IMPACT OF THE GROWTH KINETICS ON DEEP LEVEL DEFECT PRODUCTION IN GaN FILMS GROWN BY MOLECULAR BEAM EPITAXY

By

HSING-LONG LIU

A DISSERTATION PRESENTED TO THE GRADUATE SCHOOL OF
THE UNIVERSITY OF FLORIDA IN PARTIAL FULFILLMENT
OF THE REQUIREMENTS FOR THE DEGREE
OF DOCTOR OF PHILOSOPHY

UNIVERSITY OF FLORIDA

1996

ACKNOWLEDGMENTS

I would like to express my greatest appreciation to Prof. Robert M. Park, my supervisory committee chairman, for his constant professional guidance, support and encouragement during the research and the writing of this dissertation. I would also like to thank Prof. Paul H. Holloway, Prof. Joseph H. Simmons, Prof. Kevin S. Jones and Prof. Sheng S. Li who kindly served on my dissertation committee.

I extend special thanks to George Kim and Paul Precure, my fellow graduate students, whose assistance in this research is gratefully acknowledged, especially thanks to George for providing AFM images of the sapphire substrate morphology. Special thanks also go to Lynn Calhoun for sharing his knowledge of RHEED intensity monitoring. Thanks also to George, Lynn, Paul and Brent Gila for their friendship.

I would also like to acknowledge Dr. Matthias Ludwig of Dr. Hummel's group for his assistance with the PL measurements and for helpful discussions.

I would like to thank my parents, especially my father who passed away in 1993, for their prayers and love. And finally, I thank my Savior, Jesus Christ.

TABLE OF CONTENTS

Abstract of Dissertation Presented to the Graduate School
of the University of Florida in Partial Fulfillment of the
Requirements for the Degree of Doctor of Philosophy

IMPACT OF THE GROWTH KINETICS ON DEEP LEVEL DEFECT PRODUCTION IN GaN FILMS GROWN BY MOLECULAR BEAM

By

Hsing-Long Liu

December, 1996

Chairman: Robert M. Park
Major Department: Materials Science and Engineering

As is presently understood, the luminescence behavior of GaN epitaxial material is dictated by the presence of both extended defects (dislocations) and also native point defects. Near-band-edge luminescence at around 365 nm (ascribed to excitons bound to dislocations) is typically observed in addition to a, so-called, yellow band luminescence centered around 550 nm (2.3 eV) whose origin is the subject of speculation.

The specific objective of this research was to establish a relationship between growth kinetics and the production of deep level defects in GaN epitaxial films by correlating morphological changes monitored *in-situ* and in real-time during epitaxial growth with yellow band emission intensity variations recorded post-growth and *ex-situ*.

The role of Ga adatom migration on growing GaN surfaces was found to be critical with regard to the production of deep level defects and it was found that a nitrogen-free surface condition was optimum to promote efficient Ga adatom migration as

was the provision of a sufficient time delay following Ga flux exposure prior to subsequent N flux exposure.

The critical kinetic processes, such as Ga migration, were monitored in real-time during epitaxial growth using reflection high energy electron diffraction (RHEED) specular reflection beam intensity monitoring. Based on this analysis and the noted correlations between surface morphological changes and the yellow band luminescence intensity variations, it is speculated that Ga vacancies (associated with insufficient Ga adatom migration) are responsible, in association with dislocations, for the deep level emission.

An activation energy of 1.46 ± 0.25 eV has been determined for Ga adatom migration on N-free GaN surfaces and a model is presented that accounts for the kinetic processes taking place during both Ga adsorption and migration phases of growth under N-free (no N-flux arriving) conditions

CHAPTER 1
INTRODUCTION

Motivation and Objectives

Gallium nitride (GaN) has a direct band-gap of about 3.4 eV at room temperature (RT) and when alloyed with aluminum nitride (AlN) and indium nitride (InN) has the potential to be applied to the fabrication of light-emitting diodes (LEDs) and laser diodes (LDs) operating in the blue-green and ultraviolet (UV) wavelength regions of the optical spectrum.

World-wide interest in GaN was intensified by the recent realization of GaN-based blue LEDs, blue LDs, and solar-blind photodetectors. The high-output GaN-based blue LEDs are in high demand for outdoor giant displays, desktop flat-panel displays, and traffic lights, as well as devices which emit white light by combining red, green and blue emitters. Moreover, the blue LD will have far-reaching implications for space and under-sea communications, as well as high-density optical data storage. Such short-wavelength blue emitters will provide the small spot size needed to increase the storage capacity of optical storage systems over that of the current near-IR emitter-based technologies and provide faster data-transfer rates for computer and multimedia use, thus meeting the growing demands of the computer industry. GaN also is a promising semiconducting material having potential applications in electronic devices operating at high temperature, high frequency, and high power.

Despite some impressive technological achievements of the last few years, particularly by Nakamura *et al.* [1] of Nichia Chemical Industries in Japan (demonstrating the first electrically-pumped blue laser based on the InGaN/GaN multiple quantum well

system), much work remains to be done to realize a low-threshold long-lived LD suitable for commercial application. Further progress toward the development of stable, continuous wave (CW) operation of III-V nitride LDs will require a thorough understanding of how impurities and defects influence the quantum efficiency of these materials. For instance, it will be important to understand the origin of deep level defects in GaN which are known to cause yellow band luminescence, suppressing the more desirable band-edge luminescence. The yellow emission band is commonly observed in the photoluminescence (PL) spectra recorded from nominally undoped GaN epilayers regardless of the substrates used (a-plane sapphire [2,3] , c-plane sapphire [2,4,5,6] , silicon carbide (α–SiC) [7,8], Si (111) [9] , and bulk GaN [10,11]). It is also observed regardless of the crystal growth technique used (low-pressure metalorganic chemical vapor deposition (LPMOCVD) [8], metalorganic chemical vapor deposition (MOCVD) [4,11,12], metal-organic vapor phase epitaxy (MOVPE) [2,3,5,9], MBE [6,8, 10, 13,14] or high pressure methods [10]). Ramsteiner *et al.*. observed electronic Raman scattering in resonance with the yellow luminescence transition and concluded that the deep-level concentrations must be rather large to make Raman resonance observable [15].

There is little understanding of the deep-level defects in n-type GaN, however, sources of the deep-level defects have been proposed, such as Ga vacancies (V_{Ga}) [16,17,18,19,20], antisite defects (N_{Ga} and Ga_N) [21,22,23] and Ga interstitials (Ga_I) [22,23,24]. All of these theories are based on the assumption of thermodynamic equilibrium, but GaN films are currently grown under conditions that deviate significantly from equilibrium. In addition, these calculations use atomic structure factors calculated for neutral, spherical atoms. They do not take into account the effects of the charge redistribution due to chemical bonding (ionic bonding) and the stress field induced by high densities of dislocations and strong inhomogeneities present in the films. CL images, in fact, have shown strong inhomogeneities [25]. A hypothesis has recently been proposed that states that the deep-level broadband emission arises directly from the atomic structure

of dislocations or is associated with the clustering of native point defects (vacancies, interstitials) at dislocations due to the lattice distortions induced by the dislocations [25,26].

The work described in this dissertation was inspired by a desire to minimize the concentration of deep level defects occurring in GaN epitaxial films through an understanding of the factors affecting their production.

The highest quality GaN films grown today are produced by conventional MOCVD and MBE at substrate temperatures in the neighborhood of 1000° C and 700° C, respectively. Such high growth temperatures could result in Ga rich material due to desorption of the N adatoms. At low substrate temperatures, however, the diffusion rate of Ga atoms is slow compared to the growth rate of the GaN film, which can result in Ga accumulating into small Ga droplets on the growing surface which can impede the migration of nitrogen atoms [27]. Ponce *et al.*. reported that Ga droplets on the order of 10-100 μm in size were found in the GaN substrates obtained from high pressure growth methods [11]. These Ga droplets are very common even in MBE-grown GaN films, particularly in films grown at low growth temperatures. In fact, Crawford *et al.* [28] recently reported that excess surface Ga decreases the GaN formation rate when the substrate temperature is too low or the Ga flux is too high in the MBE growth case.

A systematic study of Ga migration and incorporation at some optimum growth temperature therefore seems important at this juncture with a view to controlling the deep-level defects in GaN.

Ga-migration has been investigated on GaAs surfaces. For instance, Horikoshi *et al.* [29] employed an alternate element supply technique using As and group III species to grow AlGaAs/GaAs quantum well structures. These authors reported excellent PL characteristics and smooth interfaces for films grown at a relative low growth temperature and attributed these results to a dramatic increase in the Ga atom migration rate under As-free conditions. Ewing and Greene [30] reported that growth on the Ga-terminated

(111) A face of GaAs was slow and produced films which had a tendency to form planar surfaces. On the other hand, growth on the As-terminated $(\bar{1}\ \bar{1}\ \bar{1})$ B face was fast and film surfaces were rough. The {111} planes of cubic GaAs are similar to the (0001) (or basal) plane of wurtizite GaN grown on, for instance, the (0001) plane of sapphire. The GaN basal plane has a polar configuration with two atomic subplanes, each consisting of either the cationic or the anionic component of the binary compound. Therefore, an alternating supply of Ga and N atoms may, in principle, be used to grow (0001) GaN epitaxially, possibly at growth temperatures lower than those used for MBE-growth. Such an alternate element exposure growth method has not, however, been reported previously for MBE-GaN.

In the presently described work, a growth technique which we call, alternate element exposure epitaxy (AEEE), is introduced in which the Ga and N fluxes do not impinge on the surface at the same time. During AEEE, the Ga adatoms are assumed to migrate rapidly on the growing surface under N-free conditions and by virtue of forming a Ga-covered surface and, hence, a chemically active surface, the N sticking coefficient is expected to be enhanced as well. In addition, the insertion of a Ga delay time (the time allowed to elapse between closing the Ga shutter and opening the N shutter) should allow Ga adatoms to migrate to step or kink sites and, hence, to be incorporated into the GaN film. In this manner, point defects, such as Ga vacancies and Ga interstitials, which are thought to be associated with the deep level emission in GaN may be minimized.

The specific objective of this research was to establish a relationship between growth kinetics and the production of deep level defects in GaN epitaxial films by correlating morphological changes monitored *in-situ* and in real-time during alternate element exposure epitaxy with yellow band emission intensity variations recorded post-growth and *ex-situ* .

Background

Theoretical Models of Deep-Level Defects in GaN

There are three main theoretical models which attempt to explain the origin of the deep-level emissions observed from unintentionally doped n-type GaN. All of the models predict that the deep-levels are related to native defects and impurities. Applying a tight-binding Hamiltonian model, Jenkins and Dow [21] suggested that a Ga vacancy (V_{Ga}) can act as either an electron or a hole trap with a p-like level in the gap, and the antisite defect (Ga_N) can also act as either an electron or a hole trap. Jenkins and Dow also suggested that an N vacancy (V_N) results in a shallow donor state with a p-like level in the conduction band, and its s-like deep level occupied in the gap. This will be discussed later.

By performing first-principles calculations under the assumption of thermodynamic equilibrium ,Van de Walle and co-workers [16-19] predicted that nitrogen vacancies have a rather high formation energy (~4 eV) in n-type, as-grown GaN; however, n-type behavior has traditionally been attributed to nitrogen vacancies. Van de Walle claimed that self-interstitials (Ga_i and N_i) and antisite defects (N_{Ga} and Ga_N) also have high formation energies as shown in Fig. 1.1; therefore, they are also very unlikely to occur in significant concentrations. However, these authors added that the quality of the GaN epilayers can depend strongly on the concentration of line defects such as dislocations and stacking faults, etc. The first-principles total-energy equation for a native defect in a charge state q is as follows:

$$E^f(q) = E^{tot}(q) - n_{Ga}\,\mu_{Ga}\,n_N\,\mu_N - qE_F \quad \text{----------} \quad (1.1)$$

where n_{Ga} and n_N are the number of Ga and N atoms, μ_{Ga} *and* μ_N are the Ga and N chemical potentials, E_F is the Fermi energy, and E^{tot} is the total energy for a given charge state. The chemical potentials for Ga and N are not independent, since both species are in equilibrium with GaN. If boundary conditions such as $\mu_N < \mu_{N2}$ and $\mu_{Ga} < \mu_{Ga(bulk)}$ are

not satisfied, the system would be thermodynamically unstable and would segregate into different components. Figure 1.1 shows that a Ga vacancy may have a low enough formation energy to occur in high concentrations. Van de Walle *et al.* suggested that Ga vacancies may play a role in the yellow band luminescence.

Boguslauski *et al.* [22,23,24] used an *ab initio* molecular dynamics approach in which the computations were carried out for the case of the perfect crystal using quantum molecular dynamics (MD) and the local density approximation (LDA) in supercells containing 72 atoms. Due to the wide-gap of nitrides, the formation energies of defects depend strongly on the position of the Fermi level. It is important to point out that because of the inaccuracy due to the use of LDA theory which seriously underestimates band-gap and overestimates the cohesive energy, an uncertainty on the order of 0.5 eV for the formation energy of the deep levels may occur. This is especially true if the growth process involves local excitations due to a plasma source or due to specific kinetic conditions.

In n-type GaN, the high formation energy of V_N (4.8 eV) would indicate that the N vacancy cannot be formed in sufficient concentrations to account for the n-type character of the as-grown material. However, since the formation of a Ga vacancy creates N dangling bonds, its quasi-triplet level is located about 0.4 eV above the valence band edge. V_{Ga} can trap both electrons and holes because the quasi-triplet is populated by 3 electrons in the neutral charge state. In spite of the proximity to the valence band, the quasi-triple wave functions are very localized. The formation energy of neutral V_{Ga} may appear large at 8 eV; however, since V_{Ga} can release or accept three electrons, its formation energy depends very strongly on the position of the Fermi level. In particular, in n-type GaN films the formation energy of V_{Ga}^{-3} may become very small. The thermodynamic levels for Ga vacancies are at 0.5, 0.8, and 1.3 eV above the top of the valence band maximum, respectively. Boguslauski [23] concluded that the small formation energy defects in n-type GaN are V_{Ga}, Ga_N and N_I.

Experimental Observations of Deep-Levels.

Ogino and Aoki [31] investigated the mechanism causing yellow band luminescence in GaN. A yellow band emission was observed in microcrystals synthesized from Ga and NH_3 by direct reaction, but did not appear in needle-like crystals grown by sublimation-recrystallization. These authors proposed a mechanism for the zero-phonon transition assigning the yellow-band emission to a radiative transition from a shallow donor (25 meV below the conduction band minimum) to a deep acceptor (860 meV above the valence band maximum). The deep acceptor was assigned to a complex consisting of a Ga vacancy and a carbon atom. Ramsteiner *et al.* [15] recently confirmed that shallow donors are involved in the yellow luminescence by studying the electronic Raman scattering in resonance with yellow luminescence transitions in a 1 μm thick GaN film grown on GaAs (001) by conventional MBE. No specific deep localized state was assigned by Ramsteiner *et al.*

Tansley and Eagan [20] compared the experimental data on the location of the levels associated with native point defects in the group-III nitrides with the theoretical estimates. These authors found strong evidence for the existence of a triplet of donorlike states associated with N vacancies and suggested that the three electron states associated with N vacancies in GaN are located at about 30 meV, 100 meV, and 400 meV below the conduction band minimum as shown in Fig. 1.2 (groups A, B, and C respectively). A deep level has been observed with thermal activation energies between 0.8 and 1.1 eV below the conduction-band edge as shown in Fig 1.2 as group D. This deep level has been attributed to Ga vacancies [16] and N antisite defects [21]. Both Tansley and Eagan [20] and Van de Walle *et al.* [16] proposed that group D is the obvious candidate for the yellow band luminescence due to transitions between the deep-level state and the valence band. Zhang *et al.* [32] observed a dramatically reduced deep-level luminescence in a highly Ge doped ($n \sim 10^{20}$ cm^{-3}) GaN film and suggested that the deep-

level luminescence emission may be related to Ga vacancies since Ge acts as a donor by occupying Ga sites. Glaser *et al.*. [33] found an energy level for the deep-donor state from optically detected magnetic resonance (ODMR) spectroscopy studies to be ~1 eV below the conduction-band minimum in GaN epitaxial layers grown by OMCVD, thus agreeing with the group D energy level theory. Other deep traps (group E of Fig 1.2) which are observed as a band-tail absorption feature at ~1 eV above the valence band maximum are believed to be related to Ga_N [21] or V_{Ga} [23].

Perlin *et al.* [22] investigated the pressure dependence of the energy of the yellow band luminescence for n-type GaN films at hydrostatic pressures up to 30 GPa and showed that the energy of the luminescence band changes linearly with pressure up to about 18 GPa. Thus, at the highest pressure, the yellow band luminescence becomes blue. Similarly, Shan *et al.* [34] studied the PL emission as a function of applied hydrostatic pressure using the diamond-anvil-cell technique on a 4.2μm thick single-crystal GaN film grown by MOCVD. The exciton emission lines were found to shift almost linearly toward higher energy with increasing pressure and the yellow emission band showed a similar blue shift behavior under applied pressure. Along with the conclusions of Ogino and Aoki [31] and Ramsteiner *et al.* [15], the report of Perlin *et al.*. supports group E as a candidate for yellow band luminescence due to transitions between shallow donors and deep acceptors. However, Shan *et al.* [34] attributed the yellow band emission to transitions involving s-like levels associated with group D defects and the top of the valence band maximum.

With a view to determining the distribution of the defects responsible for the 2.3 eV yellow band luminescence, Asif Khan *et al.* [35] performed low temperature PL analysis on a 9.3-μm-thick LPMOCVD grown GaN/sapphire sample from the front and back sides; the same yellow band emission intensity was found in both cases. Thus, these authors concluded that the defects that were responsible for the yellow band emission had a uniform distribution in the film. However, Cowan *et al.* [14] used

Cathodoluminescence (CL) to provide an analysis of traps as a function of depth in their GaN films. For low accelerating voltage (V_{acc}), the electron probe had little penetration so data were generated from the film surface. At higher V_{acc}, the electron beam penetrated the film-substrate interface, giving a profile of yellow emission versus depth. They observed that the intensity of the deep-level emission was higher at depths close to the film-substrate interface than at depths just beneath the film surface. Shan *et al.* [36] reported the results of time-resolved studies on the radiative decay on a 7 μm, thick MOCVD-grown GaN film in which they found that the stronger the yellow emission, the shorter the decay times for free-excitons and for bound-excitons. These authors suggested that the fast decay behavior of the PL intensity indicated that the capture of excitons and trapping of carriers at deep level defects through nonradiative combinations dominate the decay of exciton population.

On the other hand, Gotz *et al.* [37] and Hacke *et al.* [38] used a transient capacitance method to analyze traps occurring in unintentionally doped n-type GaN. By virtue of the sensitive measuring technique (deep-level transient spectroscopy [DLTS],) Gotz *et al.* detected two deep-levels having thermal activation energies for electron emission to the conduction band of 0.16 eV and 0.44 eV. However, Hacke *et al.* found three majority-carrier traps occurring at different energies below the conduction band having activation energies, 0.26, 0.58, and 0.66 eV, respectively. The detected activation energy levels mentioned above belong to group B and group A of Fig. 1-2. Although DLTS is a sensitive spectroscopic tool for the characterization of electronic levels in the bandgap of semiconductors, conventional DLTS is of limited use in wide bandgap materials as the accessible range of level energies in the gap is restricted to about 1 eV. Optical deep-level transient spectroscopy (O-DLTS), also called photoemission capacitance transient spectroscopy, can overcome this limitation by using monochromatic light for carrier emission so that levels in the entire bandgap become accessible for characterization. Using O-DLTS, Gotz *et al.* detected four new deep levels with

optical threshold energies for electron photoemission of 0.87 eV, 0.97 eV, 1.25 eV, and 1.45 eV which are relatively fitted to group D of Fig. 1.2. Very recently, Sanchez *et al.* [39] investigated yellow band and other deep level emissions in undoped MOVPE GaN samples using photocapacitance and photoinduced current transient spectroscopy (PICTS). Photocapacitance reveals in all samples two specific signatures at photon energies of 1 eV and 2.5 eV below the conduction band and the capacitance step at 1 eV is only seen after photoionization at an energy above 2.5 eV. In addition, Sanchez *et al.* observed the correlation between PICTS amplitude and the PL intensity of the yellow emission, and they concluded that both transitions are linked to the same trap which is at 2.5 eV below the conduction band. It is assigned to group E as shown in Fig. 1.2.

Lin *et al.* [40] investigated the intensity of low temperature PL as a function of annealing temperature in GaN films grown by MBE. These authors found a reduction of the donor-bound exciton (I_2) peak intensity and an enhancement of the yellow-band emission at high annealing temperatures (900° C). These authors annealed their samples for 30 minutes in a nitrogen ambient, and attributed their observations to the formation of intrinsic point defects such as Ga vacancies and antisite defects.

Migration Enhanced Epitaxy With Reference to GaAs

Migration enhanced epitaxy (MEE) is a modified version of conventional MBE in which the constituent element fluxes are supplied separately rather than simultaneously to the substrate [28,40,41,42,43].

The basic advantage of MEE over MBE is that rapid migration of adatoms on the growing surface is ensured even at relatively-low growth temperatures, adatom migration being very important with regard to the growth of high quality epitaxial layers. During conventional MBE growth of GaAs and AlAs, for instance, the group III atoms on As-stabilized surfaces migrate very slowly especially at low growth temperatures due to their

reaction with As atoms. Utilizing reflection high-energy electron diffraction (RHEED) analysis, Neave *et al.* [44] determined the activation energy of Ga surface diffusion to be, E_D = 1.3 eV, on an As-stabilized (2x4) surface. For the diffusion of Al during the growth of AlAs, a higher E_D value of 1.6 eV was estimated from the ratio of the cohesive energies of AlAs and GaAs by Joyce *et al.* [45]. These large activation energies, apparently caused by the formation of GaAs and AlAs molecules, control the growth process in conventional MBE. It is believed that such large activation energies may make the surface group-III adatoms almost immobile when the growth temperature is lower than 400° C, and this is the reason why high-quality GaAs and AlAs films have not been grown at temperature lower than 400° C using conventional MBE. Nagata and Tanaka [46] used a shadowing method to determine the Ga surface diffusion distance on (001) oriented GaAs under both Ga- and As-stabilized surface conditions. These authors concluded that at temperatures less than 550° C, the diffusion length of Ga under Ga-stabilized surface conditions was 1900Å, which is about 10 times larger than the diffusion length under As-stabilized conditions. In conventional MBE, the growth of GaAs and AlAs films is usually under As over pressure conditions, which means that the surface is As-stabilized. For this situation, migrating species on the growing surface may move as Ga-As and Al-As molecules rather than isolated Ga and Al atoms since impinging atoms immediately react with arsenic to form Ga-As and Al-As molecules. The large activation energy of surface diffusion as reported in ref. 43 makes these molecules migrate extremely slowly. On the other hand, when Ga and Al atoms arrive on an As-free growing surface, such as in the case of MEE growth, migration takes place in atomic rather than molecular form. Therefore, surface migration is effectively enhanced under Ga- or Al-stabilized conditions.

Migration Kinetics During MEE with Reference to GaAs

To illustrate how the migration of surface adatoms affects the quality of epitaxial layers, the kinetic energy of migrant atoms versus temperature is presented in Fig. 1.3 [29]. As shown in Fig. 1.3, E_m represents the minimum energy necessary for surface adatoms to move to the neighboring site, E_k and E_s are the potential energies at kinks and steps, respectively, and E_0 denotes the kinetic energy of the migrant atom. Because $E_m >> E_0 = kT$ (where k is the Boltzmann constant and T is the absolute temperature), the migration of surface adatoms during conventional MBE is usually very slow. The large value of E_m is caused by the fact that the growing surface has a high density of small islands of GaAs, and E_m includes the decomposition energy of GaAs molecules at the outermost region of the islands. In contrast, excess Ga adatoms are expected to migrate actively during MEE growth in the absence of As, thus, E_m in the MEE case is not much greater than E_0 even at relatively low temperatures. The Ga atoms diffuse until they find more stable lattice sites at kinks and ledges on the growing surface where Ga-As bonds are formed. Thus, the energy relationships in the MEE case can be expressed as E_o , $E_m << E_k$, E_s . The migration mechanisms occurring during growth of GaAs by MEE are discussed below.

The first case is the migration of Ga atoms on an As-atom plane. When only Ga atoms are supplied to the As-plane, each surface Ga atom shares two sp^2 bonds with As atoms in the underlying As-plane which leaves one unsatisfied sp^2 bond perpendicular to the surface [29]. Because of the strong acceptorlike nature of this unsatisfied sp^2 bond, the sp^2 bonds between surface Ga and the underlying As atoms could be unstable. Thus, it can be expected that the surface Ga atoms are very mobile compared to GaAs molecules.

The second case is the migration of Ga atoms on a Ga-atomic plane, especially when about two monolayers (ML) of Ga atoms are supplied during a Ga exposure.

Impinging Ga atoms will form metallic bonds with underlying Ga atoms. In metallic bonds the electron distribution is wide, which makes the migration of Ga atoms bonded to Ga atoms very easy. This characteristic holds even below the melting point of metals. Ga has a particularly low melting temperature; therefore, Ga atoms on a Ga-atomic plane move freely, even at low temperature, until they reach active sites such as locally exposed As-islands and other ledges and kinks. This characteristic is important for the MEE process at low temperatures because it is expected that Ga atoms supplied on either As- or Ga-atomic planes tend to form a two-dimensional atomic sheet rather than a three-dimensional cluster.

The third case is the migration of As molecules on a Ga-atomic plane. It is well known that the Ga-atomic plane surface is very active chemically because of the unsatisfied sp^2 bonds perpendicular to the surface. Thus, the impinging As molecules at these sites will decompose into As atoms which are incorporated into the epitaxial layer to form stable sp^3 bonds with underlying Ga atoms and neighboring As atoms [29,47]. Therefore, migration of As atoms on a Ga-atomic plane could be slow; on the other hand, isolated group V atoms on a Ga-atomic plane cannot form sp^3 bonds, and in this case they may migrate easily.

The fourth possible case of diffusion concerns As molecules on an As-atomic plane. An As surface is less chemically active than a Ga surface because the As atoms of an As-atomic plane stabilize themselves by forming p^3 or sp^3 bonds with each pair of adjacent As atoms [29,47]. The arriving As molecules are weakly adsorbed on the As-plane and migrate actively along the surface. As a matter of fact, Foxon and Joyce [48] reported a surface diffusion activation energy of As_4 molecules on As-planes to be 0.25 eV.

However, the growth of more ionic bonded materials such as Group III nitrides may be different from that of mostly covalent bonded materials such as Si and GaAs, because of the larger electronegativity difference between the components of the III-V

nitrides [49,50]. Lester *et al.* [51] suggested that Fermi level pinning at the crystal surface during epitaxial growth may not occur in the case of n-type GaN. In addition, almost all as-grown unintentionally-doped GaN films are n-type [52]. Any attempt to increase the V/III ratio results in a rough growth front. As a matter of fact, unlike GaAs in which the growth rate is controlled by the impinging Ga flux alone, GaN growth is controlled by both the Ga flux and the nitrogen flux [53].

MOCVD Growth of GaN Using An Alternate Source Exposure Method.

There have been three reported attempts to grow GaN films by MOCVD using alternate source exposure. Hwang *et al.* [54] alternately exposed a sapphire substrate to trimethylgallium (TMG) and N+H plasmas via a rotating suscepter, but most of the resulting GaN films were polycrystalline. Sumakeris *et al.* [55] alternately exposed an α - SiC substrate to triethylgallium (TEG) and ammonia. The film thickness was measured by ellipsometry to study the effect of the exposure time to the reactant species on the amount of material deposited per cycle. A self-limited growth was found to occur at a substrate temperature of 120° C and was limited to about 67 % of a monolayer. The films grown at this temperature were amorphous. The crystallinity improved with increasing temperature but the chemically self-limiting growth characteristic disappeared. Khan *et al.*. [56] used switched MOCVD to supply TEG and NH_3 to a sapphire substrate at 450° - 900° C at a pressure of 76 Torr. The growth rate was about 0.75 monolayer per cycle with a 10% margin of error. The band-edge PL signal intensity and linewidth for the alternate source exposure-grown sample grown at 900° C were comparable to those observed from samples grown by conventional MOCVD at 1040° C.

Dissertation Outline

This dissertation is subdivided into six chapters. Chapter 1 includes the motivation and objectives for this work and a review of the deep-level defects which result in yellow band luminescence in GaN.

Chapter 2 details the growth techniques employed in this work and the *in-situ* analytical techniques used to characterize the growth are also detailed.

Chapter 3 describes the substrate preparation and the conventional MBE growth procedures used to synthesize GaN films on c-plane sapphire substrates, and reports PL, Hall-effect and SEM analyses of these films.

Chapter 4 presents the novel AEEE growth method used in this investigation and growth parameters are correlated with the observed RHEED specular reflection beam intensity variations. In this chapter, PL and SEM data are reported as functions of the Ga and N delay times.

Chapter 5 presents a discussion of the GaN growth kinetics and their correlation with deep level defects. A model is presented to explain the experimental observations.

Finally, Chapter 6 summarizes the principal conclusions drawn from this investigation and presents suggestions for future work in this area.

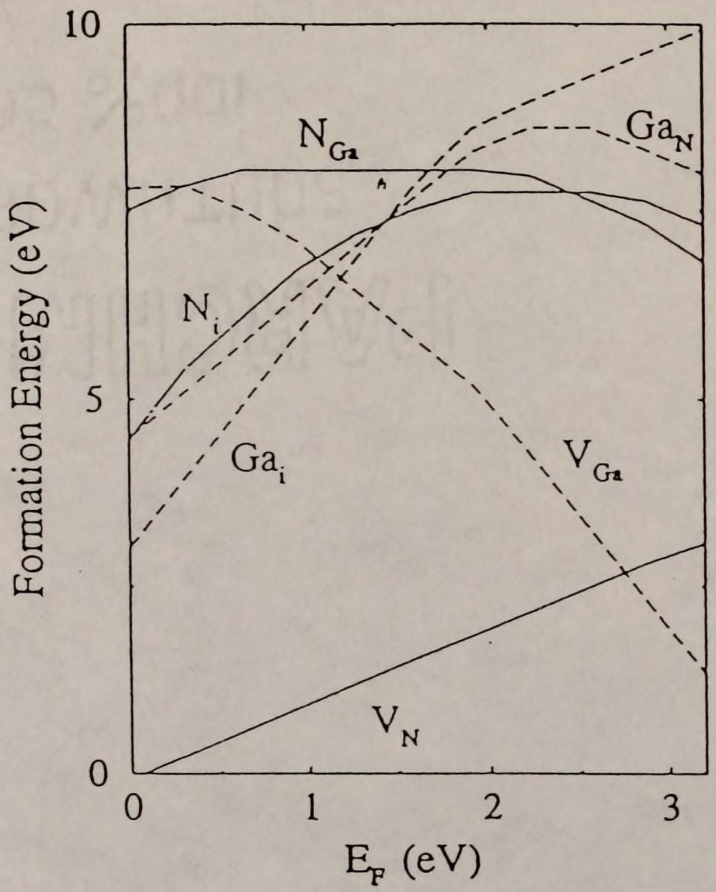

Figure 1.1 The predicted formation energies of native deep-level defects in GaN as a function of the position of the Fermi level, E_F (after Ref. 20).

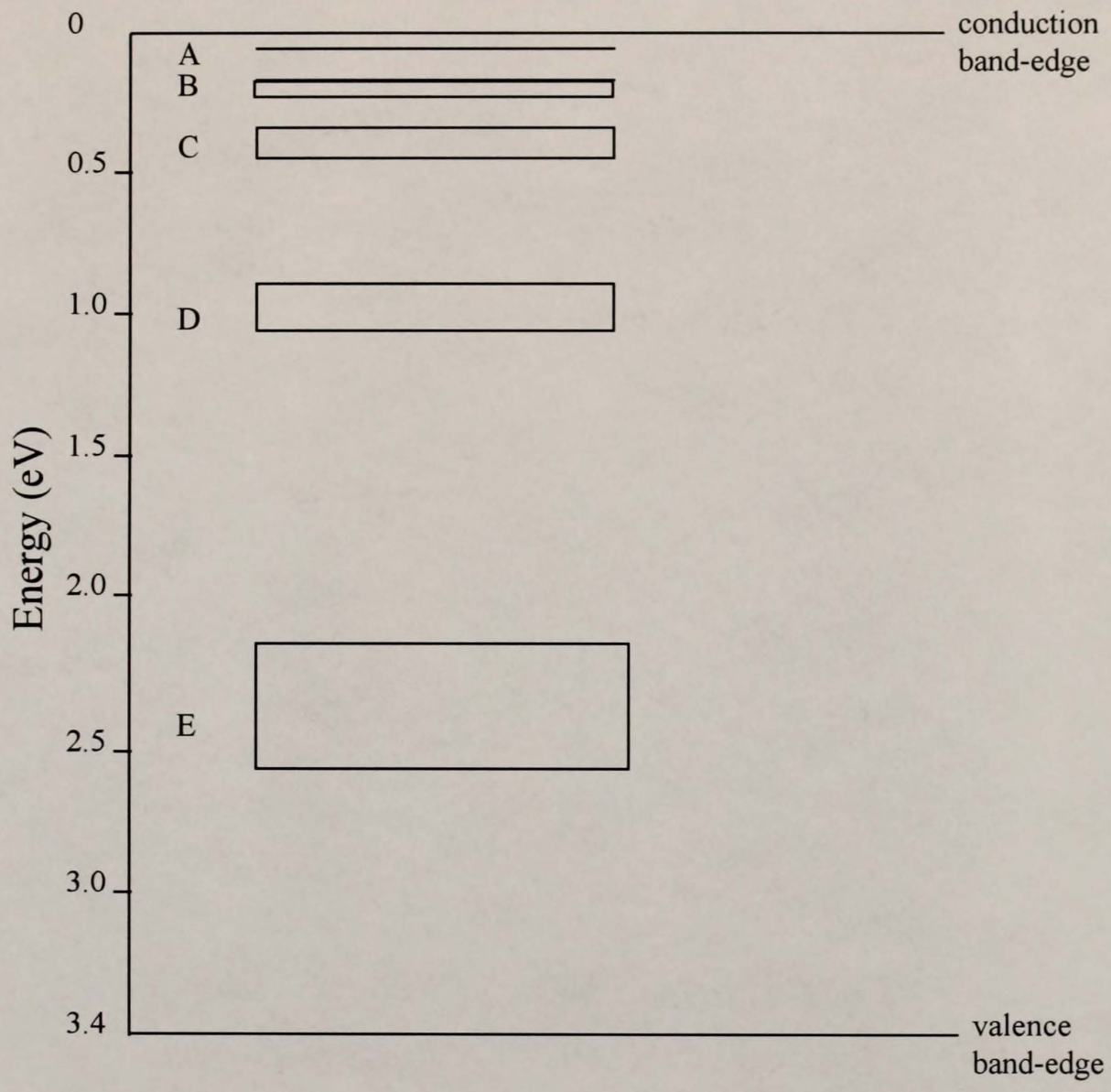

Figure 1.2 Native defect levels in as-grown GaN summarized from the literature. A,B,C (V_N), D (N_{Ga} , V_{Ga}), and E (Ga_N , V_{Ga}).

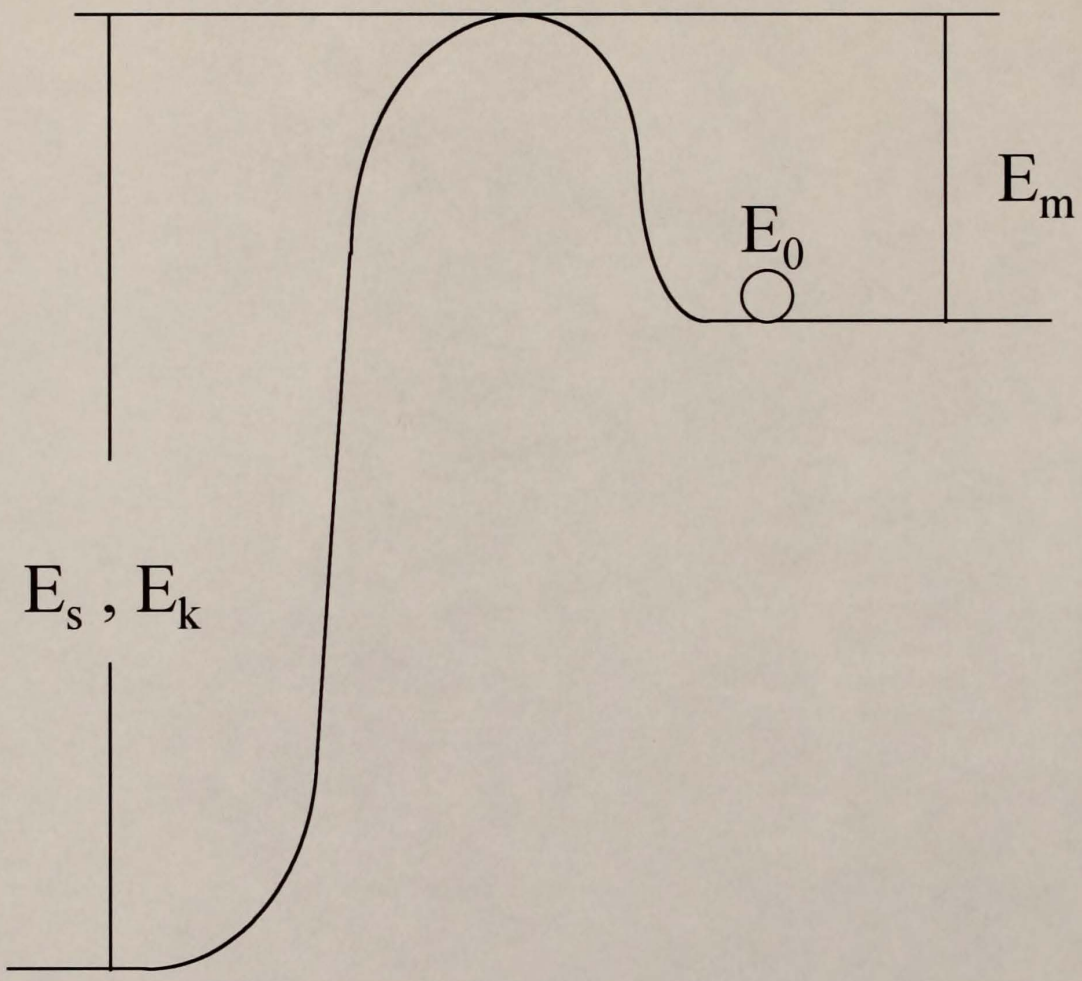

Figure 1-3 Potential energy diagram for surface migration. E_m represents the minimum energy necessary for surface adatoms to move to the steps and kinks, E_k and E_s are the potential energies at kinks and steps, respectively. E_0 is the kinetic energy of migrant atom.

CHAPTER 2
MBE SYSTEM AND CHARACTERIZATION TECHNIQUES

Introduction

All of the samples in this work were grown in a Varian GEN II MBE system. This system was previously employed to grow zinc blende-GaN films [59,60]. All samples were characterized *in-situ* using RHEED analysis as well as *ex-vacuo* using other analytical techniques including scanning electron microscopy (SEM), Hall-effect measurements and photoluminescence (PL) measurements. All samples were grown and characterized by the author with the exception of the PL analysis which was carried out by Dr. Matthias Ludwig in Dr. Hummel's research laboratory at the University of Florida. The MBE growth conditions employed, as well as important considerations and procedures pertaining to the growth, and the characterization techniques mentioned above are outlined in the following chapter.

Molecular Beam Epitaxy

Molecular beam epitaxy has become a powerful growth technique particularly suitable for manufacturing advanced electronic and photonic devices. In a MBE system, constituent elements and dopants are supplied in the form of molecular or atomic beams, either thermally generated or formed in a plasma. The beams are directed toward a suitably heated single-crystal substrate on which epitaxial growth occurs. Since the molecular or atomic beams can be individually shuttered, complex superlattice structures can be fabricated using this technique with precise control down to the atomic-level.

Varian GEN II MBE System Configuration

The Varian GEN II MBE system at the University of Florida consists of three connected ultra-high vacuum (UHV) chambers; an entry/exit (EE) chamber, a buffer chamber, and the growth chamber. Each UHV chamber is of stainless steel construction and has an independent pumping system. The chambers are isolated by gate valves and all system components are bakeable to 200° C.

The entry/exit chamber allows samples to be loaded into and out of the system while maintaining the buffer and growth chambers under ultrahigh vacuum conditions. To reduce contamination, the EE chamber opens into a clean room where the *ex-vacuo* cleaning of substrates take places while the opened chamber is vented using dry nitrogen gas. Two molecular-sieve and liquid nitrogen cooled sorption pumps are used to evacuate the chamber, in addition to a CTI-100 cryogenic pump which produces ultra-high vacuum conditions. After entry into the EE chamber, the substrates are heated to 150 °C using a pair of quartz halogen lamps in order to desorb water vapor from the substrate surface and the sample holder.

A transfer trolley facilitates sample movement between chambers. A magnetic force is employed to transfer the trolley from the EE chamber to the buffer chamber once the valve separating the two chambers is opened. The buffer chamber is evacuated by a VacIon pump. A heater station inside the buffer chamber is employed to evaporate any impurities whose vapor pressures are too low at 150° C (the EE bake-out temperature). The temperature used for buffer bake- out is 450° C. There are two magnetically-coupled transfer arms, one for transferring a substrate to the buffer chamber heater station, the other for the substrate mounting block, which is attached to the continuous azimuth rotation (CAR) substrate holder, inside the growth chamber. The pressure difference between the buffer and the growth chamber is minimized before the gate valve between the chambers is opened.

The growth chamber is illustrated schematically in Fig. 2.1. Different types of pumps, a CTI-200 cryogenic pump, a VacIon pump, and a titanium sublimation pump, are employed to maintain the UHV environment required for growth. When attached to the CAR, the substrate can be rotated (180°) from the transfer position to the growth position and vice-versa, and rotated (360°) in its own plane for RHEED analysis. Heater filaments for elevating the substrate temperature are mounted on a pyrolitic boron nitride (PBN) plate inside the substrate mounting block. A W-Re thermocouple is isolated from the heater filaments by a PBN tube in a radiation cavity which is located in the center of the substrate mounting block. The water-cooled substrate mounting block can heat the substrate to 800° C by radiation through the PBN plate which gives uniform heat distribution for the entire substrate holder, while the thermocouple serves to monitor and control the substrate temperature. In addition, the rotation speed of the CAR substrate holder can be controlled which further improves the substrate temperature uniformity during epitaxial growth.

Conventional effusion cells are used to supply the atomic and molecular beams, with the exception of the nitrogen source. There are eight furnace ports to house different source materials. For the conventional effusion cells, each solid or liquid source material is placed into an ultraclean PBN crucible. The liquid sources are mounted on upward-facing ports, while the solid sources are mounted on downward-facing ports. A W-Re thermocouple is held by spring force tightly against the bottom of each crucible. To maintain the high purity of the source materials, the crucibles are idled at relatively high temperature in the range, 200° C to 820° C, depending on the source. Cryoshrouds surround the effusion cells and the growth chamber itself to dissipate excess heat. A beam flux monitor (nude ion gauge) is utilized to measure the beam flux from the effusion cells. The beam flux monitor is mounted on the CAR 180° away from the substrate position in order that beam fluxes can be monitored without exposing the substrate to the fluxes. Control over the beam fluxes is achieved using pneumatically controlled shutters

in front of each source orifice. For practical purposes, the beams can be considered as unidirectional so that the insertion of a mechanical shutter will stop a beam from reaching the substrate and allow different crystal compositions to be grown. The precise control of the opening and closing of the shutters plays an important role in this research.

Substrate Temperature Calibration

The actual temperature at the substrate surface is different from that monitored by the W-Re thermocouple, since the thermocouple is not physically attached to the substrate. In this work, Omega Temperature Indicating Liquids (OTIL) which have a time response to temperature changes on the order of milliseconds and an accuracy of ± 1% were used to calibrate the surface temperature. By applying a small amount of OTIL on a test sapphire surface which was mounted on a Mo block, it was easy to pinpoint at which monitored temperature the OTIL turned black, an irreversible change, indicating that the substrate had reached a particular temperature. In this fashion, a calibration was obtained and a plot of actual sapphire substrate surface temperatures versus monitored temperatures is presented in Fig. 2.2.

In Situ Analysis

Reflection High Energy Electron Diffraction (RHEED) was utilized to perform real-time *in-situ* analysis of the substrate and epilayer surfaces. The RHEED electron beam energy was in the range of 0 - 10 keV and the electron beam was incident at a glancing angle of 1-2° to the substrate surface. Since monochromatic electron beams are sensitive to atomic order in solids and are ideally suited for the study of crystalline surfaces, this *in-situ* surface analyzer was invaluable in providing information about the surface structure, orientation, and the degree of surface roughness during epitaxial

growth. RHEED is particularly useful in studying structure changes as functions of temperature or time during epitaxy.

Ex-vacuo RHEED Specular Reflection Beam Intensity Monitoring System

In addition to observing diffraction patterns, the RHEED specular reflection beam intensity was monitored in this work and the monitoring system employed during growth consisted of a CCD camera, video monitor, Si-photodiode, bias circuit, and chart-recorder as shown schematically in Fig. 2.3. The RHEED specular beam intensity was captured by the CCD camera and displayed on the monitor and the Si-photodiode placed over the spot on the monitor. The bias circuit placed a potential across the photodiode causing output (voltage) to be linearly related to the input (light intensity). The chart recorder logged the output voltage of the photodiode.

By monitoring the variation of the RHEED specular reflection beam intensity during growth, the migration process and surface conditions on the growing surface could be evaluated. Because the specular reflection beam intensity is sensitive to the degree of surface roughness, a decrease of the RHEED specular reflection beam intensity indicates an increased surface roughness, such as might be associated with island formation for instance. To illustrate this point a typical RHEED specular reflection beam intensity trace recorded in this work during alternate element (Ga and N) exposure growth is presented in Fig. 2.4. As can be seen from the figure, the specular reflection beam intensity is a strong function of the status of the surface in terms of species present and the particular kinetic processes taking place. The interpretation of such data will be discussed at length in the following chapters.

Nitrogen Free-Radical Source

In this work, an Oxford Applied Research (OAR) radio frequency (rf) plasma discharge source as shown schematically in Fig 2.5 was used to generate nitrogen free-radicals. The same type of source has been successfully used to supply atomic nitrogen for p-type doping of ZnSe [57,58] and to grow zinc blende-GaN [59,60]. The source operates at 13.56 MHz and has a maximum output power of 500 W. The radical source is mounted on the MBE growth chamber, replacing a conventional effusion cell. A distance of 15 cm separates the end of the radical source from the substrate.

High-purity molecular nitrogen gas (99.9995%) was introduced through a precision UHV leak valve into a PBN discharge tube capped with a PBN aperture. The PBN aperture had 37, 0.3 mm diameter holes to release reactive nitrogen species to the substrate surface. The gas line between the nitrogen cylinder and the UHV leak valve was pumped by two liquid nitrogen cooled sorption pumps before opening the valve on the cylinder to ensure the purity of gas that was introduced into the growth chamber.

In this work a nitrogen plasma was maintained using a forward power of 200W and a nitrogen chamber pressure of 1×10^{-5} Torr. Under these conditions, an optical emission spectrum was recorded from the plasma using a wavelength spectrometer/OMA apparatus. The emission spectrum shown in Fig. 2.6 is indicative of the presence of both ground state nitrogen atoms (1^{st} Positive System of N_2 transitions) and excited nitrogen atoms (direct transitions) in the plasma and therefore in the flux emanating from the source.

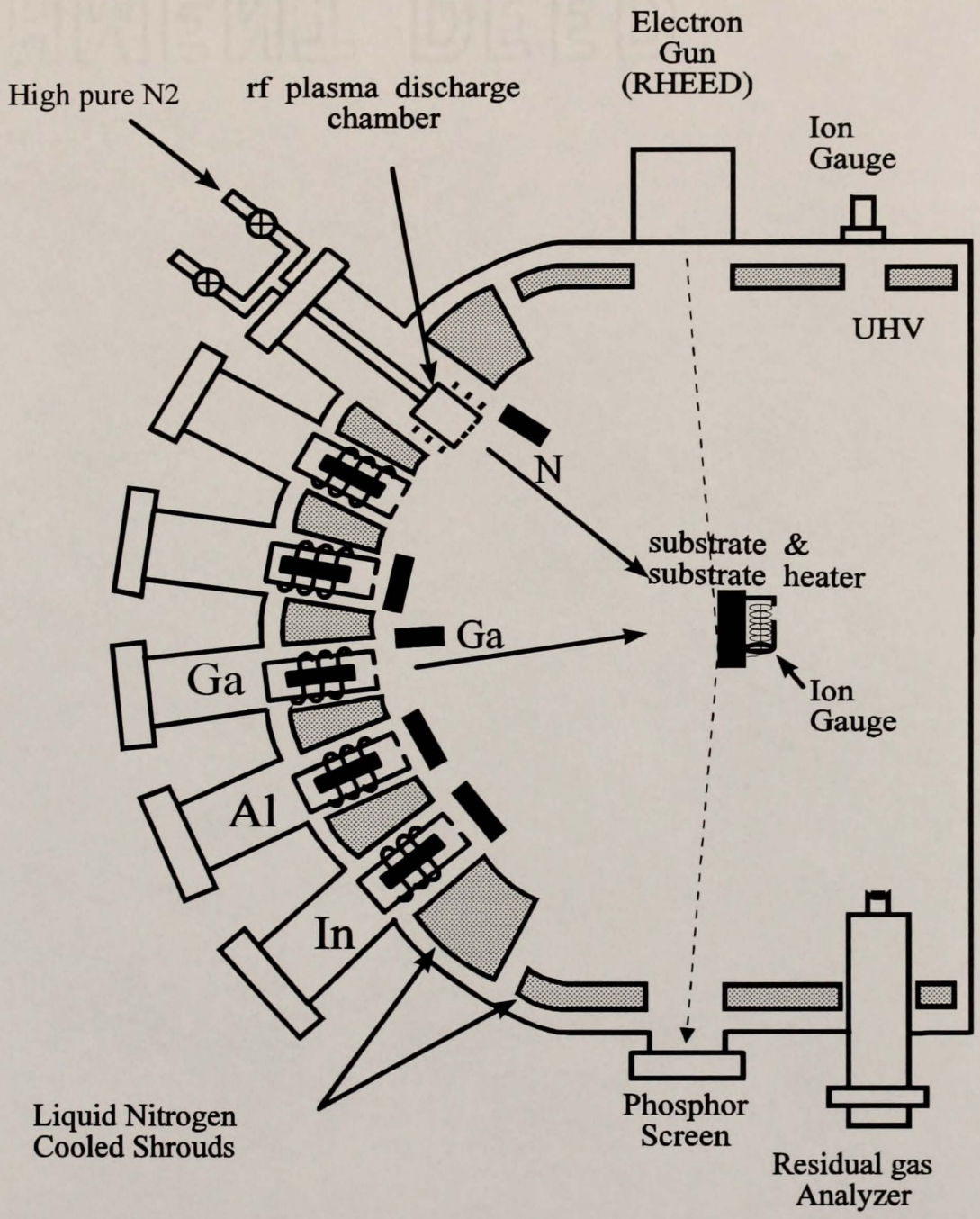

Figure 2.1 Schematic of the MBE growth chamber used to grow GaN/sapphire films by conventional growth and by AEEE techniques.

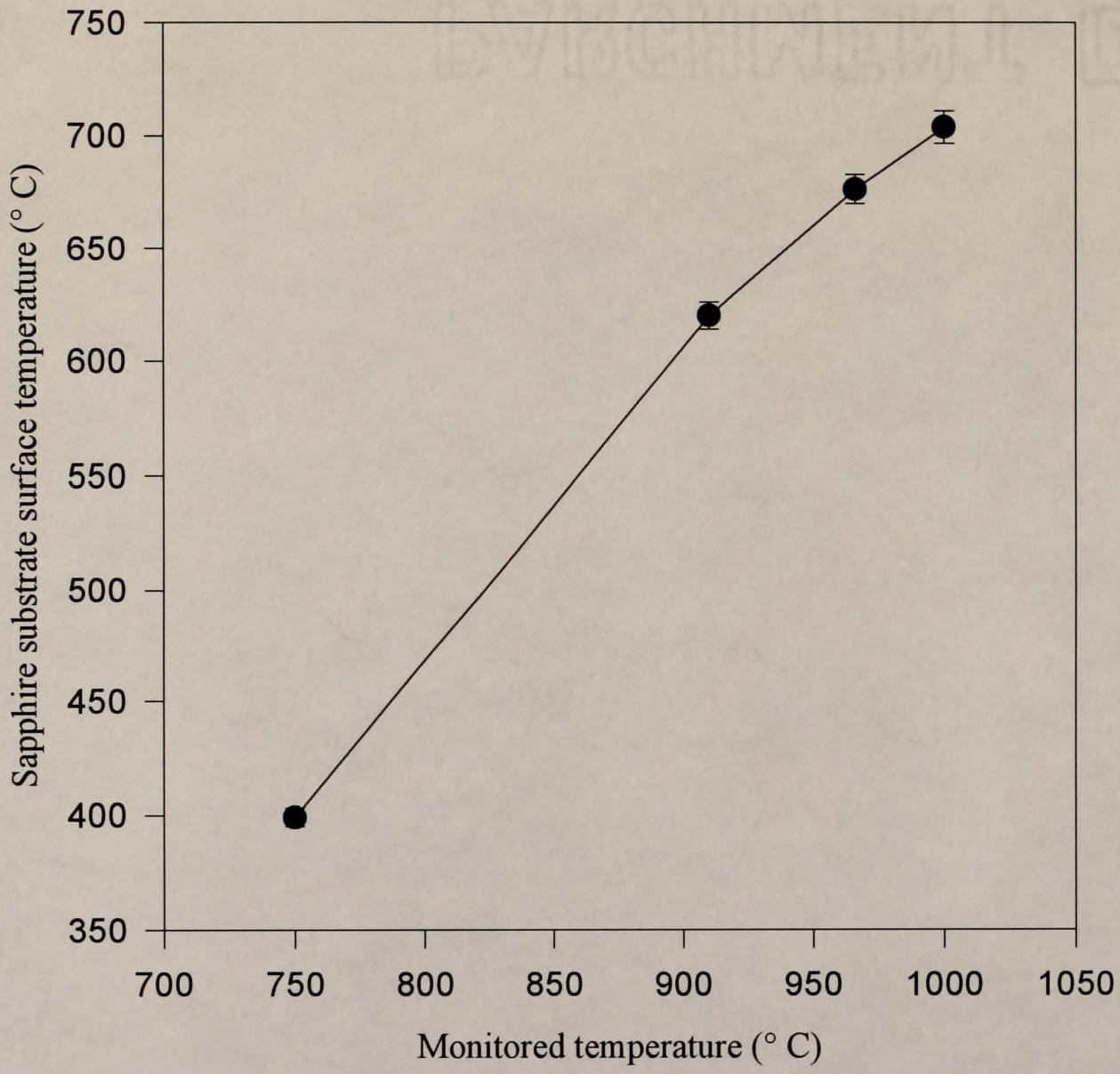

Figure 2.2 Plot of sapphire substrate surface temperature vs. monitored temperature obtained using Omega Temperature Indicating Liquids (OTIL).

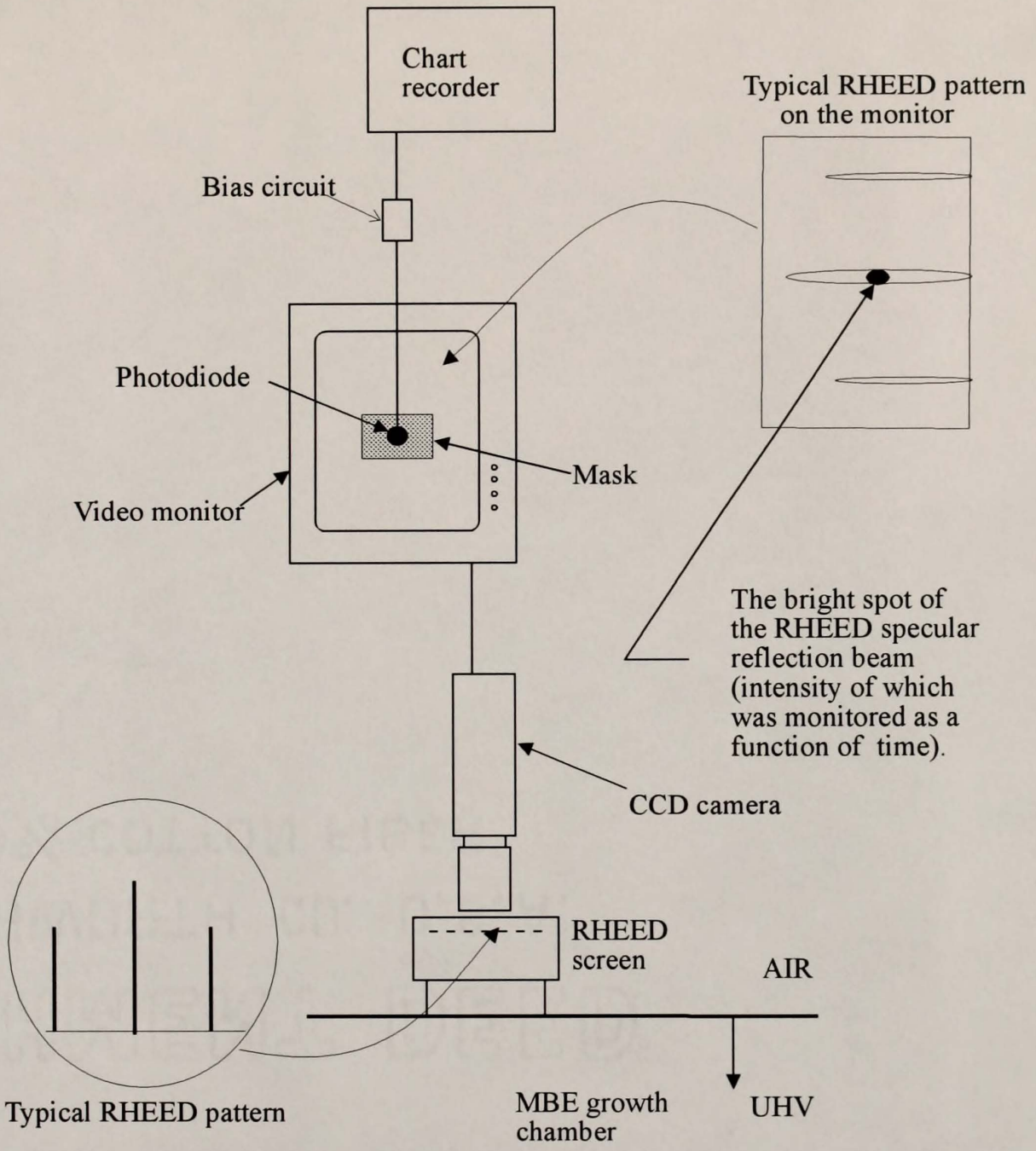

Figure 2.3. Experimental set-up used to monitor the RHEED specular reflection beam intensity as a function of time during growth.

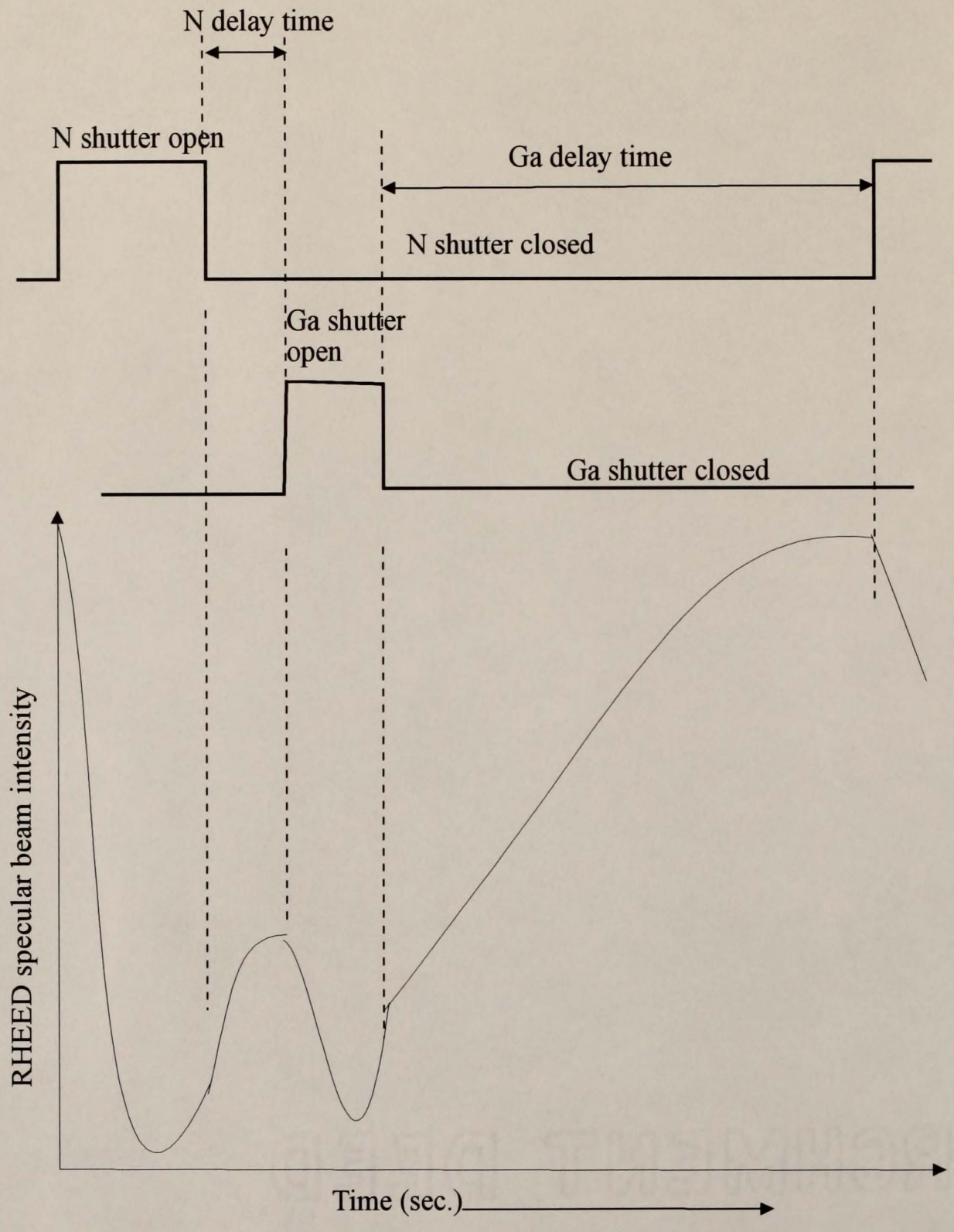

Figure 2.4 A typical specular reflection beam intensity trace recorded during one cycle of alternate element (Ga + N) exposure growth.

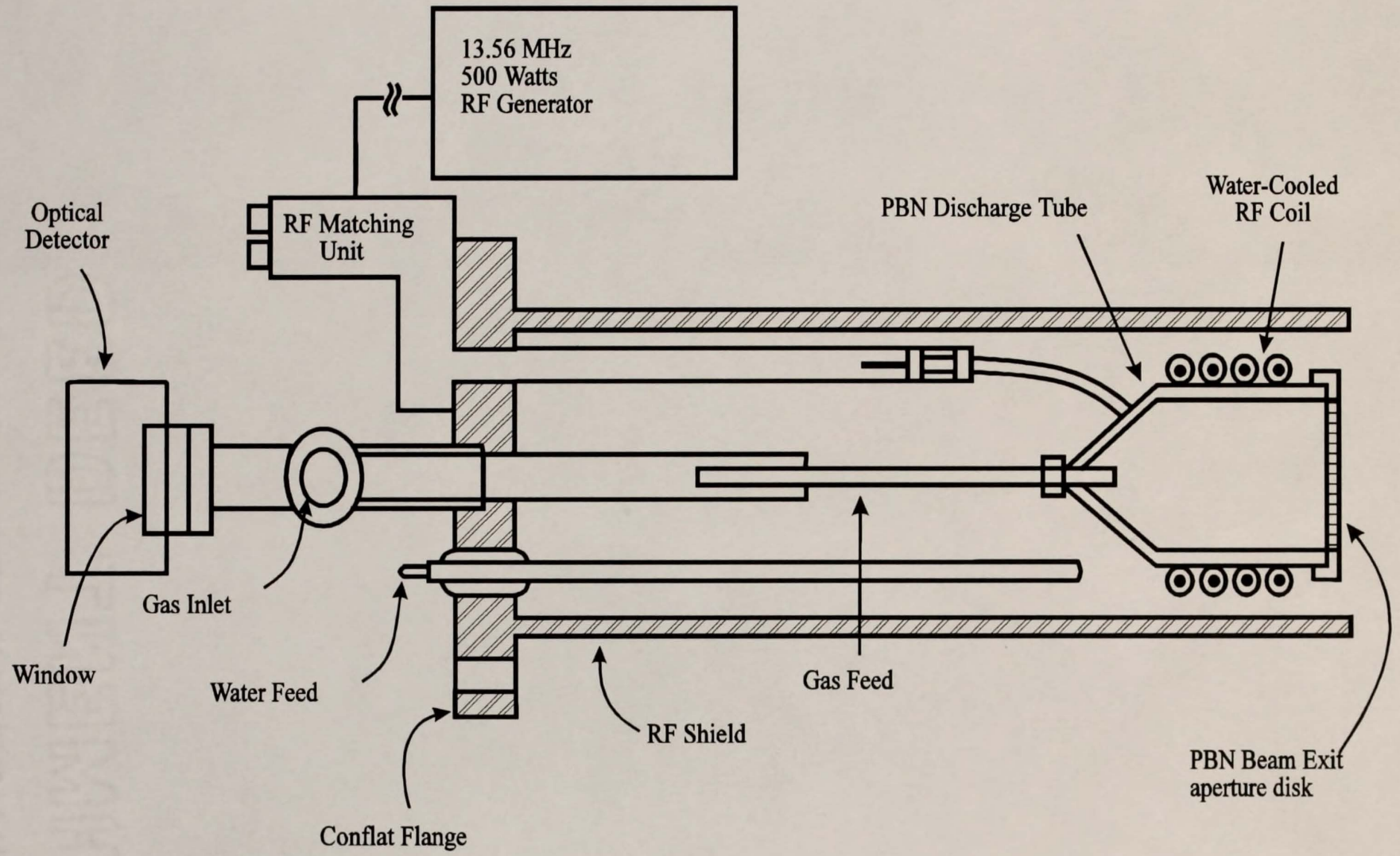

Figure 2.5 Schematic of rf plasma discharge source used to generate nitrogen free radicals (N).

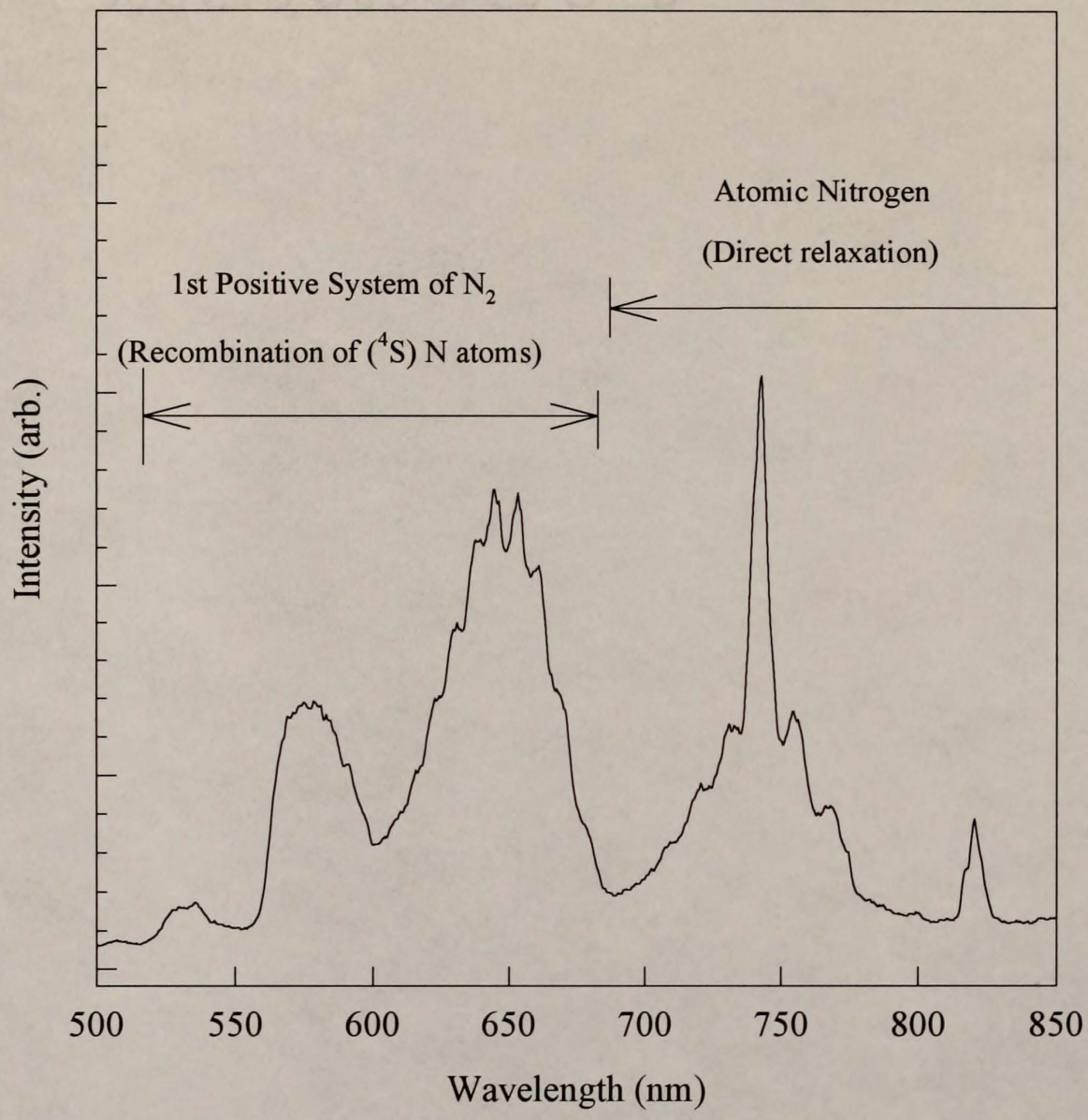

Figure 2.6 Optical emission spectrum of nitrogen plasma generated from a 190 W, 13.56 MHz, rf plasma discharge with a nitrogen background pressure of 2 x 10^{-5} Torr.

CHAPTER 3
GROWTH BY CONVENTIONAL MBE AND CHARACTERIZATION OF GaN / SAPPHIRE FILMS

Ex-vacuo Substrate Preparation

All of the c-plane sapphire (Al_2O_3) substrates used in this work were obtained from Union Carbide Crystal Products in Washougal, WA. The specifications of these substrates are listed in Table 3.1.

Table 3.1 Specifications of Union Carbide c-plane sapphire substrates

Wafer Size	10 x11 mm
Wafer Orientation Surface Edges	 normal to the (0001) or c-axis to within 3° longer edges normal to $(1\,\bar{2}\,1\,0)$ or a-axis
Wafer Thickness	500 microns
Surface Finish	one side polished
X-ray Rocking Curve linewidth	~12 arc seconds
Lattice Parameter a-axis c-axis	 a=4.758 Å c=12.991Å
Thermal Expansion Coefficients a-axis c-axis	 7.5×10^{-6}/K 8.5×10^{-6}/K

Ex-vacuo substrate preparation procedures were performed in the clean room. The Al_2O_3 (0001) substrates were degreased by successive rinses in trichloroethane, acetone and methanol and then etched in H_2SO_4 : H_3PO_4 (3:1) at 160° C for 15 minutes. The etching was used to eliminate any surface contaminants and mechanical damage due to polishing. Atomic force microscopy (AFM) analysis showed that the surface morphology of the etched sapphire substrate was smoother than that of the un-etched substrate as shown in Fig. 3.1 (rms roughness = 0.398 nm compared to as-received sapphire, rms roughness = 2.458 nm). The wafers were then rinsed in de-ionized water and blown dry using dry nitrogen. The backside of the substrates were metallized with Mo using electron-beam (E-beam) evaporation. In the vacuum ($< 5 \times 10^{-7}$ Torr) environment of the E-beam evaporation system, a high-intensity beam of electrons was focused on a high-purity Mo source target. With the shutter closed, the source target was outgassed for 5 minutes. The shutter was then opened and Mo was deposited at a rate of ~3 Å/sec. as measured by a quartz crystal monitor. The resonant frequency of the crystal shifted in proportion to the thickness of the deposited film. By monitoring the shift in resonant frequency of the crystal, the deposition rate could be measured with an accuracy of better than 1 Å/sec. The total thickness of the Mo metallization was 0.25 μm. The metallization on the backside of substrate greatly improved the thermal uniformity across the substrate during growth. Just before loading into the EE chamber, the metallized substrates were re-rinsed in methanol, de-ionized water, and strain-free mounted on a hollow molybdenum block which was loaded on a trolley. A stream of dry nitrogen was used to remove particles from the substrate surfaces and the trolley. The trolley was then introduced into the EE chamber which was then pumped down.

In-situ Substrate Preparation

All substrates were preheated at 150° C for one hour in the EE chamber and at 450° C for 20 minutes in the buffer chamber to desorb impurities such as water vapor on the substrates and substrate holders. Before carrying out the preheating procedures in both the EE and the buffer chambers, it was important to make sure that the background pressure in both chambers was lower than 10^{-8} Torr. After transfer to the growth chamber, the substrate was heated slowly (~30 °C/min.) to 750° C; this temperature was held for 60 minutes for thermal cleaning. All substrate temperatures quoted in this dissertation are the actual sapphire surface temperatures calibrated using the OTIL method described in the previous chapter. The RHEED system was used to monitor the surface morphology and crystallinity through the thermal cleaning and nitridation processes. The thermal cleaning resulted in a (1 x 1) RHEED pattern with Kikuchi lines indicating a clean Al_2O_3 (0001) surface. A 9 keV electron beam was oriented along (a) [1 $\bar{1}$ 0 0] (ϕ=0°) and (b) [1 $\bar{2}$ 1 0] (ϕ=30°) as shown in Fig. 3.2 (a,b). Then, the thermally cleaned substrate was exposed to the nitrogen free-radical beam (at a forward power of 250 W) while at the same temperature (750° C) for 20 minutes to form a thin AlN layer whose RHEED pattern is shown in Fig. 3.3.

Conventional MBE Growth of GaN on Sapphire

With both Ga and N shutters closed, the substrate temperature was lowered to 500° C at which temperature a thin GaN buffer layer was deposited. A Ga effusion cell temperature of 780° C was used to provide a low Ga flux (J= 7.6 x 10^{13} cm $^{-2}$ s^{-1}) in order to grow the buffer layer. Growth was initiated by simultaneously opening both Ga and N shutters for 10 minutes to grow a ~300 Å thick GaN buffer layer. An elongated spotty RHEED pattern was observed during the growth of this layer. The basal plane of the GaN overlayer was rotated 30° with respect to that of the substrate during growth; the

orientation relationship between the single crystal GaN film and the substrate was [0001] GaN // [0001] Al_2O_3, [$1\bar{1}00$] GaN //[$1\bar{2}10$] Al_2O_3, and [$2\bar{1}\bar{1}0$] GaN // [$\bar{1}100$] Al_2O_3. Immediately following buffer-layer deposition, the substrate temperature was ramped to 750 °C, 700 °C, 640 °C or 600 °C in 5 minutes, during which time both source shutters were kept closed. A streaky RHEED pattern developed during the ramp in each case. Also during the ramp, the Ga cell temperature was increased to 820° C to provide a flux of J = 2.3×10^{14} cm^{-2} s^{-1}. When the appropriate substrate temperature was reached, both the Ga and N shutters were opened simultaneously, producing a growth rate of 0.1-0.2 μm/hr depending on the growth temperature. The growth parameters employed are summarized in Table 3-2. The surface morphology during growth was very sensitive to the Ga/N beam flux ratio as well as the growth temperature. For a fixed N flux (1×10^{-5} Torr), the RHEED pattern changed from streaky to spotty at 750° C when the Ga beam equivalent pressure (BEP) was lower than 5×10^{-8} Torr (J=1.8×10^{14} $cm^{-2}s^{-1}$). However, the same Ga flux resulted in a milky surface at 600° C. Hence, a lower Ga BEP of 2×10^{-8} Torr (J=7.6×10^{13} $cm^{-2}s^{-1}$) was used for conventional growth at 600° C, and 6×10^{-8} Torr (J=2.3×10^{14} $cm^{-2}s^{-1}$) was used for growth temperatures of 640° C , 700° C and 750° C. A streaky (1x1) RHEED pattern, as shown in Fig. 3.4, was maintained throughout growth for all conventionally-grown samples. In order to provide a uniform thermal distribution, the CAR was rotated at a speed of 1 rpm for all conventional growths. The total growth time in each case was 4 hours and about 0.8 μm of GaN was deposited. For the sample grown at 600° C, a 0.4 μm thick film was deposited since Ga droplets prevented it from growing thicker, as suggested in references 28 and 29. In each case, growth was terminated by simultaneously closing both shutters and cooling the sample to room temperature in 20 minutes in a nitrogen environment. The thermal expansion coefficient of sapphire is about 26-34% [34% in the case of $c_{\perp}$ (GaN) // $c_{//}$ (sapphire) and 26 % in the case of $c_{\perp}$ (GaN) // $c_{\perp}$ (sapphire)] larger than that of GaN. Therefore,

the epitaxial GaN film suffered compressive stress in the plane parallel to the c-face when the sample was cooled, hence a slow cooling rate was necessary.

Table 3.2 Growth parameters used for both conventionally-grown and AEEE-grown films.

Nitrogen source parameters	
RF forward power	200 W
Nitrogen beam flux	1×10^{-5} Torr
Plasma emission intensity	80 ~ 100 mV
Ga source condition	
Ga beam flux for epilayer growth	6.0×10^{-8} Torr ($J=2.3 \times 10^{14}$ $cm^{-2}s^{-1}$)
Ga beam flux for buffer layer growth	2×10^{-8} Torr ($J=7.6 \times 10^{13}$ $cm^{-2}s^{-1}$)
Growth parameters	
Buffer layer	
Growth temperature	500 °C
Buffer layer growth time	10 min.
Conventionally-grown epilayer	
Growth temperature	600° C, 640 °C, 700 °C, 750° C.
Growth rate	0.1 - 0.2 μm/hr
Film thickness	0.4 and 0.8 μm

Characterization of Conventionally-Grown GaN Films

SEM Analysis

The surface morphology of MBE grown samples was examined by SEM. The surface morphology of the sample grown at 750° C showed a typical micrometer range rough surface as shown in Fig. 3.5. The surface morphology of the sample grown at

600° C was smoother in most areas, however, ~15 μm diameter Ga droplets were distributed over the surface with a density around, 6 x 10^4 cm^{-2}, as shown in Fig. 3.6. The sample grown at 640° C had a similar surface morphology, however, the Ga droplet size was smaller (< 5 μm) in this case. In order to observe what was under the Ga droplets, samples were etched in (1:10:100) HF : NHO_3: H_2O before re-performing SEM. It was found that crack-like voids were observable beneath the Ga droplets as shown in Fig. 3.7.

Hall-Effect Measurement and Photoluminescence Analysis

The Van der Pauw method was employed to measure carrier concentrations and mobilities at room temperature using Hall-effect analysis. Small pieces of indium were pressed in place at the four corners of square-shaped samples to make ohmic contact (the I-V characteristic was linear) to the GaN. All of the unintentionally doped GaN films showed 10^{18} cm^{-3} n-type carrier concentrations except the sample grown at 600° C which had a 3 x 10^{19} cm^{-3} carrier concentration. The carrier mobility was 35 cm^2 V^{-1} s^{-1} for the sample grown at 640° C and was in the single digit range for those samples grown at 600° C and 700° C.

In the PL analysis, the samples were excited by the 325 nm wavelength output of a 25 mW HeCd laser. The power density at the sample was about 30 $mWmm^{-2}$. The luminescence signal was dispersed by a 0.3 m single-grating monochromator and detected by a photomultiplier tube. Room-temperature and low-temperature PL spectra were recorded from the samples grown at 700, 640, and 600 ° C and these spectra are presented in Fig. 3.8-3.13. As can be seen from these figures, the yellow band emission was observed in all of the spectra in addition to the near-band-edge emission.

A detailed discussion on luminescence peak assignments (both near-band-edge and deep level emission) is presented in Chapter 5 based on the results detailed in this chapter and also Chapter 4.

(a) rms roughness = 2.458 nm

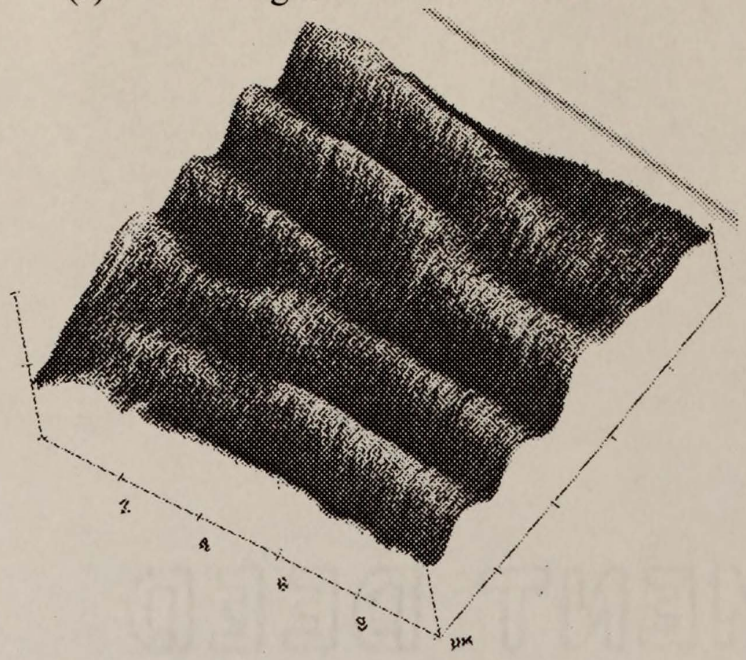

(b) rms roughness = 0.398 nm

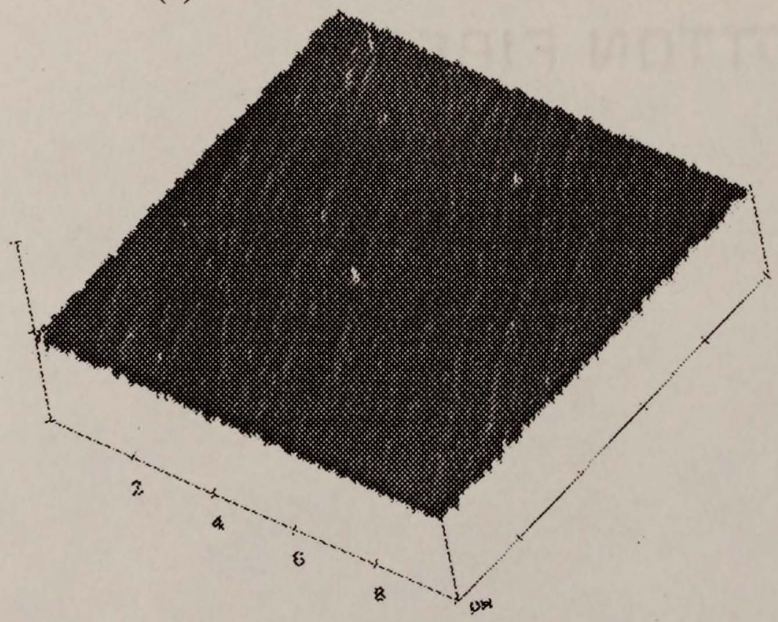

Figure 3.1 Atomic force microscopy tapping mode images showing the morphology of c-plane sapphire
(a) as-received, rms roughness = 2.458 nm
(b) etched in $H_2 SO_4 : H_3PO_4$ at 160° C for 15 minutes, rms roughness = 0.398 nm.

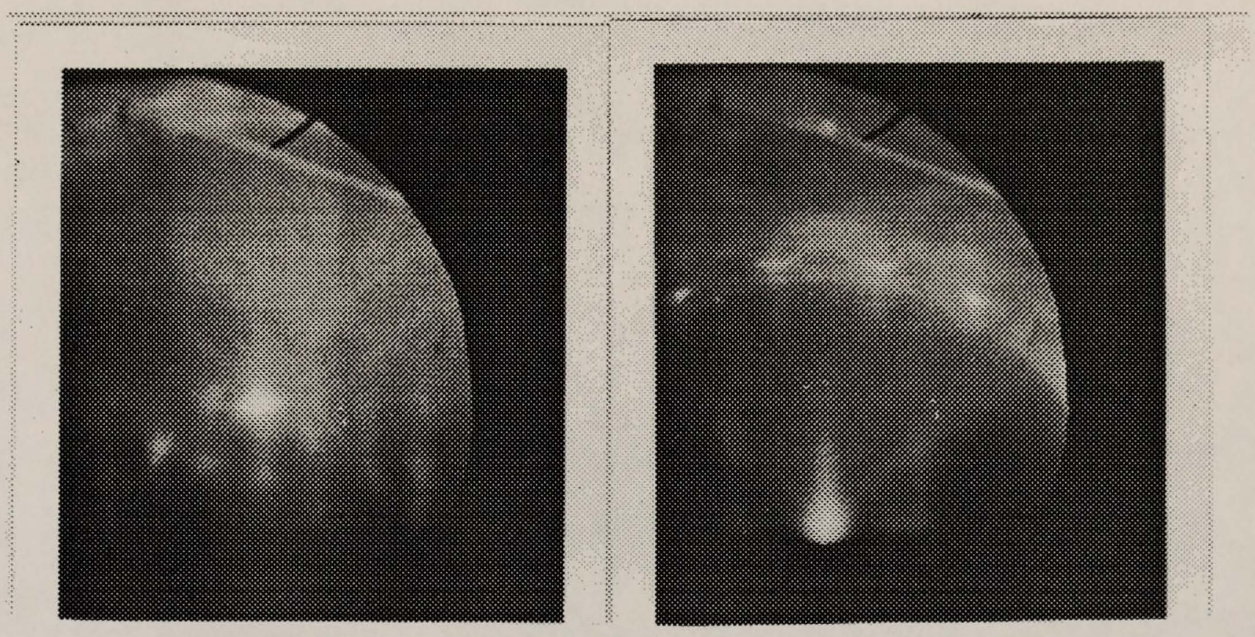

(b) (a)

Figure 3.2 RHEED patterns recorded from thermally cleaned sapphire (0001) surface, (a) electron beam oriented along [1$\bar{1}$00] (ϕ = 0 °), (b) [1$\bar{2}$10] (ϕ = 30 °)

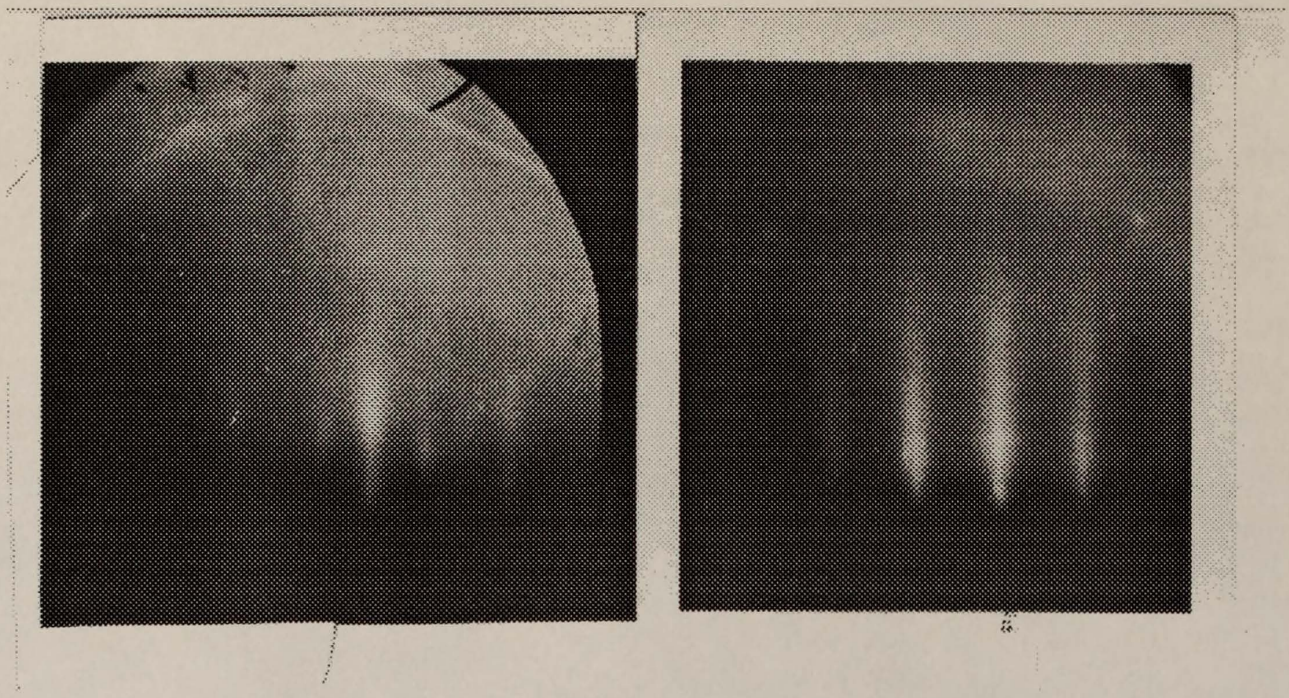

(b) (a)

Figure 3.3 RHEED pattern recorded from a thin AlN layer formed during nitridation at 750° C after 20 minutes exposure to the N-flux (a) [$2\bar{1}\bar{1}0$] AlN // [$1\bar{1}00$] sapphire, (b) [$1\bar{1}00$] // [$1\bar{2}10$] sapphire.

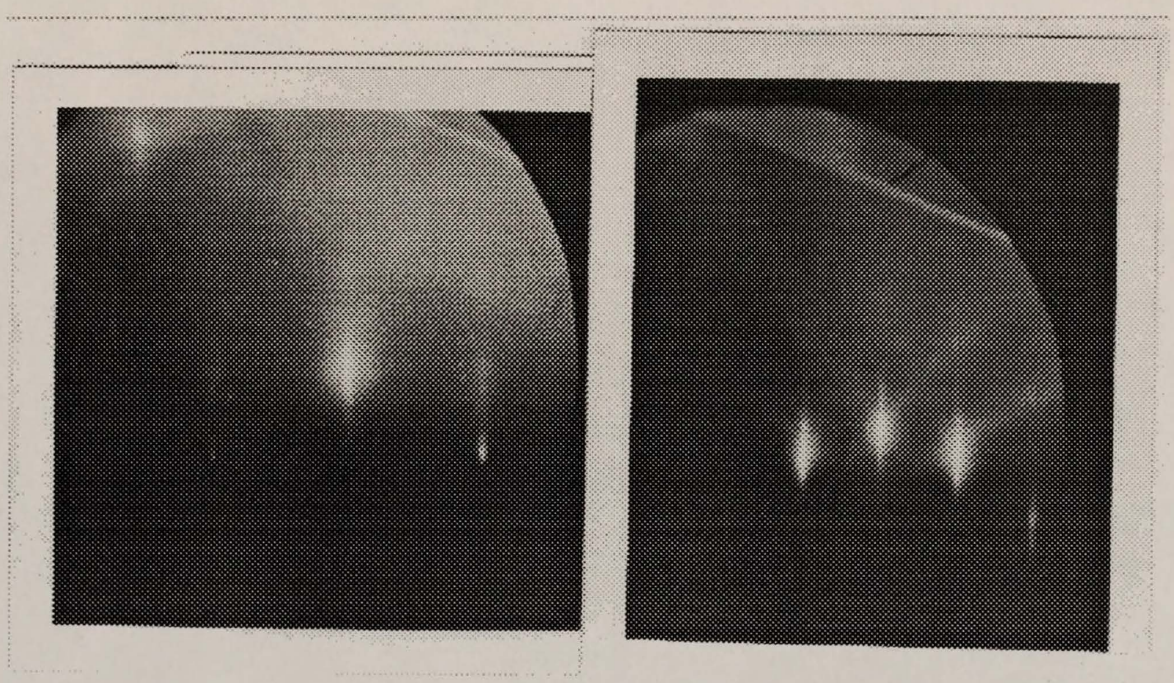

(b) (a)

Figure 3.4 RHEED patterns recorded from a conventionally grown GaN film, (a) [$2\bar{1}\bar{1}0$] GaN // [$2\bar{1}\bar{1}0$]AlN // [$1\bar{1}00$] sapphire, (b) [$1\bar{1}00$] GaN // [$1\bar{1}00$] AlN // [$1\bar{2}10$] sapphire.

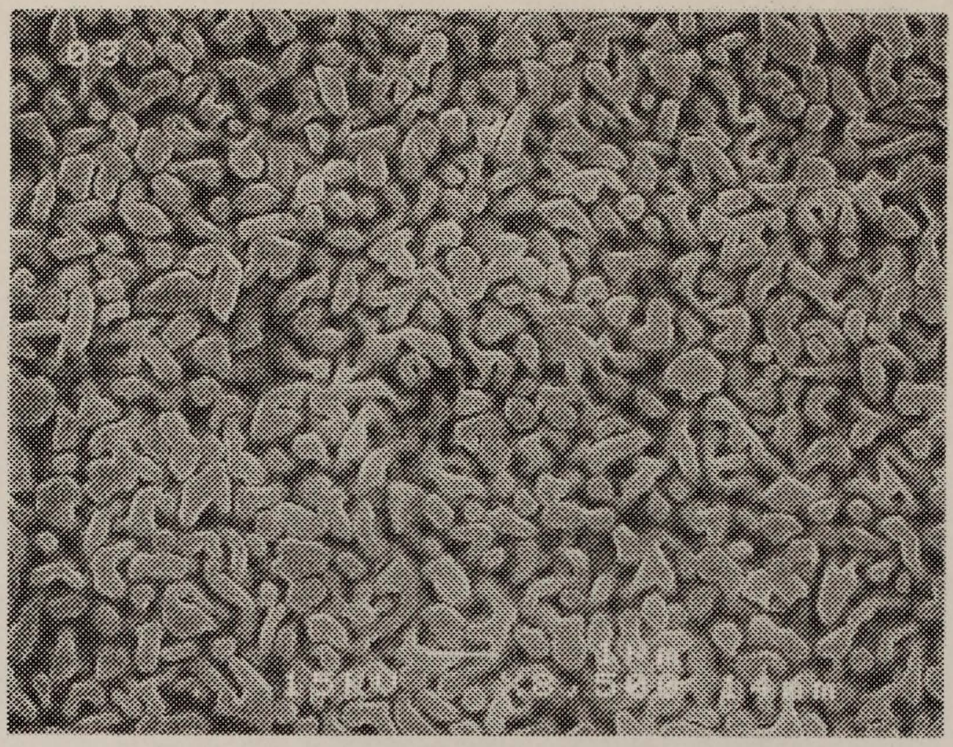

Figure 3.5 SEM micrograph showing the surface morphology of a GaN film grown by conventional MBE at 750° C.

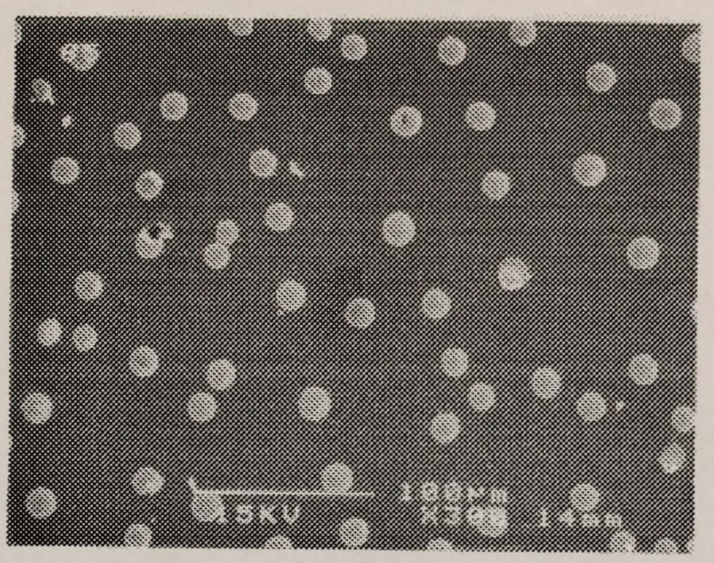

(a)

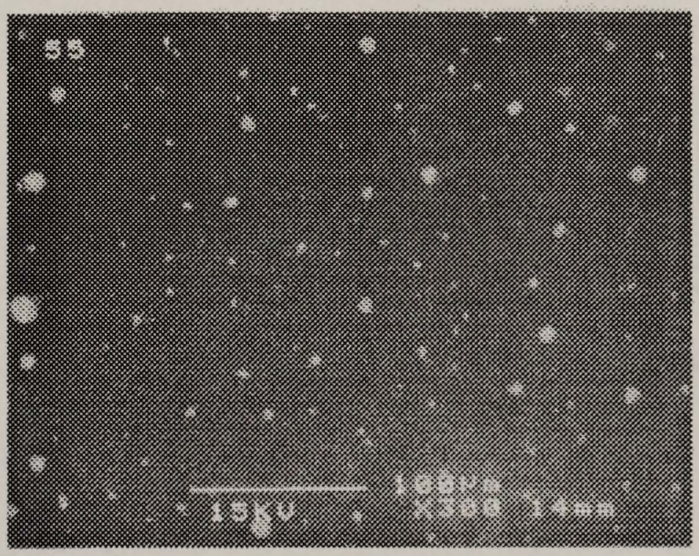

(b)

Figure 3.6 SEM micrographs of the surfaces of GaN films grown by MBE at a substrate temperature of 600° C (a), and 640° C (b). Note the presence of Ga droplets.

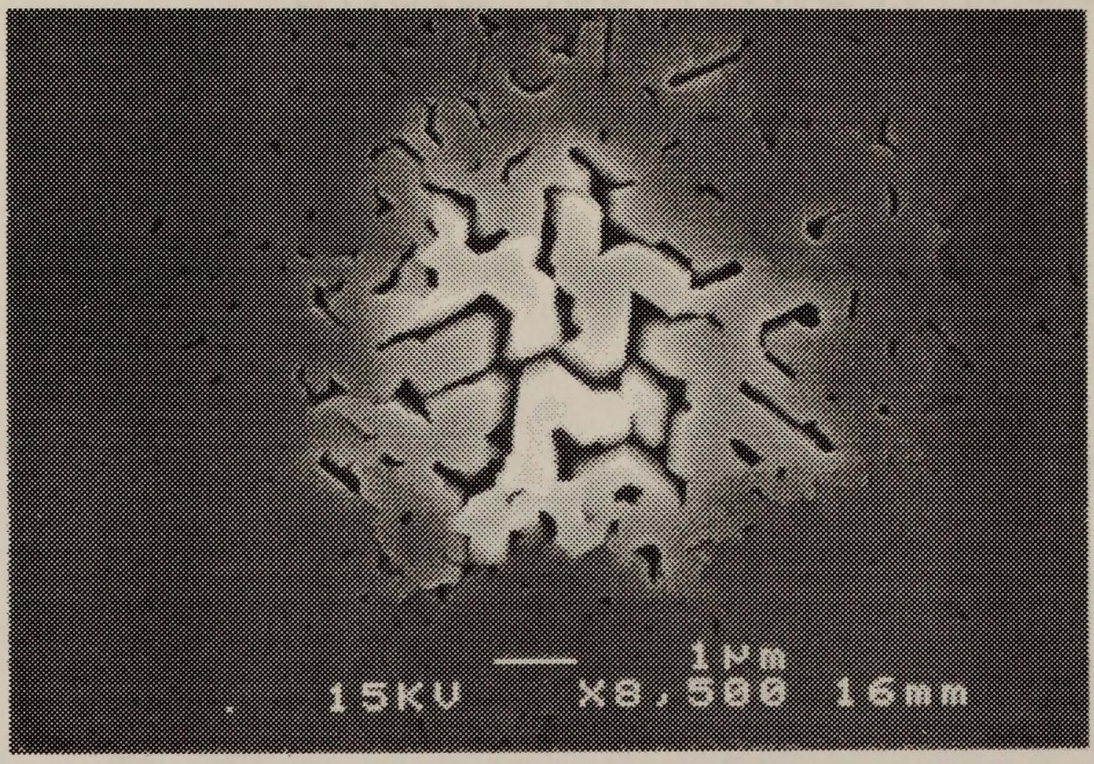

Figure 3.7 SEM micrograph showing the GaN morphology beneath a Ga droplet after removal of the Ga droplet by wet etching. The GaN was grown at 600° C.

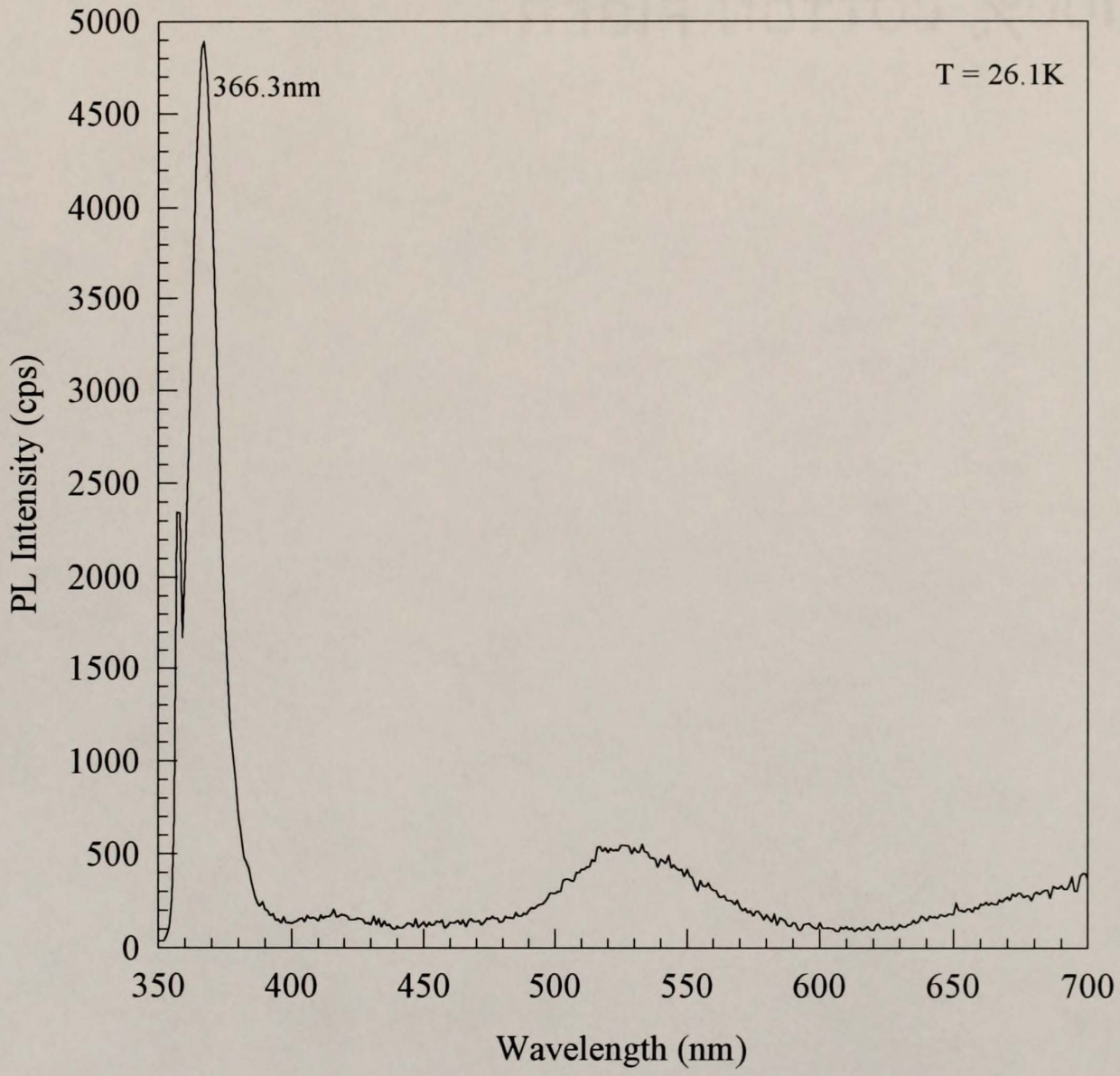

Figure 3.8 Low-emperature PL spectrum recorded from a GaN/sapphire film grown at 700 ° C by conventional MBE.

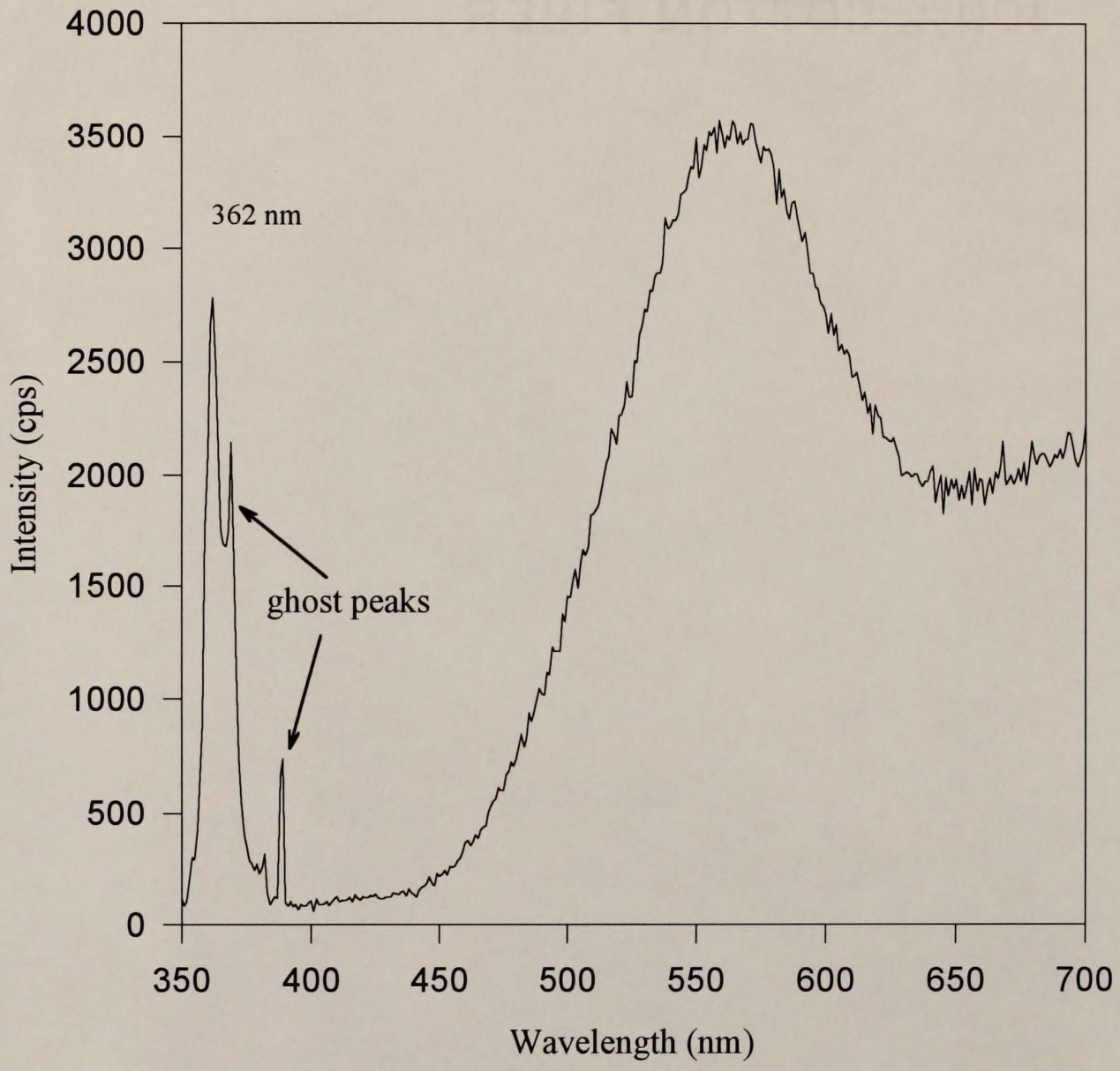

Figure 3.9 Room-temperature PL spectrum recorded from a GaN/sapphire film grown at 700° C by conventional MBE.

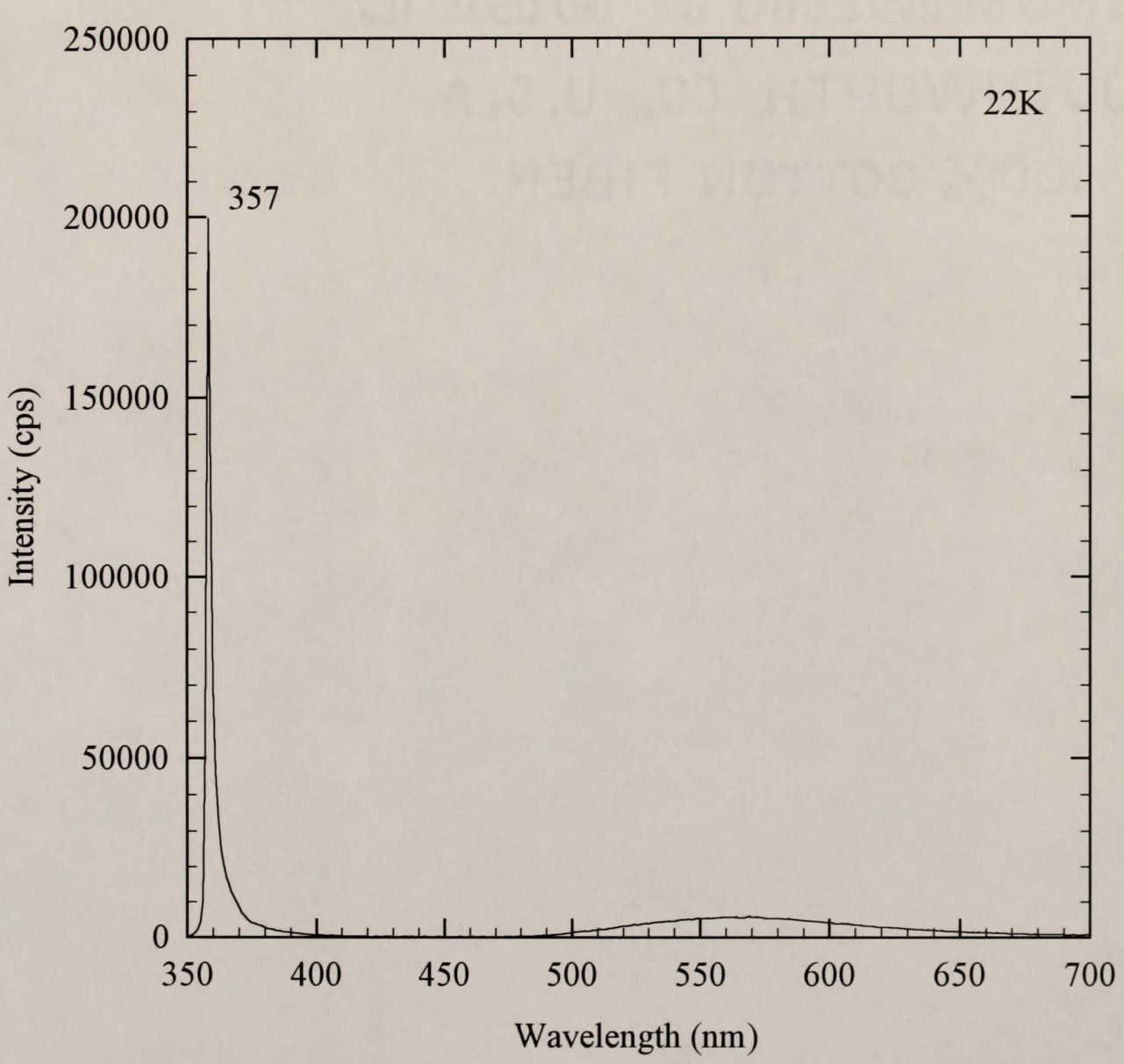

Figure 3.10 Low-temperature PL spectrum recorded from a GaN/sapphire film grown at 640° C by conventional MBE

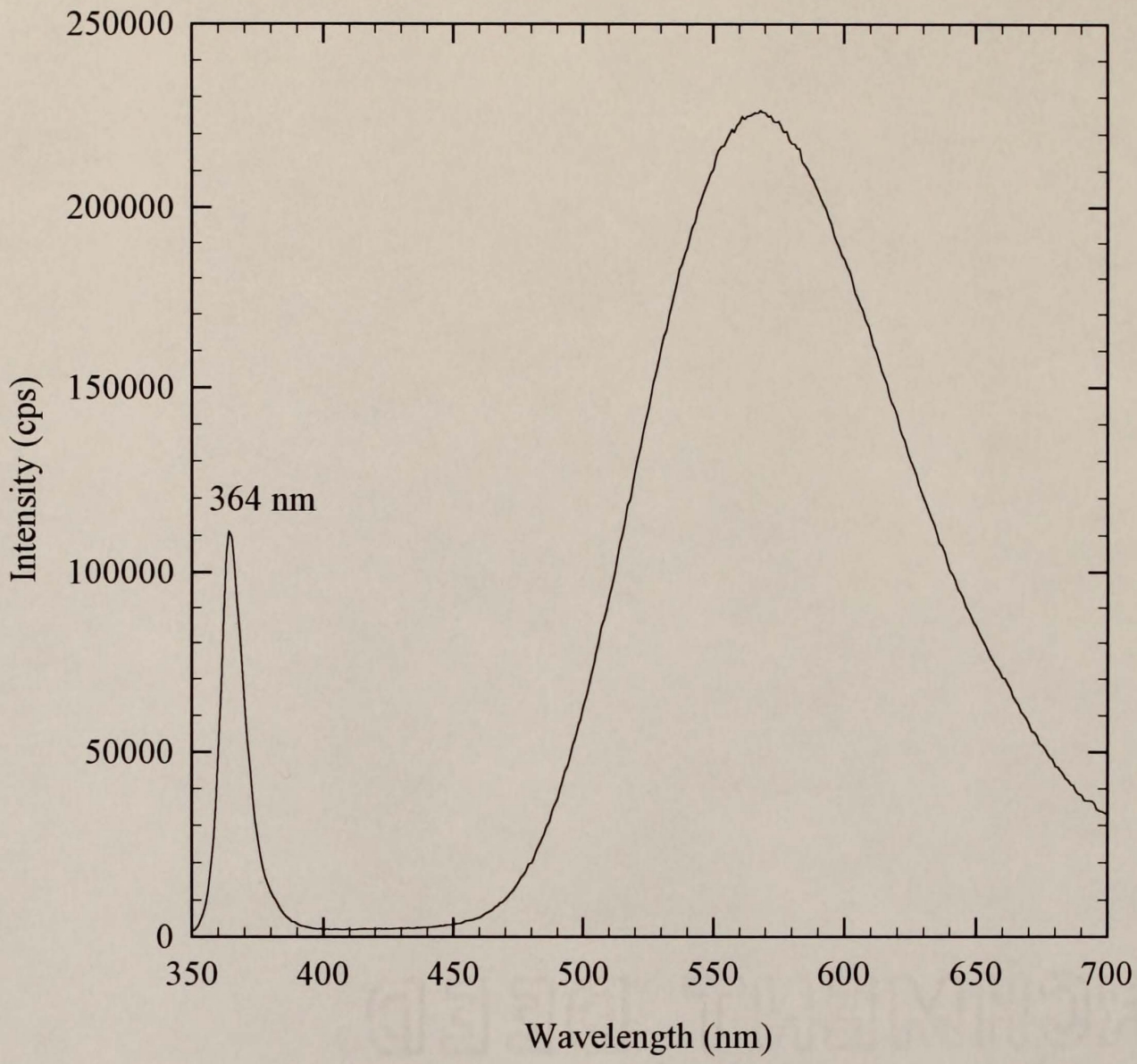

Figure 3.11 Room-temperature PL spectrum recorded from a GaN/ sapphire film grown at 640° C by conventional MBE.

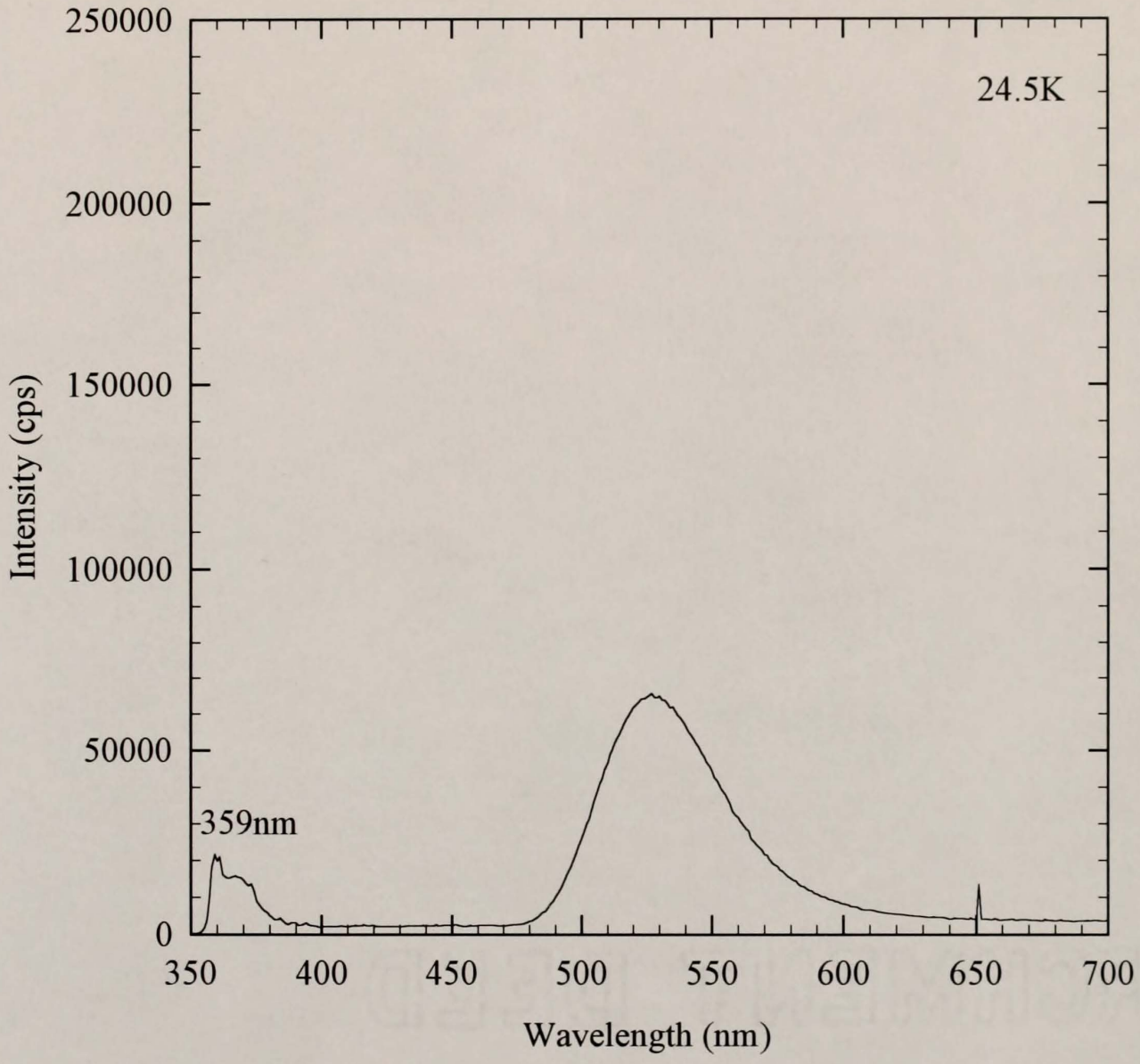

Figure 3.12 Low-temperature PL spectrum recorded from a GaN/sapphire film grown by conventional MBE at 600° C.

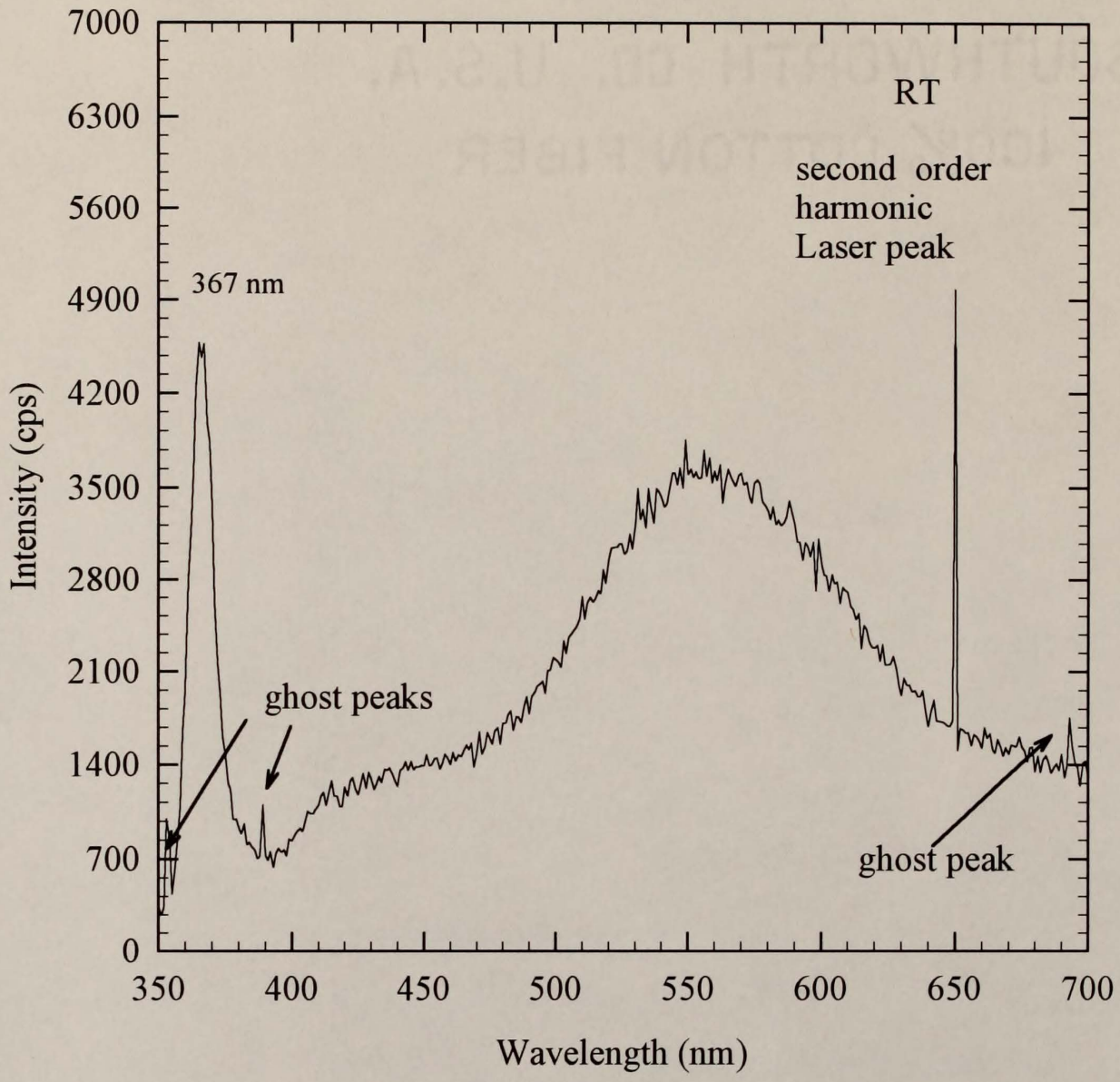

Figure 3.13 Room-temperature PL spectrum recorded from a GaN/sapphire film grown by conventional MBE at 600° C.

CHAPTER 4
INVESTIGATION OF A NOVEL GROWTH MODE

Introduction

The PL spectra recorded from all of the conventionally grown GaN/sapphire films showed near band-edge emission at around 365 nm and a yellow band emission centered around 550 nm. Decreasing the growth temperature improved the efficiency of the near band-edge emission but the deep-level defect-related yellow band emission was still present. Furthermore, decreasing the growth temperature resulted in the formation of Ga droplets on the growing surface and the yellow band emission became dominant in the PL spectra. This yellow band emission has been commonly reported in the literature regardless of the growth techniques and the substrates used [2-14]. With a view to investigating the factors that lead to deep level generation and consequently to the yellow band emission in the PL spectra recorded from GaN epitaxial films, a systematic study was conducted in which the surface morphology was examined by means of the real-time monitoring of the RHEED specular reflection beam intensity during critical phases of growth. In particular, a new growth mode was studied in which the substrate was separately exposure to Ga atoms and N atoms (as in migration enhanced epitaxy [MEE]) and, in addition, time delays were introduced following the Ga and N exposures which we term the Ga delay and the N delay, respectively. The time delays, in which a variety of kinetic processes might take place depending upon the element in question, distinguish this growth mode from MEE and we have termed the novel growth mode "alternate element exposure epitaxy (AEEE)". This work was carried out as follows; first, a systematic study was conducted to determine the optimum AEEE growth temperature, second, a

systematic search was made for an optimum N delay time at the optimum growth temperature, and, finally, a systematic investigation was conducted to find the optimum Ga delay time, also at the optimum growth temperature.

AEEE Growth Procedures

The *ex-vacuo* and *in-situ* substrate preparations were the same as those used for the preparation of conventionally-grown samples as mentioned in the previous chapter. After nitridation of the sapphire substrate at 750° C, the substrate temperature was lowered to 500 ° C, both Ga and N shutters being closed. A 300 Å thick buffer layer was deposited at this temperature by opening the Ga and N shutters simultaneously for 10 minutes. During growth of the buffer, the Ga effusion cell temperature was kept at 780° C, corresponding to a low Ga flux of $J = 7.6 \times 10^{13}$ cm^{-2} s^{-1}. After the buffer layer was deposited, the substrate temperature was increased to 600 °C with both shutters being closed. During the same substrate temperature ramping period, the Ga effusion cell temperature was gradually increased to 820 ° C, corresponding to a Ga flux of $J = 2.3 \times 10^{14}$ cm^{-2} s^{-1}.

AEEE Growth Temperature Optimization

In order to determine the optimum substrate temperature for AEEE growth, the same growth temperatures used in conventional growth were investigated here. Each growth cycle included opening the N shutter for 10 sec., simultaneously closing the N and opening the Ga shutter (Ga exposure time, 5 - 8 sec., depending on the growth temperature), closing the Ga shutter and allowing the RHEED specular reflection beam intensity to recovery to a maximum before opening the N shutter again (Ga delay time, 15 - 30 sec., depending on growth temperature). The delay time is defined as being the time elapsed between closing one shutter and opening the other shutter as indicated in Fig. 2.4 (page

28). The growth conditions for one cycle of the shutter sequence are summarized in Table 4.1. The recovery of the RHEED specular reflection beam intensity during the Ga delay was found to be a function of the growth temperature. At higher temperatures the beam intensity recovered faster but to a lower level of intensity as shown in Fig. 4.1. Films were not deposited at 750° C by AEEE because the RHEED pattern did not remain streaky and the specular reflection beam intensity decreased quickly after repeated cycles. The specular reflection beam intensity was also found to be a function of the Ga exposure time. For instance, an 8 sec. Ga exposure time was optimum to have the RHEED intensity recover to a maximum when the substrate temperature was 700° C, whereas, 7 sec and 5 sec were the optimum Ga exposure times for substrate temperatures of 640° C and 600° C, respectively. Failure to control the optimum Ga exposure time results in a loss of RHEED signal intensity following several cycles. Each of the AEEE samples was grown using a total of 2000 cycles. The growth was terminated by the last N exposure and the substrate was cooled to room temperature in 20 minutes under a N_2 overpressure in the growth chamber with both Ga and N shutters closed.

Table 4.1 AEEE growth conditions for one cycle of the shutter sequence at different growth temperatures.

Growth temperature (sample #)	N shutter open (sec.)	N delay time (sec.)	Ga shutter open (sec.)	Ga delay time (sec.)	Remark
700° C (7147)	10	0	8	15	Maximum RHEED intensity-low
640° C (7155)	10	0	7	20	Maximum RHEED intensity-moderate
600° C (7165)	10	0	5	30	Maximum RHEED intensity-high

PL Analysis

Low-temperature PL spectra were recorded from the samples grown at 700° C, 640° C, and 600° C and the spectra are presented in Figs. 4.2, 4.3, and 4.4, respectively. These spectra all indicate a dominant near band-edge emission, but a low intensity yellow band emission is still exhibited in samples grown at 700° C and 640° C. In addition, a weak peak related to N vacancies [20,37] appeared at 365.5 nm for the sample grown at 700° C and at 385 nm for the sample grown at 640° C, respectively. On the other hand, as can be seen from Fig. 4.4, the yellow band emission was absent from the PL spectrum recorded from the sample grown at 600° C.

Nitrogen Delay Time Optimization.

The basic advantages of the AEEE technique in the context of GaN are the low growth temperature and the provision of a chemically active Ga-covered surface. Both of these factors can greatly enhance the sticking coefficient of N during GaN epitaxy. In this investigation, the shutter operating sequence was the same as for the sample grown at 600° C in the previous section except that N delay times, namely, 0 sec., 15 sec., and 30 sec., were inserted between closing the N shutter and opening the Ga shutter as shown from Fig. 4.5. As can be seen from Fig. 4.5, the RHEED specular reflection beam intensity recovered only moderately during the N delay phase.

Shutter sequences employed for the N delay experiments are shown in Table 4.2. It is worth pointing out that during the N shutter open time, the RHEED specular reflection beam intensity decreased initially and then recovered moderately to a turning point beyond which the intensity again dropped (see Fig 4.5) and the RHEED pattern became spotty. The turning point occurred after an exposure time of 10 seconds and thus a 10 sec. N exposure was employed in this work.

Table 4.2 Shutter sequences for the N-delay optimization experiments.
(Growth temperature was 600° C)

Run Number	N shutter open (sec.)	N delay time (sec.)	Ga shutter open (sec.)	Ga delay time (sec.)	Remark
7160	10	0	5	30	Maximum RHEED intensity-high
7167	10	15	5	30	Maximum RHEED intensity-moderate
7156	10	30	5	30	Maximum RHEED intensity-moderate

PL Analysis

The low-temperature PL spectra recorded from samples grown using N delays of 0 sec, 15 sec. and 30 sec. are shown in Figs. 4.6, 4.7, and 4.8. As can be seen from these spectra, as the N delay time is increased, the near band-edge emission intensity decreases and additional peaks appear in the spectra. Consequently, in future growth runs a 0 sec. N delay was employed.

Ga-delay Time Optimization

In the Ga-delay optimization set of experiments, the N-delay was fixed at 0 sec. based on our previous experience and the previously determined optimum substrate temperature of 600° C was used throughout. As indicated in Fig. 4.9, various Ga-delay times were employed including 0 sec, 15 sec, 30 sec. and 50 sec. As seen in the figure, these delay

times corresponded to various RHEED specular reflection beam intensities. Shutter sequences employed in the Ga-delay experiments are summarized in Table 4.3.

Table 4.3 Shutter sequences for the Ga-delay optimization experiments. (Growth temperature was 600° C)

Run Number	N shutter open (sec.)	N delay time (sec.)	Ga shutter open (sec.)	Ga delay time (sec.)	Remark
7161	10	0	5	0	
7164	10	0	5	15	
7160	10	0	5	30	Highest maximum RHEED intensity
7168	10	0	5	50	

SEM and PL Analyses

SEM analysis was performed on samples grown with Ga delay times of 0 sec., 15 sec, 30 sec, and 50 sec. No Ga droplets were found on the surfaces of these samples as can be seen from Figs. 4.10 (a)-(d).

Low- and room-temperature PL spectra recorded from the 0 sec, 15 sec, 30 sec, 50 sec. Ga delay time samples are presented in Figs. 4.11- 4.18. The influence of the Ga delay time on the PL properties will be discussed in detail in Chapter 5.

Activation Energy of Ga Migration Under N-free Conditions

As illustrated in Fig. 4.19, the RHEED specular reflection beam intensity recovers upon closing the Ga shutter (during the Ga-delay phase) in two distinct stages. In stage 1, the recovery is fast and the RHEED intensity varies almost linearly with time. However, beyond stage 1, the recovery appears to be more sluggish in stage 2 in which the

relationship is distinctly non-linear. By assuming monatomic steps with terraces and edges on the growing surface [62-66], it is believed that the fast stage (stage 1) of the RHEED specular reflection beam intensity recovery is dominated by Ga adatom migration to step sites [44,45, 67-71]. With a view to determining the activation energy for the process, the time to complete stage 1 recovery was measured as a function of growth temperature and the migration times recorded in the range, 560° C to 640° C, are presented in Table 4.4. The data displays an Arrhenius behavior as shown in Fig 4.20. This is the same approach as that used by Foxon and Joyce [48] who determined the activation energy of As_4 migration on a GaAs surface in the absence of a Ga flux. The activation energy of Ga migration under N-free conditions was determined from Fig. 4.20 to be 1.46 ± 0.25 eV

Impact of Impinging RHEED Beam on Ga Migration

It is essential to understand the role, if any, that the impinging RHEED electron beam has on the kinetic behavior of Ga adatoms. In order to investigate this possibility, the electron gun shutter was opened continuously in the first instance during an operating cycle and the RHEED specular reflection beam intensity was recorded as shown in Fig. 4.21 (solid line). Immediately following this cycle, the chart recorder was rewound back to the start position of the previous cycle and this time the RHEED intensity was sampled by only opening the RHEED gun shutter for 1 sec. every 5 secs. In this case, the trace recorded is shown in Fig 4.21 as a dashed line. As can be seen from the figure, the sampled intensities correspond to those recorded during continuous electron beam exposure and, therefore, it is assumed that Ga migration, for instance, was not electron beam assisted.

Table 4.4 Ga migration times estimated from the RHEED intensity curves at various substrate temperatures.

Migration time (sec.)	Substrate temperature (° C)
35 ~ 40	560
25 ~30	580
13 ~17	600
10 ~13	620
6 ~9	640

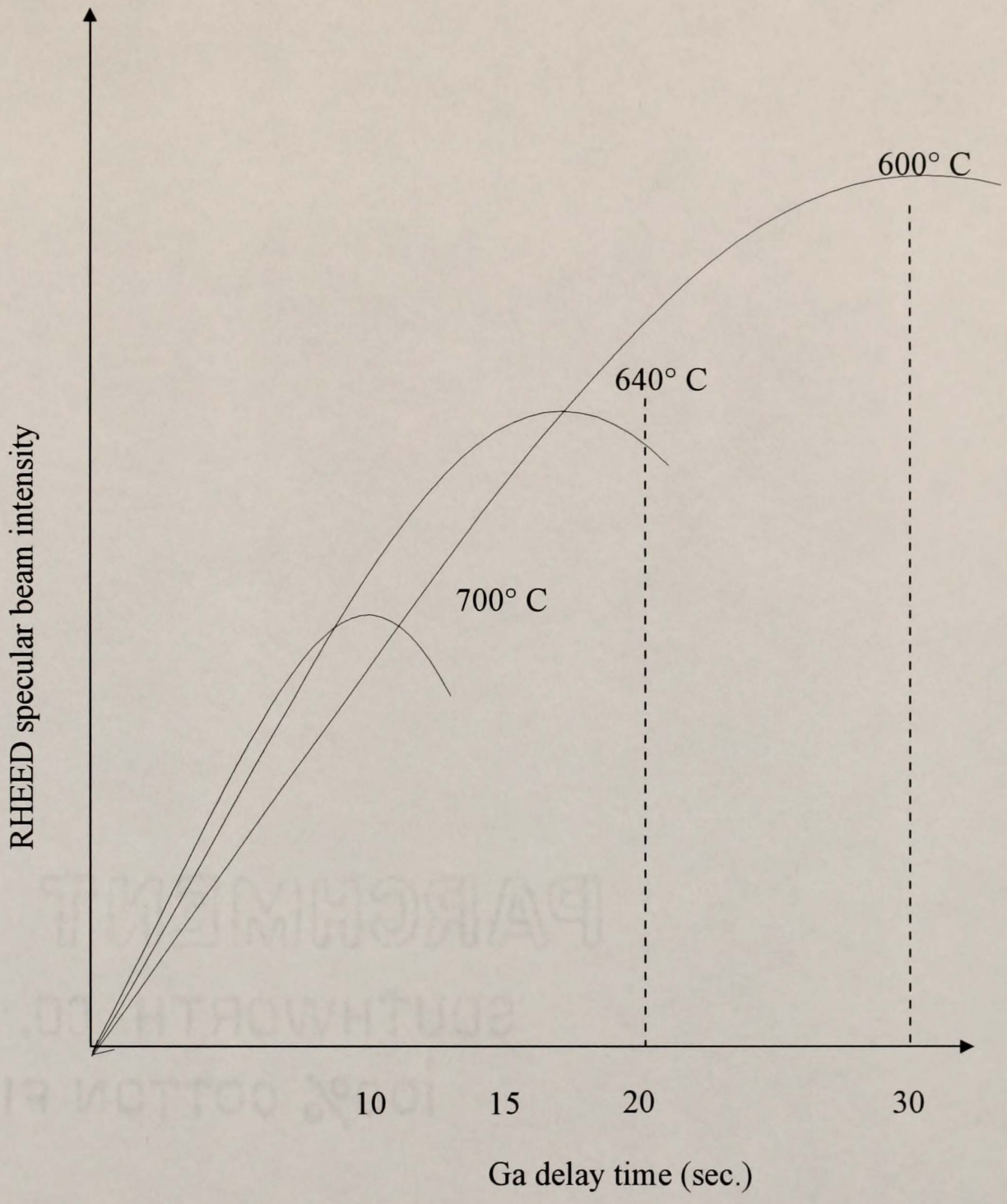

Figure 4.1 RHEED specular reflection beam intensity as a function of Ga delay time (time allowed to elapse between closing the Ga and opening the N shutter) recorded at different substrate temperatures.

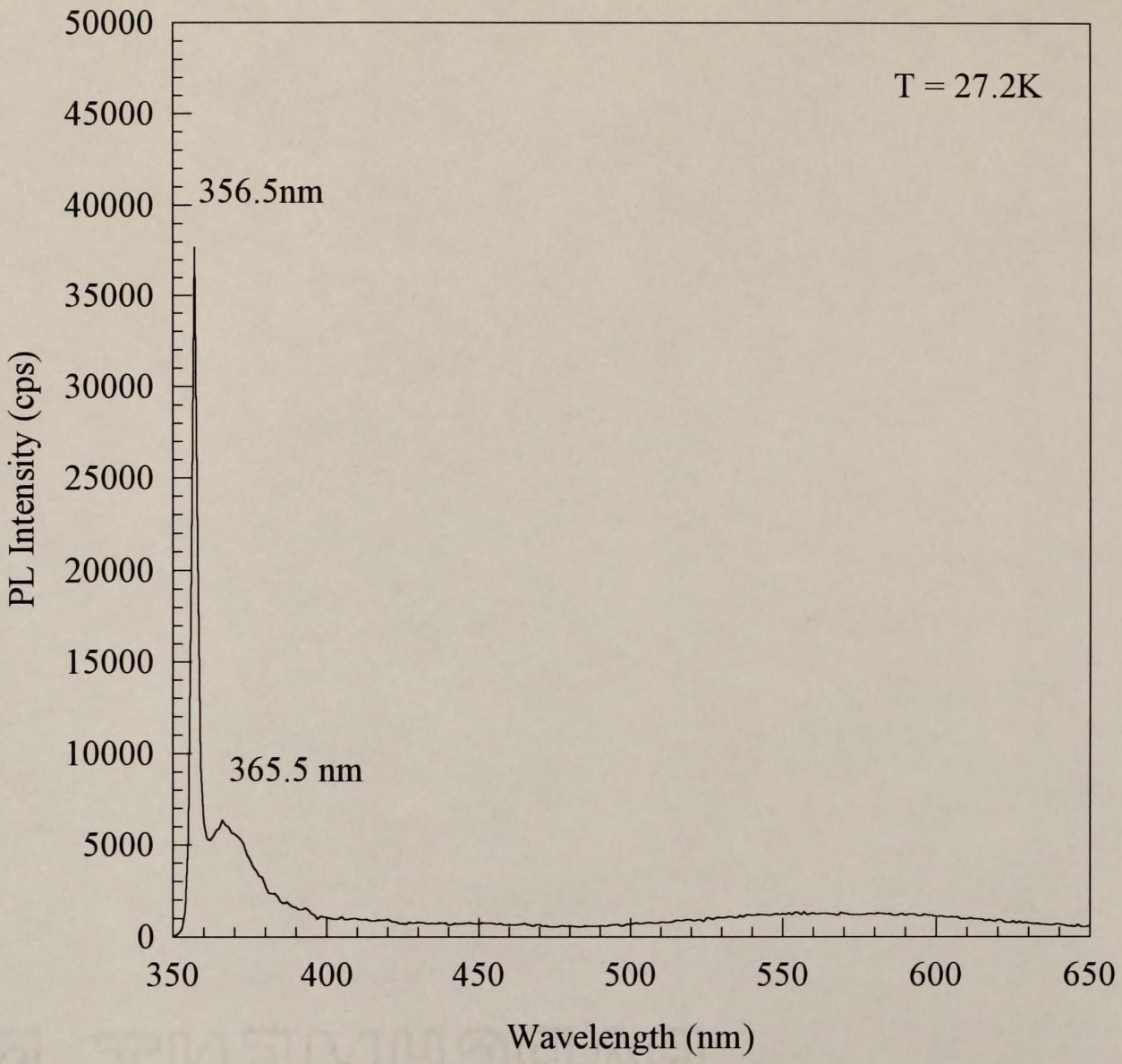

Figure 4.2 Low-temperature PL spectrum recorded from a GaN/sapphire film grown by the AEEE technique at 700° C.

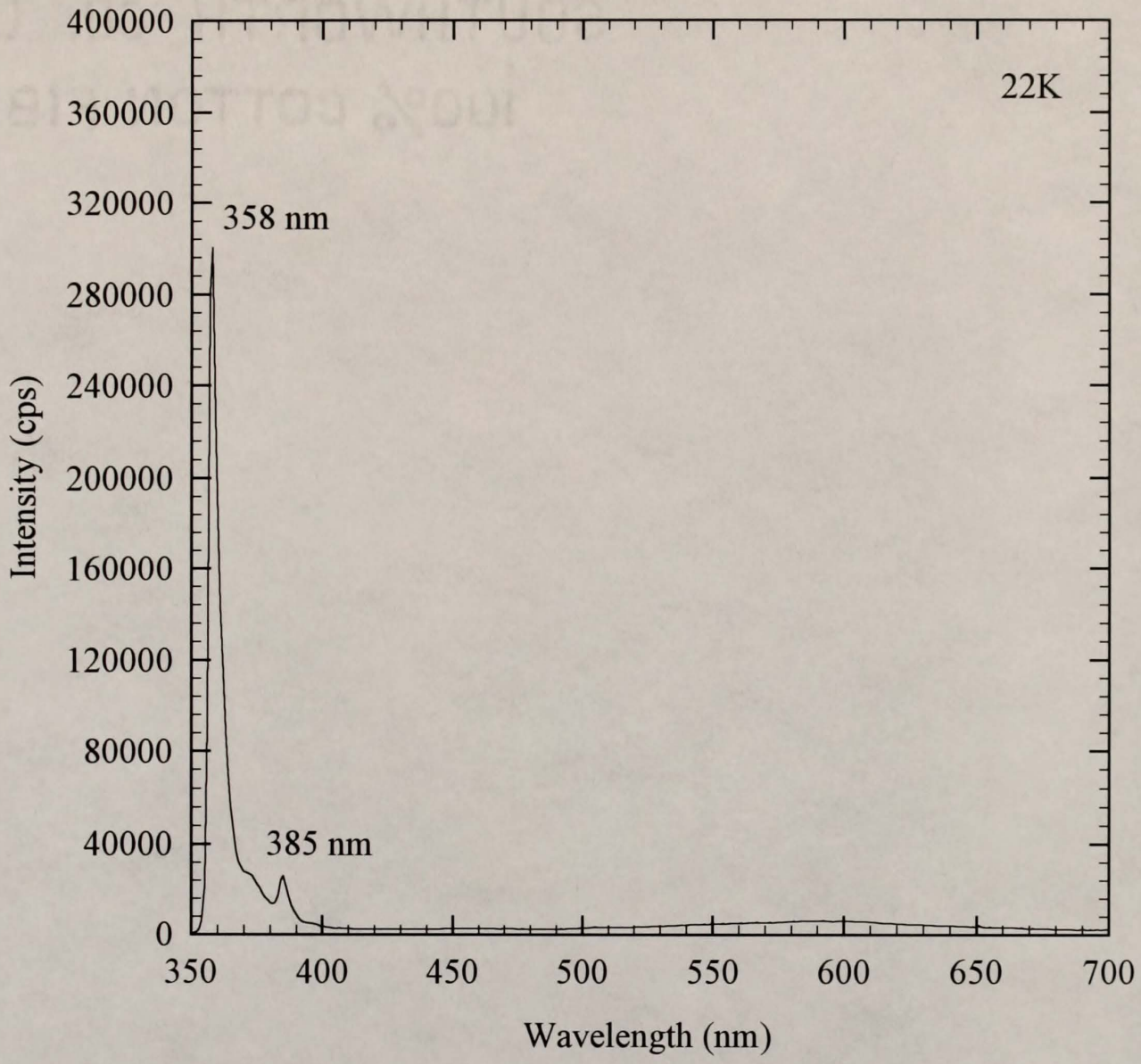

Figure 4.3 Low-temperature PL spectrum recorded from a GaN / sapphire film grown by the AEEE technique at 640° C.

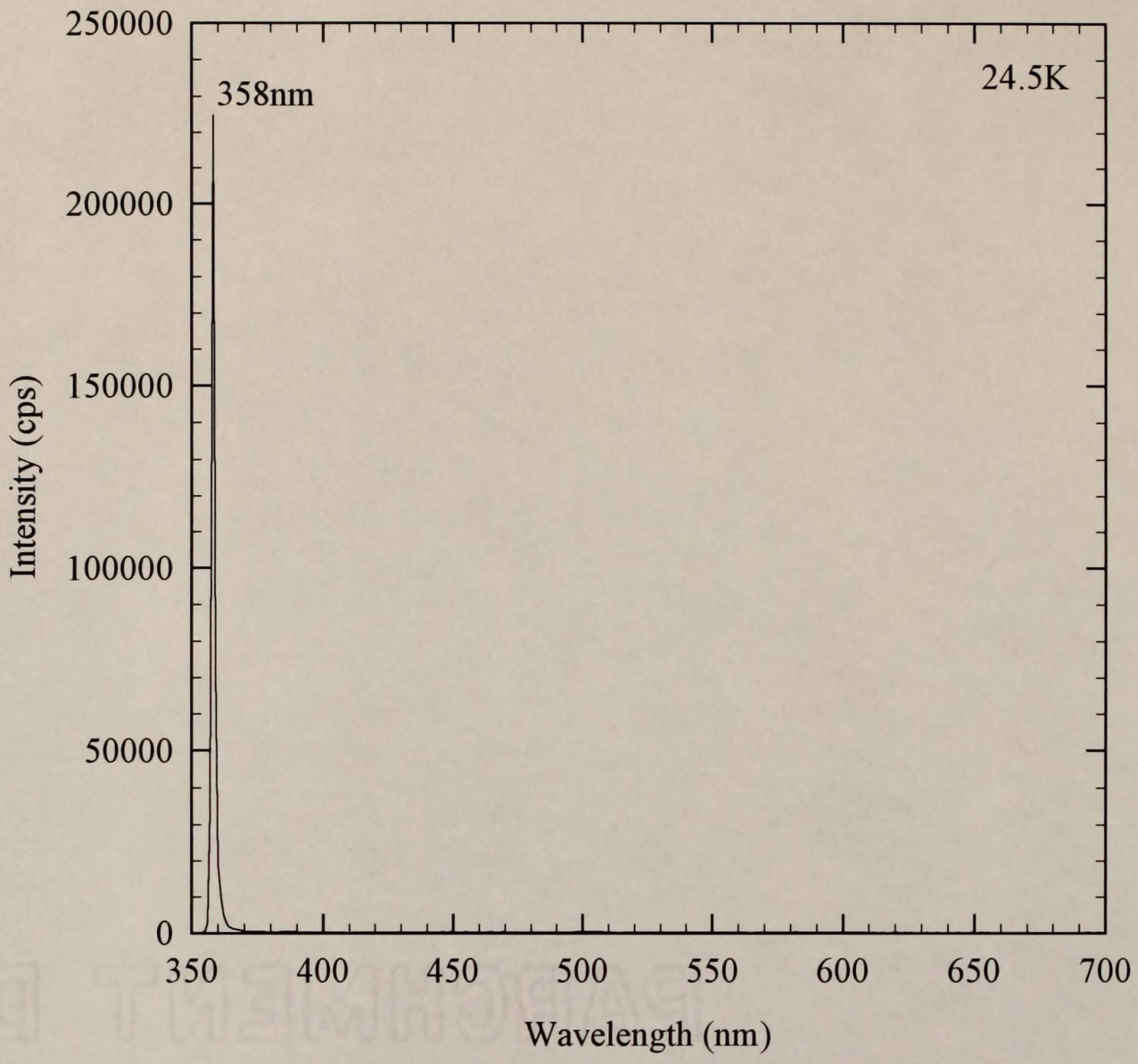

Figure 4.4 Low-temperature PL spectrum recorded from a GaN / sapphire film grown by the AEEE technique at 600° C.

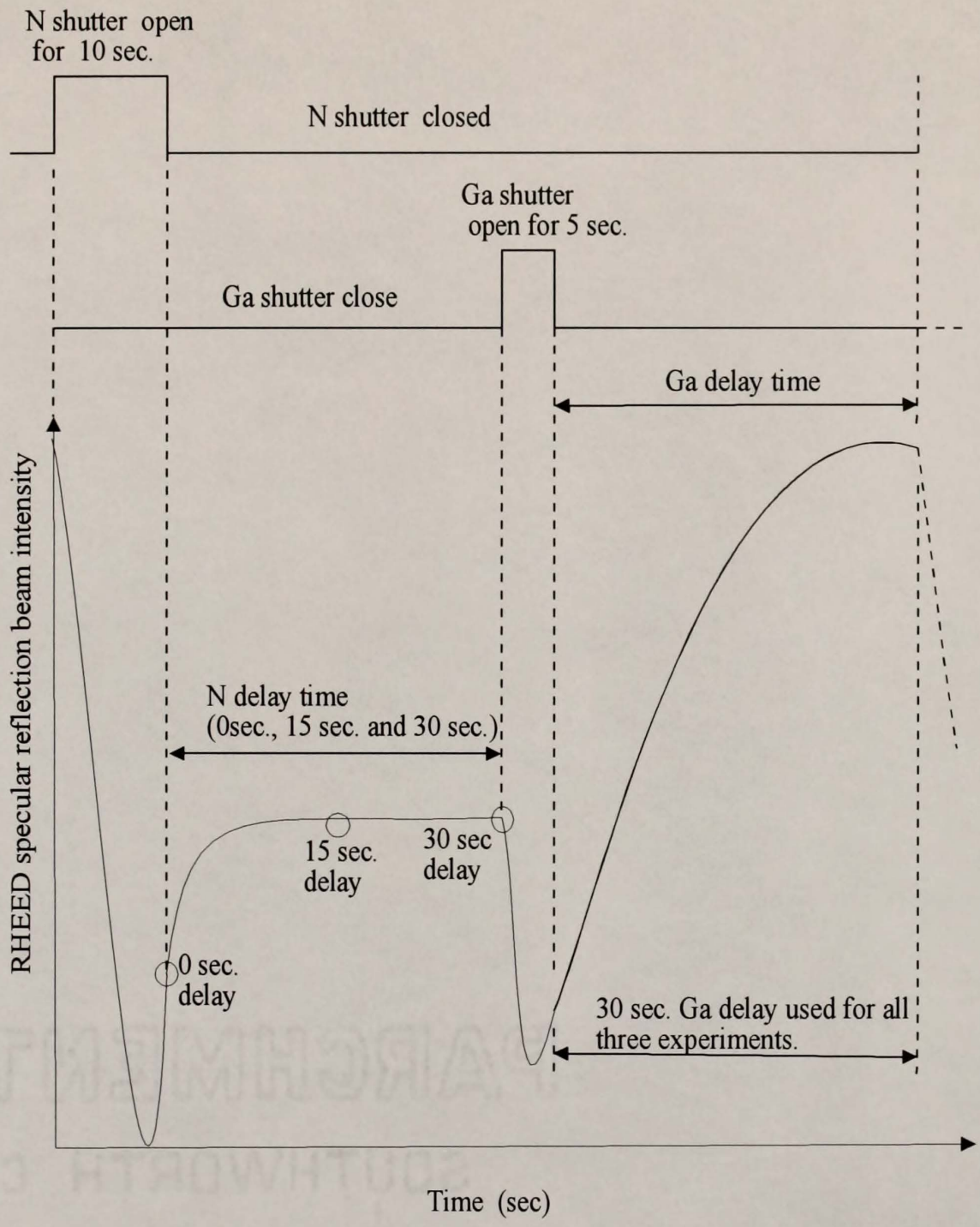

Figure 4.5 RHEED specular reflection beam intensity recorded as a function of time during a cycle of AEEE growth. The circles represent the beam intensities at the three N delay times used in the N delay optimization set of experiments. Growth temperature was 600° C.

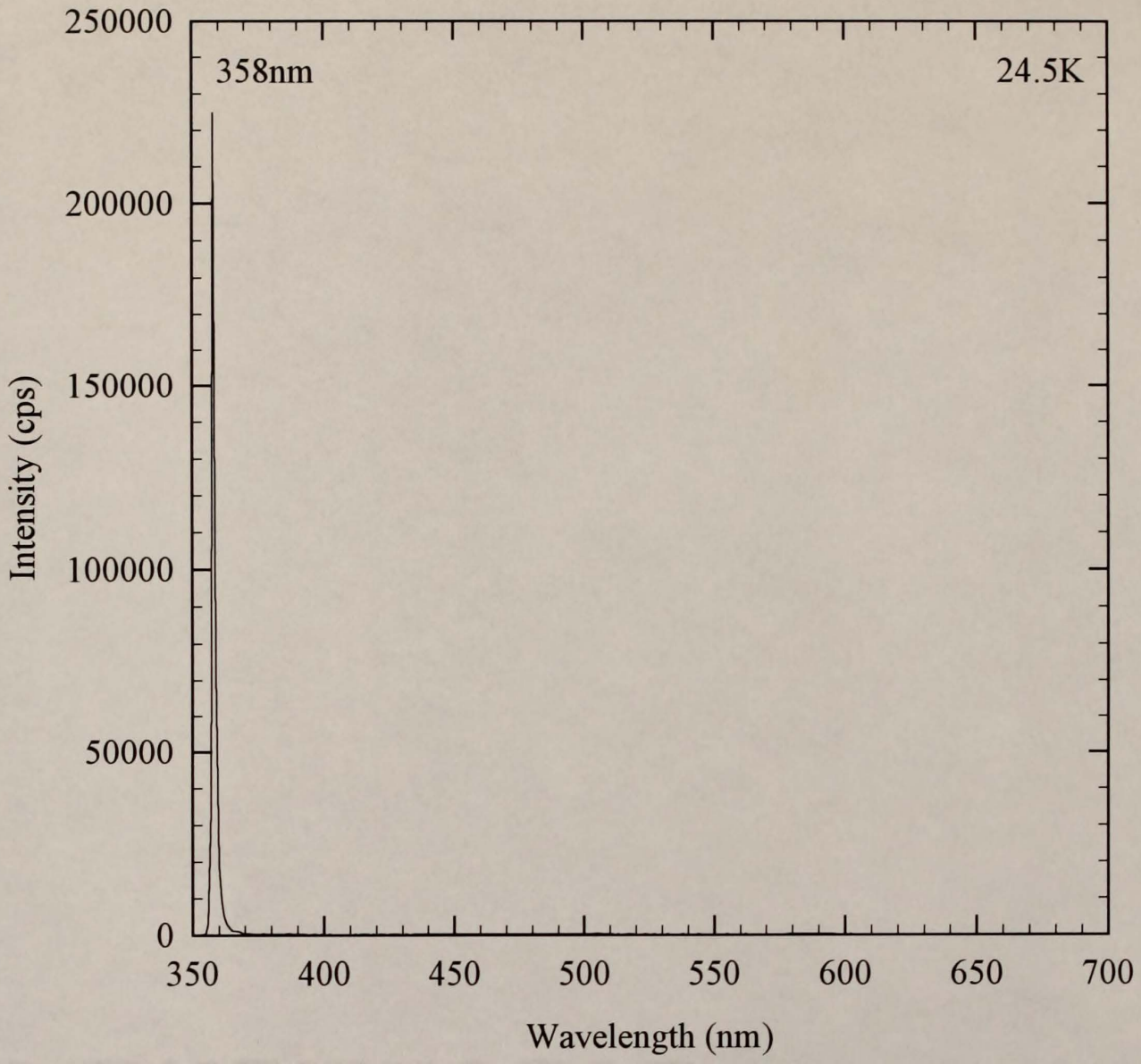

Figure 4.6 Low-temperature PL spectrum recorded from a GaN / sapphire film grown by the AEEE technique with a 0 sec. N delay at 600° C.

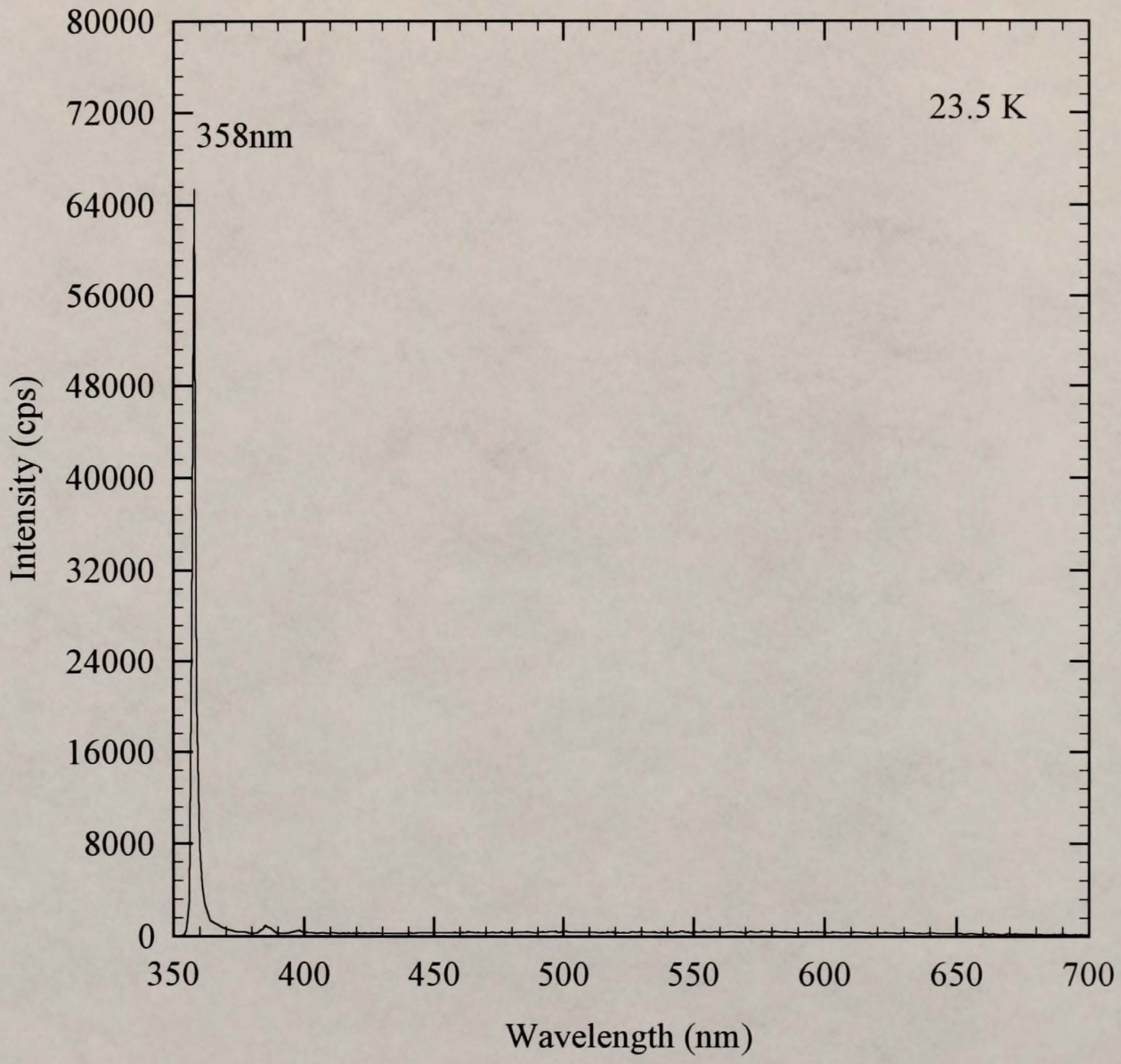

Figure 4.7 Low-temperature PL spectrum recorded from a GaN / sapphire film grown by the AEEE technique with a 15 sec. N delay time at 600° C.

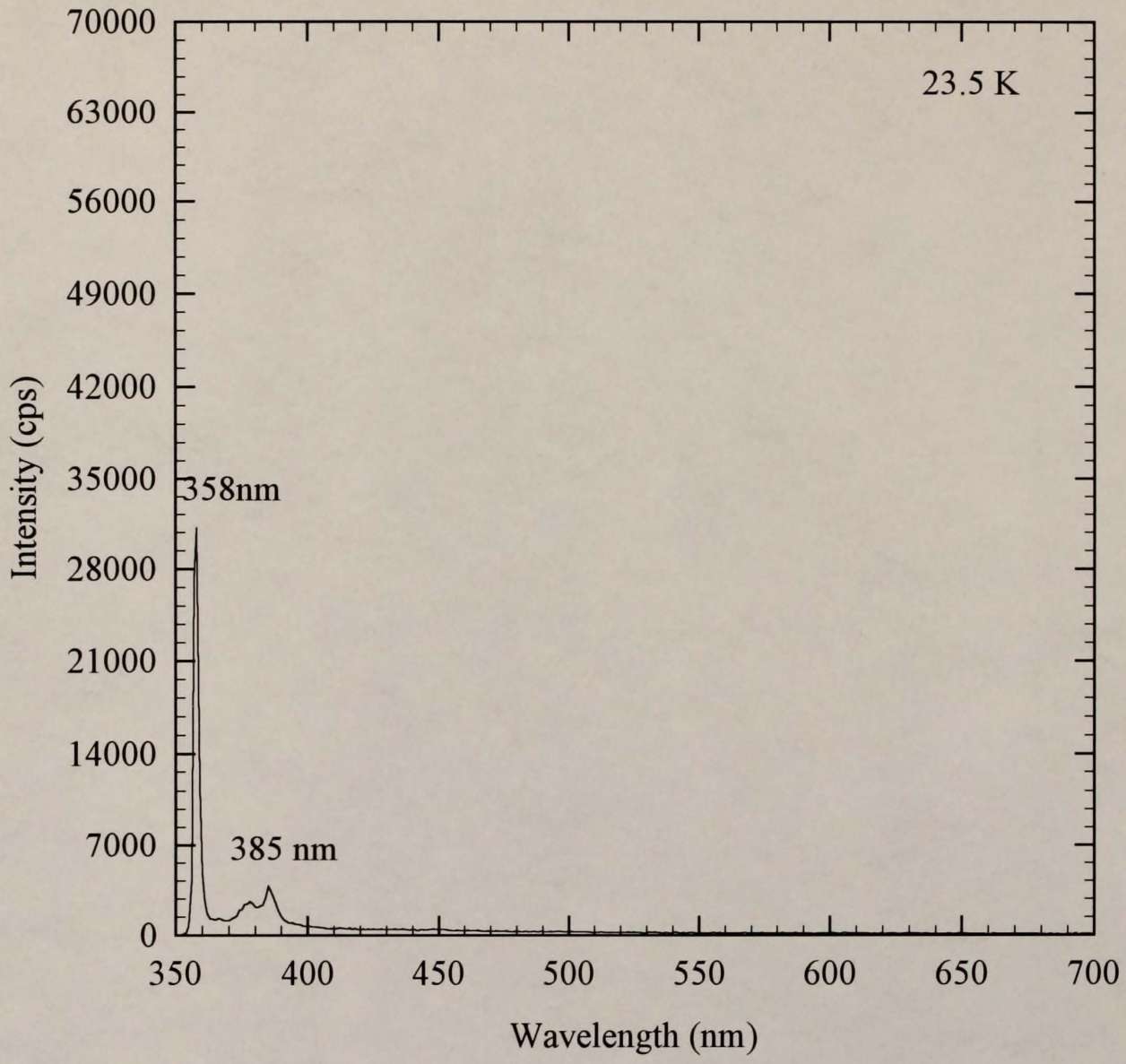

Figure 4.8 Low-temperature PL spectrum recorded from a GaN / sapphire film grown by the AEEE technique with 30 sec N delay time at 600° C

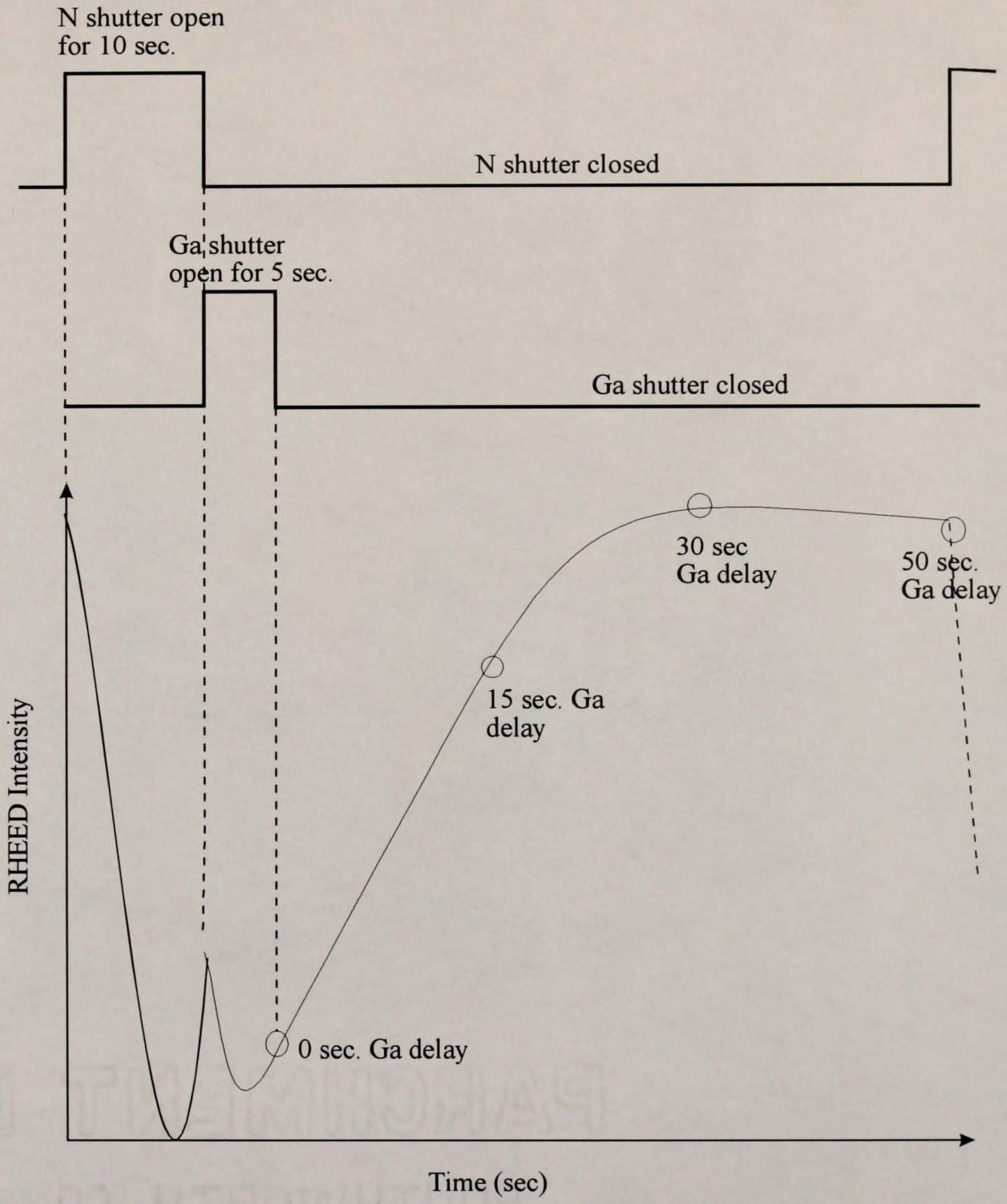

Figure 4.9 RHEED specular reflection beam intensity recorded as a function of time during a cycle of AEEE for the 0 sec. N delay case. The circles represent the beam intensities at the four Ga delay times used in the Ga delay optimization set of experiments. Growth temperature was 600° C.

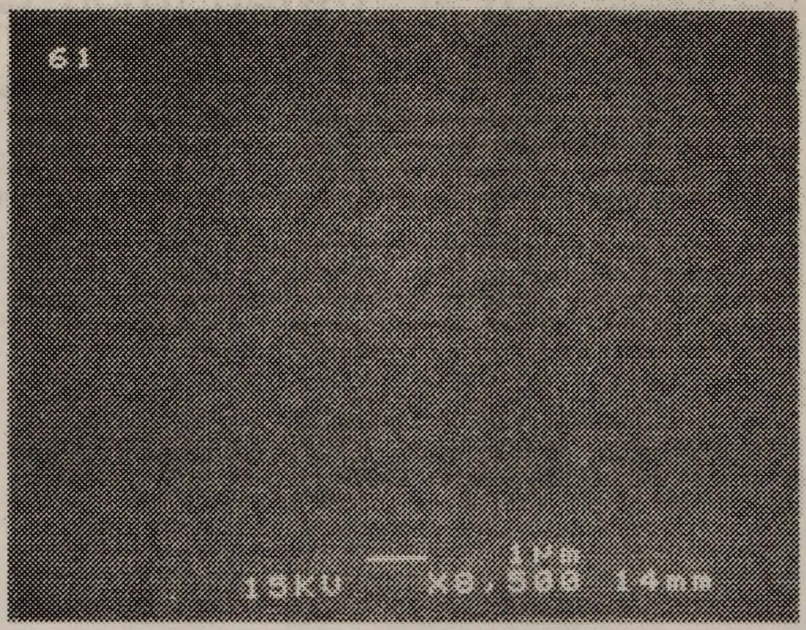

(a)

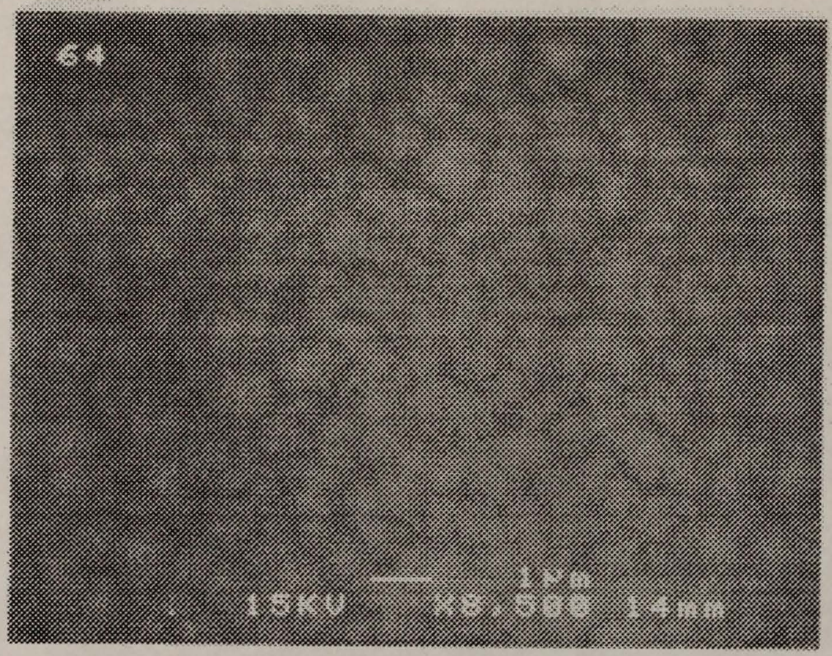

(b)

Figure 4.10 SEM micrographs of GaN film surfaces grown by the AEEE technique using various Ga-delay times ($T_{substrate}$ = 600° C) (a) Ga delay time = 0 sec. (b) Ga delay time = 15 sec.

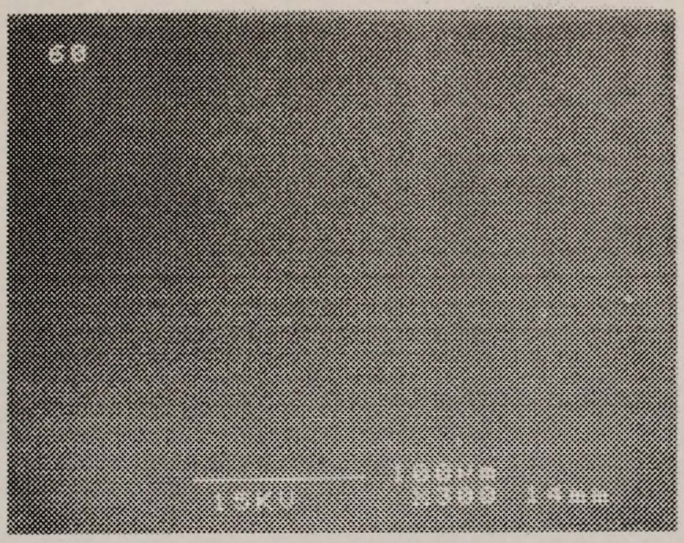

(c)

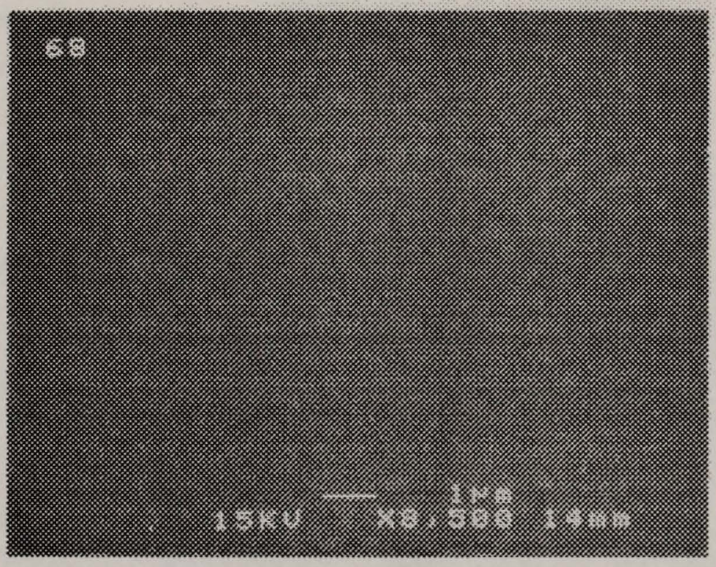

(d)

Figure 4.10 Continued.
(c) Ga delay time = 30 sec.
(d) Ga delay time = 50 sec.

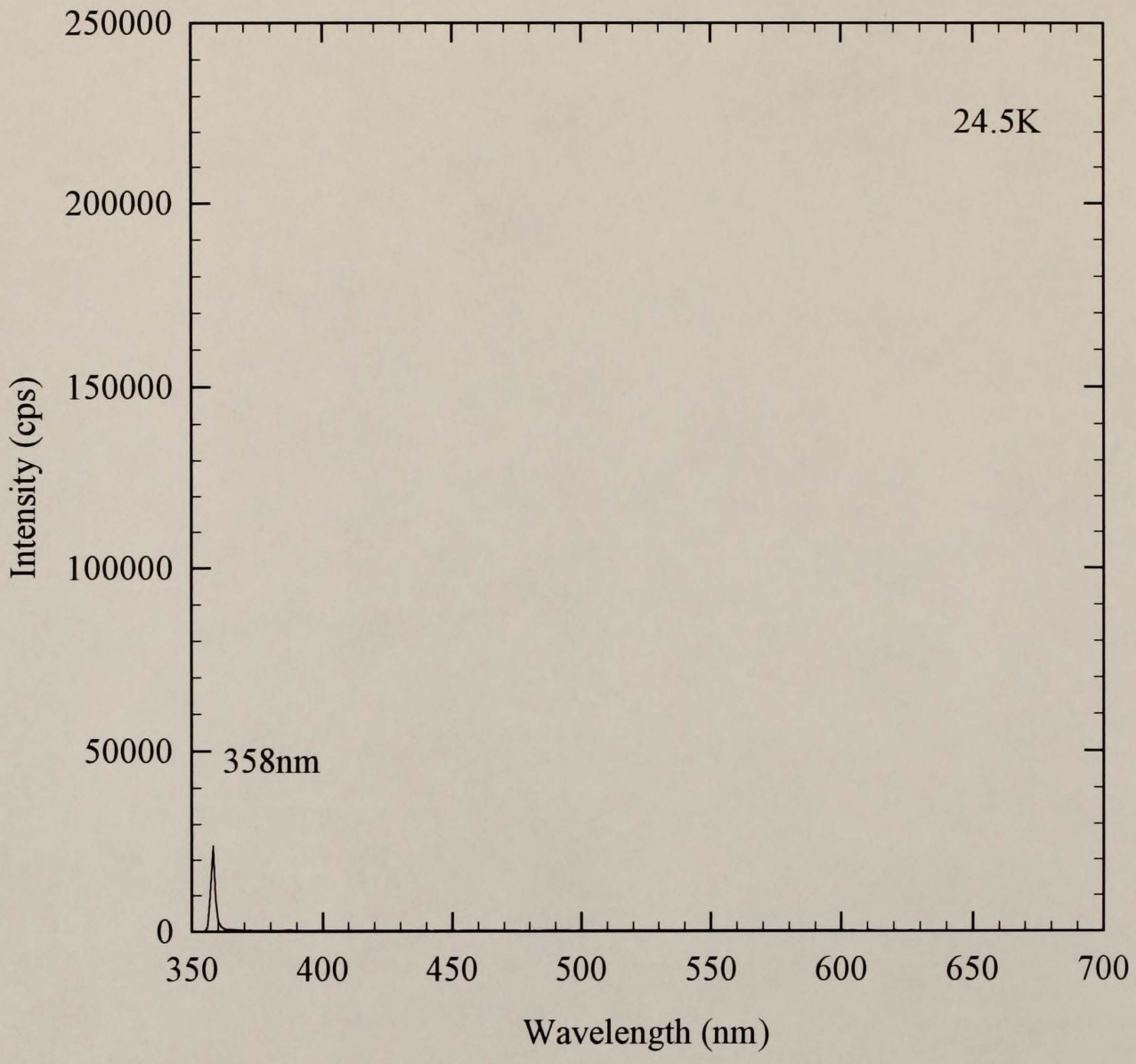

Figure 4.11 Low-temperature PL spectrum recorded from a GaN / sapphire film grown by the AEEE technique with a 0 sec.Ga delay time.

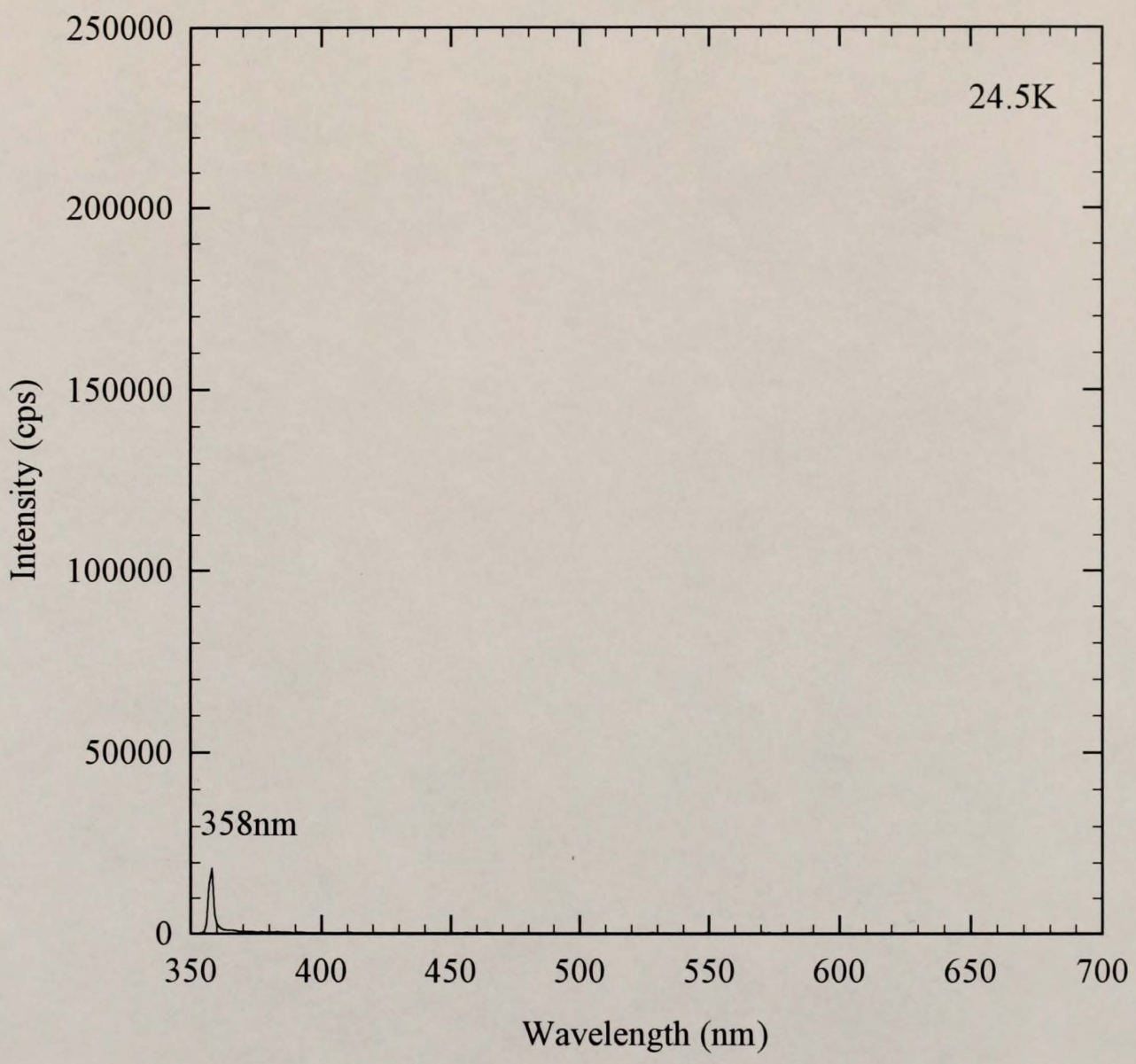

Figure 4.12 Low-temperature PL spectrum recorded from a GaN / sapphire film grown by the AEEE technique with a 15 sec. Ga delay time.

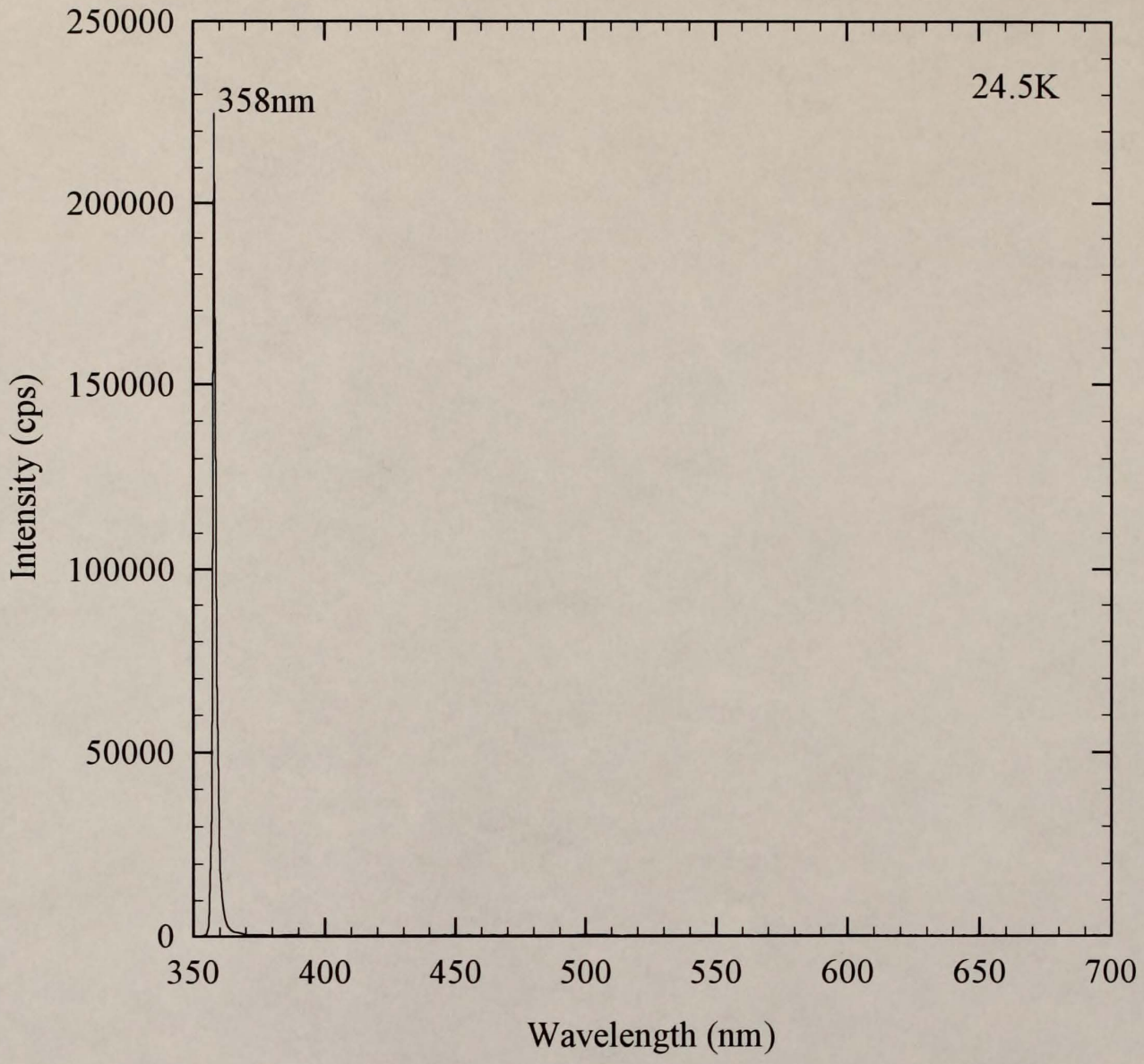

Figure 4.13 Low-temperature PL spectrum recorded from a GaN / sapphire film grown by the AEEE technique with a 30 sec. Ga delay time.

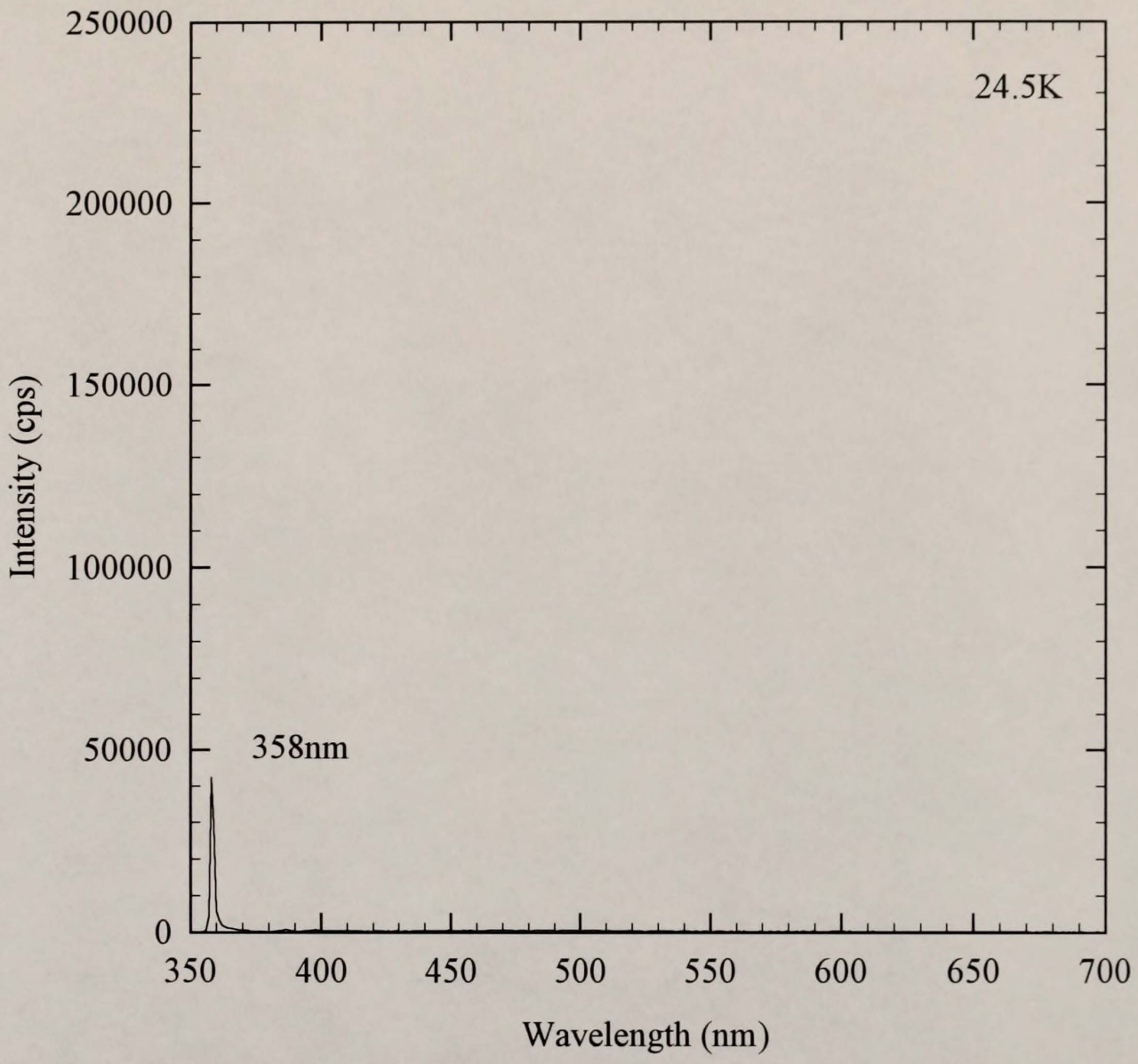

Figure 4.14 Low-temperature PL spectrum recorded from a GaN / sapphire film grown by the AEEE technique with a 50 sec. Ga delay time.

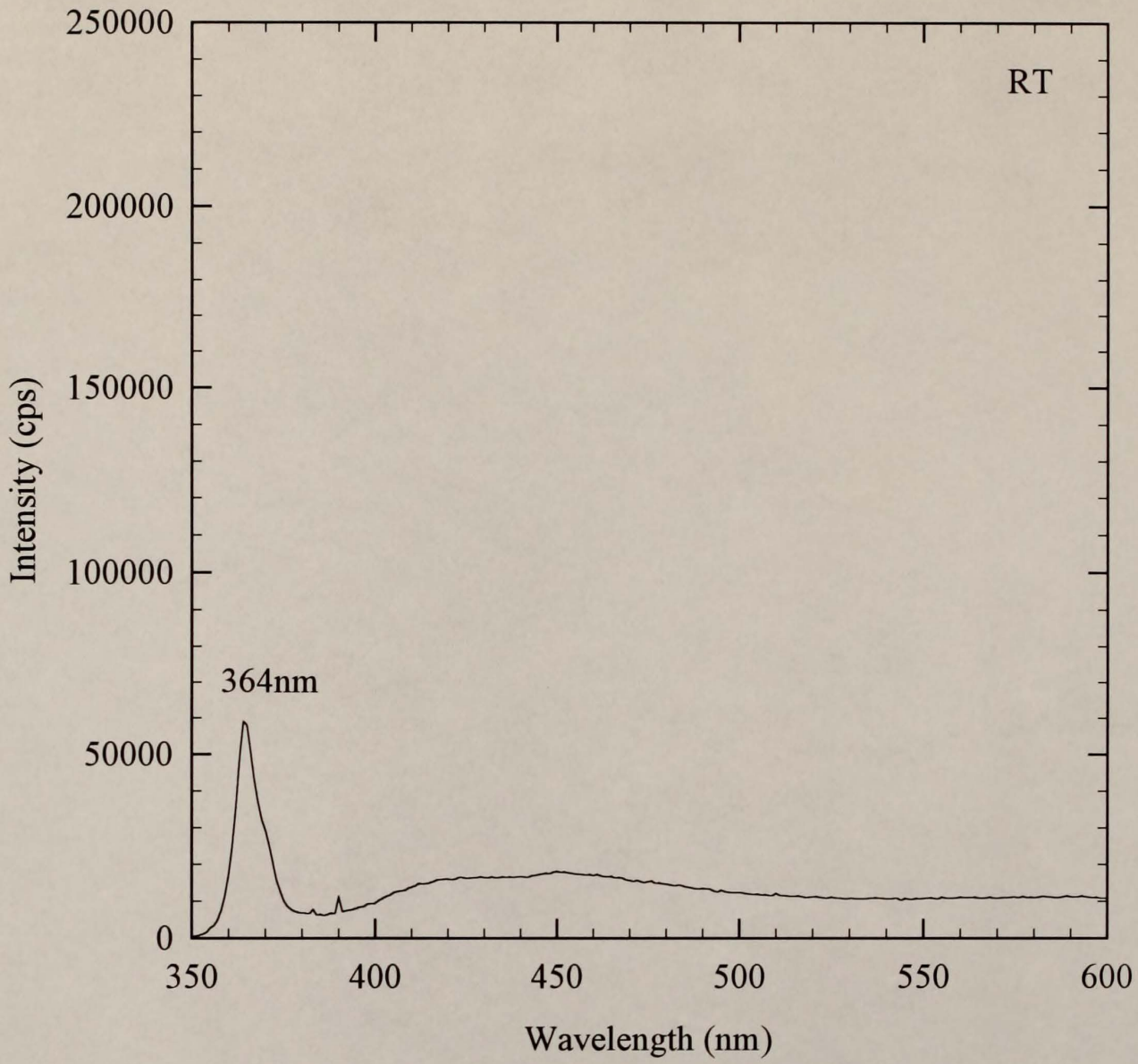

Figure 4.15 Room-temperature PL spectrum recorded from a GaN / sapphire film grown by the AEEE technique with a 0 sec. Ga delay time.

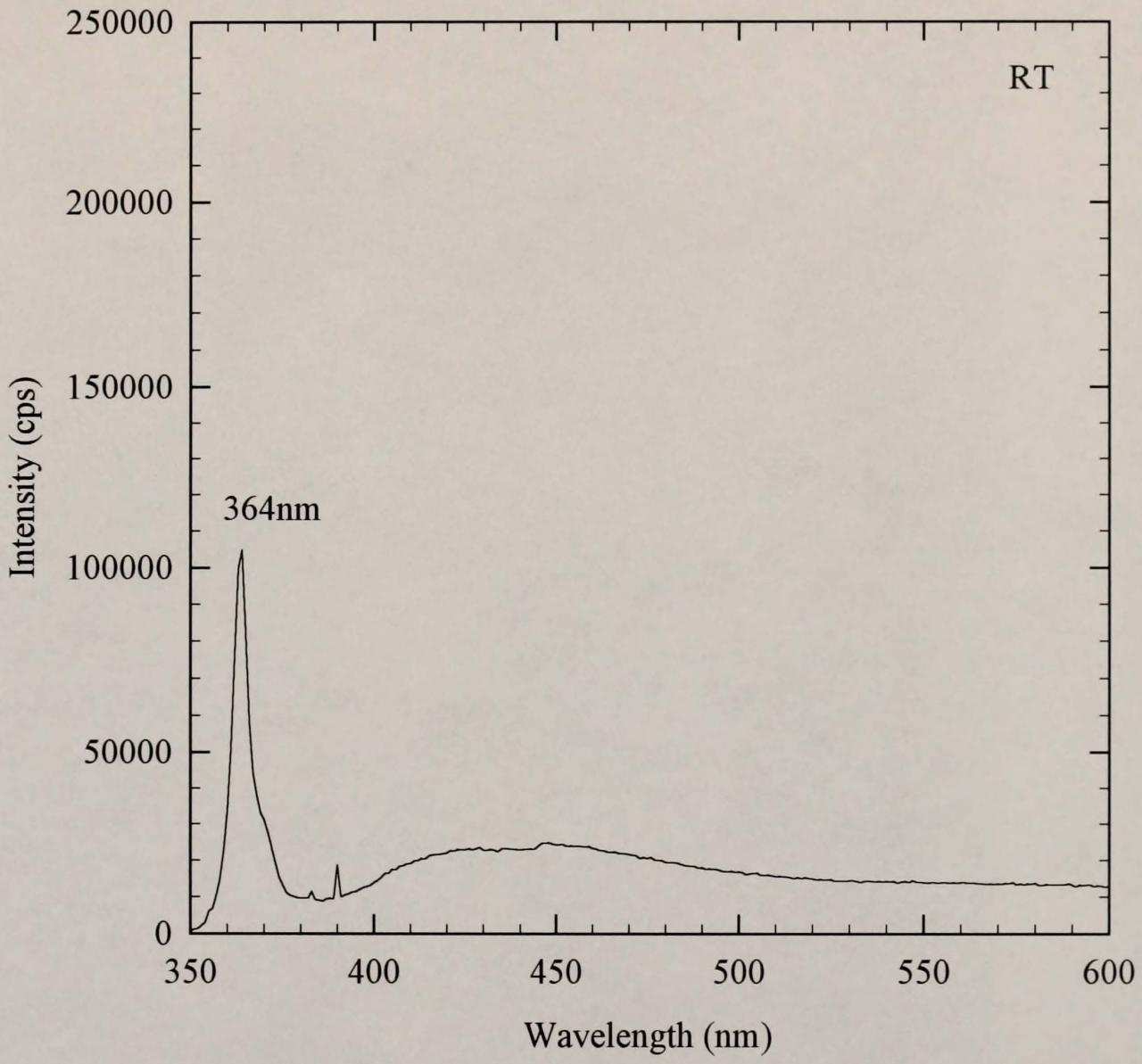

Figure 4.16 Room-temperature PL spectrum recorded from a Ga / sapphire film grown by the AEEE technique with a 15 sec. Ga delay time.

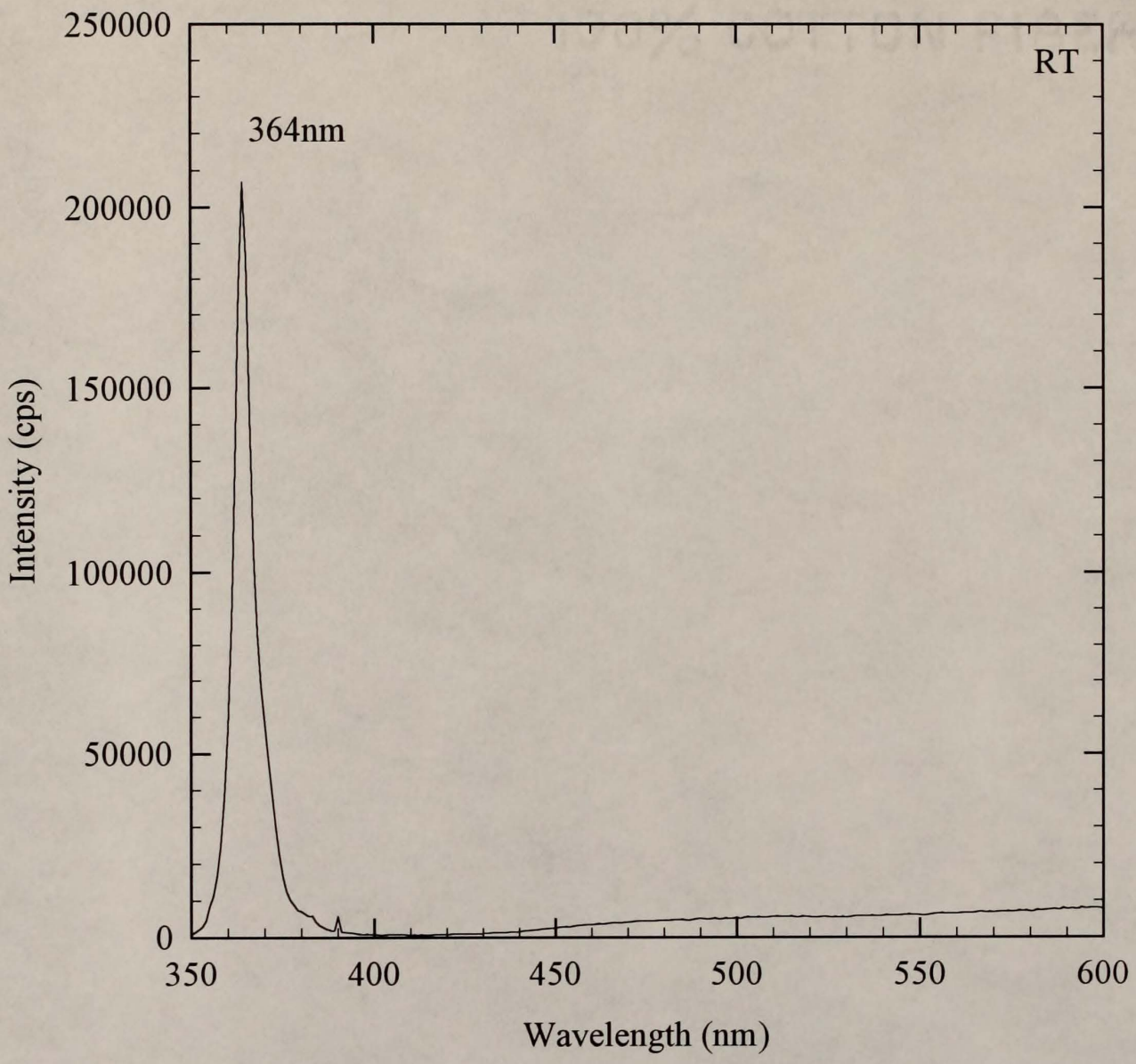

Figure 4.17 Room-temperature PL spectrum recorded from a GaN/ sapphire film grown by the AEEE technique with a 30 sec Ga delay time.

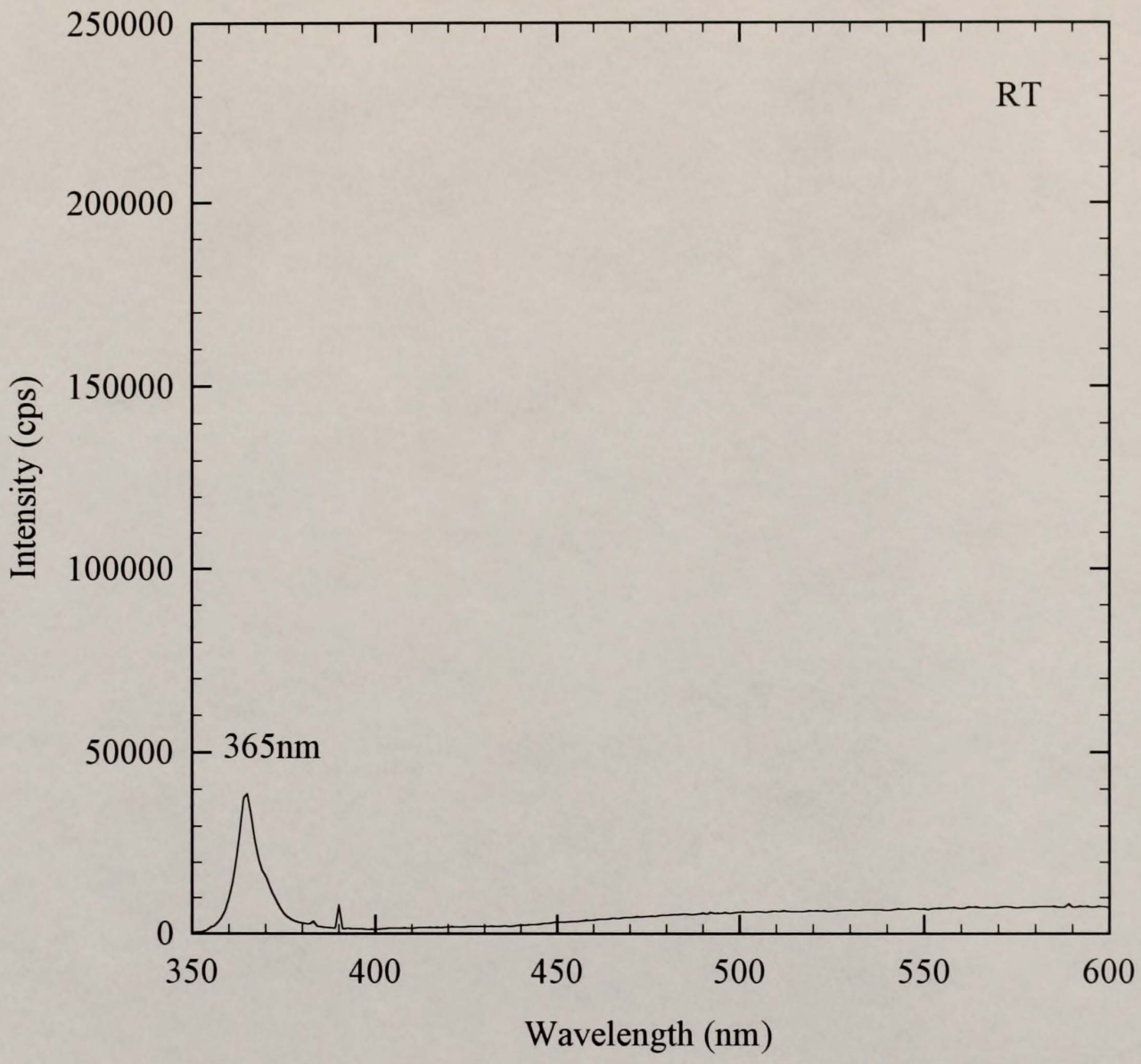

Figure 4.18 Room-temperature PL spectrum recorded from a GaN / Sapphire film grown by the AEEE technique with a 50 sec. Ga delay time.

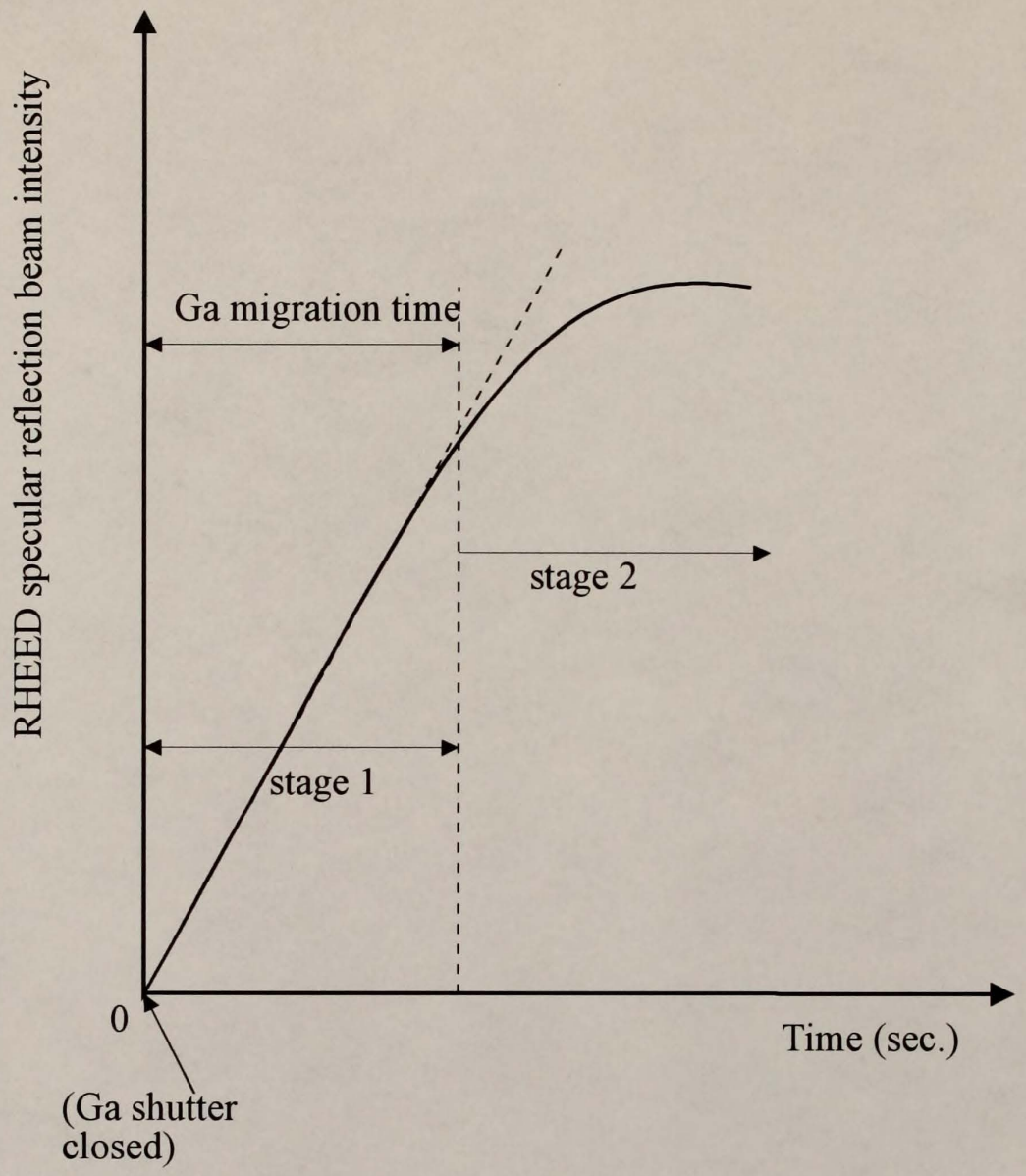

Figure 4.19 RHEED intensity recorded during a Ga-delay phase showing the two distinct stages of recovery. Ga adatom migration times were determined for a variety of substrate temperatures by noting the time required for completion of stage 1 recovery as indicated at each temperature.

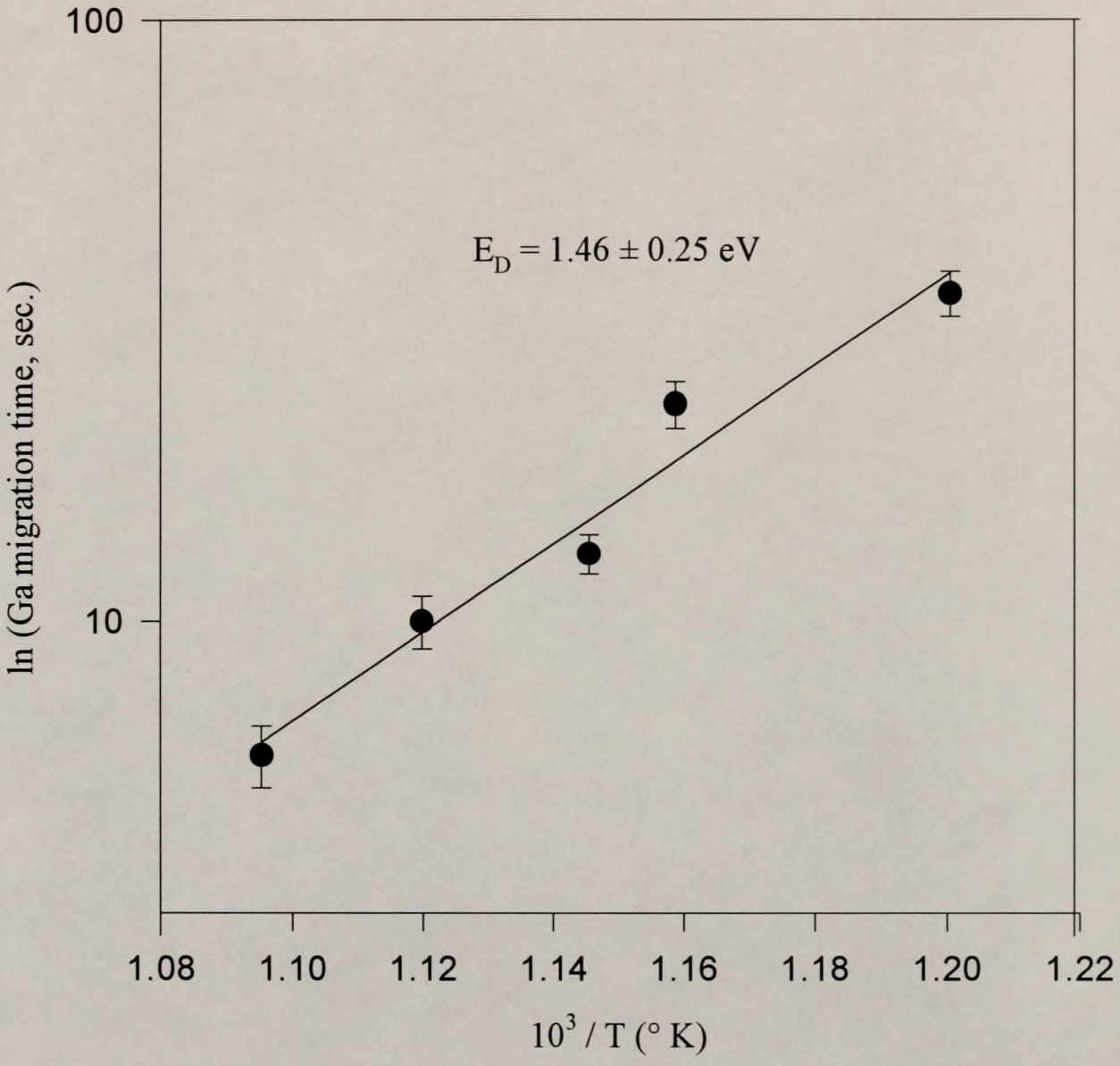

Figure 4.20 Plot of ln(Ga migration time) versus reciprocal substrate temperature.

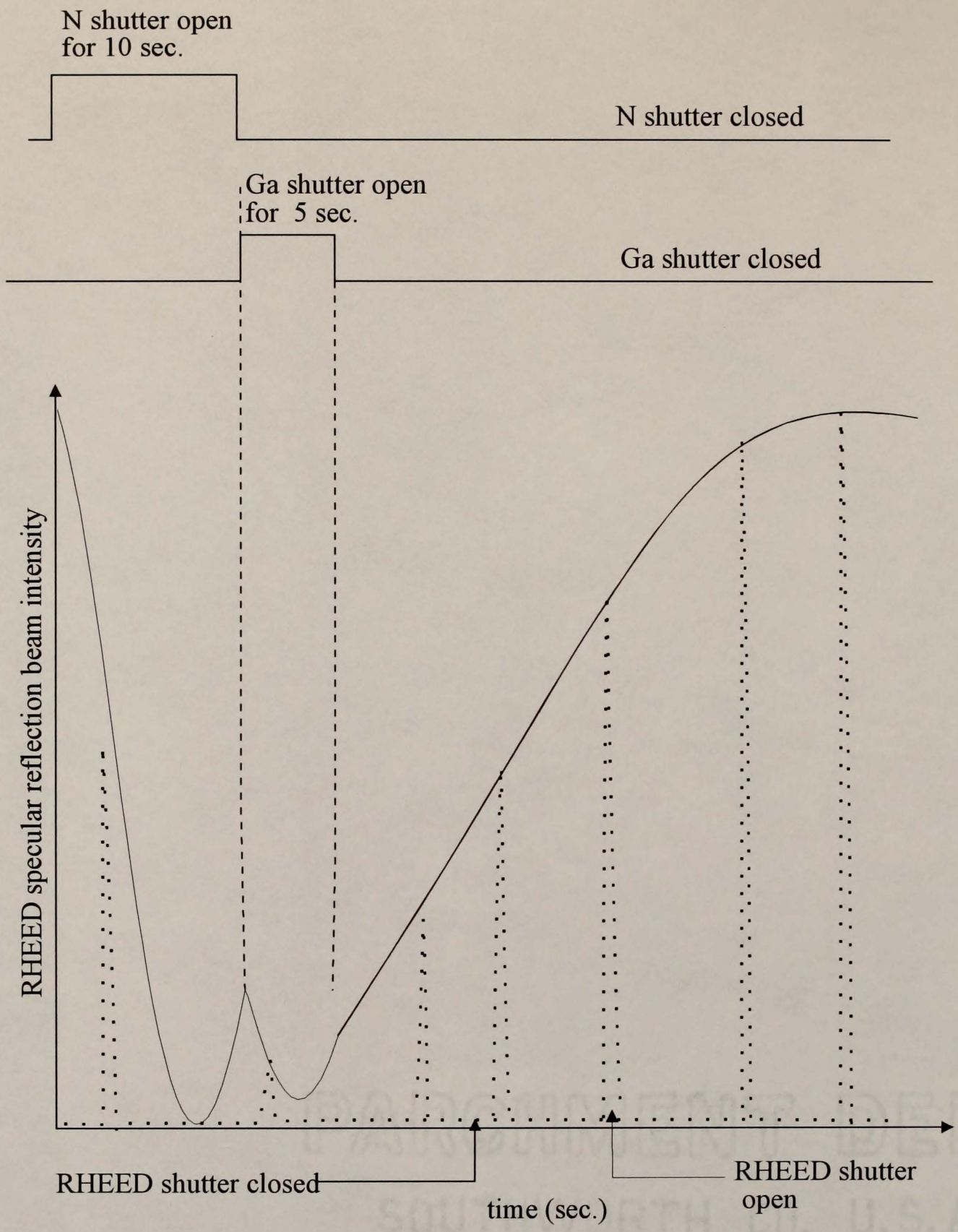

Figure 4.21 RHEED specular reflection beam intensity recorded as a function of time during one cycle. The solid line represents the RHEED intensity trace when the RHEED electron beam is continuously impinging on the surface, while the broken line represents the intensity when the RHEED electron beam shutter is periodically opened (~1 sec.) and closed (~5 sec.).

CHAPTER 5
INVESTIGATION OF GaN GROWTH KINETICS AND THEIR CORRELATION WITH DEEP-LEVEL DEFECTS

Introduction

In this chapter, the AEEE growth mechanisms will be compared with the mechanisms of conventional MBE growth, specifically, for α-GaN growth on sapphire. First, a discussion of the growth mechanisms will be given based on the growth parameters and the SEM characterization results which were presented in Chapters 3 and 4. Second, speculation will be made about the origin of the deep-level defects that are believed to cause the 2.3 eV yellow band luminescence observed in all of the PL spectra recorded from conventionally-grown α-GaN films, this speculation being based on the PL spectra discussed in Chapter 3 and on the theoretical and experimental results concerning deep-level defects discussed in Chapter 1. Finally, the optimum AEEE shuttering sequence which contributes to the elimination of the yellow band emission will be discussed. This discussion includes the presentation of a model concerning Ga adatom migration which was developed as a result of the real-time RHEED intensity observations during the Ga exposure and Ga delay phases.

Morphological Considerations

The surface morphology of conventional MBE-grown GaN films deposited on sapphire is very sensitive to the growth parameters as illustrated by the SEM micrographs shown in Figs. 3.5 and 3.6. Also, the yellow band emission appears in the PL spectra recorded from all of the conventionally-grown samples in this study regardless of growth

temperature (Figs. 3.8-3.13). The substrate temperature and Ga/N beam flux ratio play important roles in determining the GaN surface morphology. Since the nitrogen re-evaporation rate is extremely high, particularly at the high temperatures required for conventional growth, the residence time of nitrogen atoms is much shorter than that of Ga atoms. Also, the incorporation of Ga is limited by the lack of N atoms on the growing surface, especially at high temperatures. This situation is very different from the MBE growth of GaAs, for instance, in which the growth rate is controlled by the Ga flux only. Experimental evidence concerning the MBE growth of GaN indicates that the sticking coefficient of Ga is only about 0.25 and attempts to increase the Ga flux or lower the growth temperature lead to Ga-rich surfaces which are extremely rough [72]. Crawford *et al.* [28] have reported that Ga accumulation on the growing surface actually decreases the GaN growth rate when the substrate temperature is too low or the Ga flux is too high. Consequently, it could be expected that the incorporation of Ga and N are correlated in the MBE growth of GaN [53].

In this work, a strong dependence of the surface morphology of conventionally-grown GaN films on the growth temperature has been confirmed. The surface coverage of a GaN film grown at 750° C is about 90 % as can be seen from Fig. 3.5. As mentioned above, the desorption rate of N is much higher than that of Ga, hence, there are fewer incorporation sites for the Ga adatoms. The observed micro-scale discontinuity of the film will limit the surface migration length of Ga adatoms even at such a high growth temperature, producing films having localized Ga-rich and Ga-deficient areas. Reducing the growth temperature to 640° C and to 600°C decreases the N desorption rate, however, the migration rates of Ga adatoms and Ga-N molecules are also greatly reduced. The surface morphologies of the films grown at 640° C and 600° C indicate the presence of Ga droplets as can be seen from Fig. 3.6. The average size of the Ga droplets is about 15 μm for the sample grown at 600° C and about 5 μm for the sample grown at 640° C. It is noteworthy that the Ga flux used for the sample grown at 600° C was actually three times

lower than that used for the sample grown at 640° C and yet the droplet size is larger for the sample grown at 600° C. This can be explained by assuming that the Ga desorption rate is higher at 640° C than it is at 600° C and that Ga adatom diffusion is extremely slow at 600° C during conventional MBE growth.

As reviewed in Chapter 1 [29,45], with reference to GaAs growth kinetics, the Ga surface diffusion length at 550° C under Ga-stabilized conditions is about 10 times larger than that under As-stabilized conditions. The migrating species on the growing surface when GaAs is grown with an As overpressure are believed to be Ga-As molecules rather than isolated Ga atoms, since impinging Ga-atoms immediately react with impinging As molecules to form Ga-As molecules. As in conventional MBE-growth of GaAs which is normally carried out using an As-overpressure, conventional MBE-growth of GaN is normally carried out using an N overpressure. In this case, the impinging Ga-atoms have a high probability of immediately reacting with the impinging N-atoms to form Ga-N molecules; thus, surface migration takes place as Ga-N molecules (or GaN clusters) rather than isolated Ga-atoms. The large activation energy for migration of the Ga-N molecule on the GaN growing surface is believed to result in extremely slow migration. The short diffusion length of Ga-adatoms under these conditions enhances the formation of Ga-aggregates which become sinks for additional Ga adatoms. This phenomenon is believed to have caused the slow GaN growth rates observed in references 27 and 28.

In contrast, samples grown at 600° C using the AEEE growth technique had surface morphologies devoid of Ga droplets as can be seen from the SEM micrographs shown in Figs. 4. 10 (a)-(d). It is speculated that in this case rapid Ga adatom migration takes place in the absence of an N atom flux and thus Ga clustering is avoided.

Speculation Concerning the Source of Deep-Level Defects Responsible for the Yellow Band Emission

The yellow band emission intensity has a growth temperature dependence which is evidenced by comparing the PL spectra recorded from the AEEE samples grown at 600°C with those of samples grown at higher temperatures (Figs. 4.2-4.4). Yellow band emission is, in fact, completely absent from the spectra recorded from samples grown at a substrate temperatures of 600° C. It is postulated that higher growth temperatures result in the desorption of Ga during the Ga delay phase producing Ga-vacancies which when associated with dislocations result in the yellow band emission. Dislocation densities have been estimated to be in the range, 10^8 - 10^{10} cm^{-2}, in typical GaN films grown on c-plane sapphire [25,26,54,61]. The deposition of Ga on GaN (0001) surfaces followed by thermal desorption of the Ga has been reported by Khan *et al.* [73]. In that study, Ga was deposited at 620° C and was found to evaporate at temperature around 670° C which supports the Ga re-evaporation theory. Also, Schoonmaker *et al.* have reported that GaN decomposition can be enhanced via catalysis by metal Ga [74]. Furthermore, as reported in Chapter 4, it was found in this work that during the Ga delay phase, the RHEED specular reflection beam intensity recovered faster at growth temperatures of 700° C and 640° C but recovered to a lower level of intensity than was the case for a sample grown at 600° C as shown in Fig. 4.1. Also, for a Ga exposure time at 700° C of 5 sec. instead of an optimum 8 sec, the RHEED specular reflection beam intensity was found to gradually decrease as the shuttering sequence progressed. It is believed that Ga desorption under N-free conditions is more rapid at higher temperatures and Ga vacancy generation is promoted. Ga vacancies were predicted as the most likely deep-level candidate in n-type unintentionally doped GaN in the literature review section (Chapter 1). Similar observations concerning Ga re-evaporation at relatively low temperatures have been made with regard to MBE-GaAs. Arthur [75] reported that Ga deposited on a GaAs (111), Ga-rich surface, has a sticking coefficient of unity below

477°C. However, the Ga sticking coefficient is much less than unity unless an As flux is present when the substrate temperature is in the range, 500- 600° C.

Strong yellow band emission is evident in the PL spectra recorded from GaN films grown by conventional MBE as indicated in Figs. 3.8-3.13. Also, as shown in Fig. 3.6, a high density of Ga droplets is observed on the surfaces of conventionally-grown films. It is speculated that Ga vacancies are again involved in this case since the material providing the luminescence will be Ga-deficient due to the participation of Ga adatoms in Ga droplet formation.

As mentioned previously, radiative transitions in GaN epilayers are thought to be associated with dislocations [25,26,61], in particular, screw dislocations which are uncharged in hexagonal GaN [61]. The near-band-edge emission has previously been ascribed to the recombination of electrons with holes trapped at screw dislocations [61], as indicated in Fig 5.1. Based on the results of this present study, it is speculated that the yellow band emission is due to electrons recombining with holes trapped at Ga vacancy / screw dislocation complexes as illustrated in Fig. 5.1. As the concentration of Ga vacancies increases, the probability of holes being trapped at V_{Ga} / dislocation complexes will increase and correspondingly so will the intensity of the yellow band emission.

Influence of the Ga and N Exposure Times and Delay Times.

When an N atom flux impinges on a Ga-covered surface while the Ga shutter is closed, the N atoms will incorporate into the appropriate lattice-sites easily because the surface Ga atoms have one dangling sp^2 bond. As mentioned in Chapter 4, a 10 sec. N exposure time was required for the RHEED specular reflection beam intensity to decrease to its lowest level and then to recover to a saturation level beyond which the intensity again dropped. For N exposure times longer or shorter than 10 sec, the RHEED specular reflection beam intensity did not recover to the same level as it did in the case of

the 10 sec N-exposure time during subsequent cycles. Consequently, a 10 sec. N-exposure time was thought to be optimum for the substrate temperature range employed and such an N exposure time was used throughout this work.

As can be seen from Figs. 4.2 and 4.3, the PL spectra recorded from AEEE-grown GaN deposited at 700° C and 640° C show weak peaks in the range, 365-385 nm. Such emission is believed to be related to N vacancies [20,37] which provide the group B level shown in Fig 1.2. Similar emission is also observed in the PL spectra (Figs. 4.7 and 4.8) recorded from samples grown at 600° C using N-delay times of 15 sec. and 30 sec., however, this emission is absent from the spectra recorded from the samples grown with a 0 sec. N-delay time (Figs. 4.11-14). Such evidence suggests that under Ga-free conditions (no Ga exposure), the N-adatoms have a short residence time and, hence, the optimum N-delay time was selected as 0 sec. in this work. In general, an N atom arriving at a chemically-active Ga-covered surface, which has one unsatisfied sp^2 bond perpendicular to the surface per Ga atom will tend to form a stable sp^3 bond with underlying Ga and neighboring N atoms. This will make N incorporation homogeneous on a Ga-covered surface (similar to As_2 on a Ga stabilized surface [76]). However, N has a very high vapor pressure and so excess N atoms may be only weakly adsorbed on the surface. Therefore, N desorption is proposed to be the dominated mechanism contributing to the moderate recovery of the RHEED specular beam intensity during the N delay phase, as shown in Fig. 4.5.

A primary goal of the AEEE growth mode was to promote the migration of Ga-adatoms on N-covered surfaces under N-free conditions (no N exposure) at temperatures lower than those required for conventional MBE growth. The purpose of the Ga-delays was to eliminate the Ga clusters which are thought to form on Ga-exposed surfaces. Isu *et al.* [68] used a scanning reflection electron microscopy (SREM) technique to observe the formation of Ga-droplets on Ga-exposed, As-covered surfaces. These authors also observed that the Ga droplets shrank in size when the Ga supply was interrupted.

The density of available incorporation sites for impinging Ga atoms is 1.1347 x 10^{15} cm^{-2} for GaN. The Ga-exposure time in this work ($T_{substrate}$ = 600° C) was based on the maximization of the RHEED specular reflection beam intensity level. For a Ga effusion cell temperature of 830° C, corresponding to a Ga flux of 2.27 x 10^{14} cm^{-2} s^{-1}, a 5 sec. exposure provided about 1.135 x 10^{15} Ga-atoms cm^{-2}. When the Ga shutter was opened, the RHEED specular reflection beam intensity decreased to its lowest level in ~2.5 sec. and then recovered to a saturated level in an addition 2.5 sec. It was found that the RHEED specular reflection beam intensity recovered to its highest level for a Ga exposure time of 5 sec. A shorter Ga exposure time resulted in a lower intensity level for the recovered signal while a longer than 5 sec. Ga exposure resulted in a longer recovery period. The growth rate of all AEEE-grown GaN films regardless of the Ga-delay time was measured to be ~63% of a monolayer per cycle for a substrate temperature of 600° C. In MOCVD "atomic layer epitaxy "of GaN, both Khan *et al.* and Sumakeris *et al.* reported about 2/3 of a monolayer per cycle growth although the films grown by Sumakeris *et al.* were amorphous [55,56].

Model for Ga Adatom Migration

As discussed in Chapter 4 and illustrated in Fig. 4.20, an activation energy for Ga migration on an N-free surface of 1.46 ± 0.25 eV was determined in this work. To the best of the author's knowledge, this is the first time that the activation energy of Ga migration on GaN surfaces has been reported. Compared to the activation energy of Ga diffusion on GaAs, given as, E_d = 1.3 eV, by Neave *et al.* [44], the barrier for Ga migrating on a GaN surface is higher. It must be point out , however, that the arsenic flux was on during the Ga delay in the GaAs case since Neave et al. tried to simulate conventional MBE growth. E_d is expected to be smaller than 1.3 eV for Ga-adatom migration under As-free conditions.

The adatom migration rate at site i is taken to be in an Arrhenius expression:

$R^i = R_0^i \exp(-E / k_B T)$----------(5.1)

where R_0^i is a prefactor which is related to the vibration frequency of site i surface atom, T is the substrate temperature, k_B is the Boltzmann constant and E is the activation barrier for migration which depends on the local configuration of site i. E includes a substrate barrier E_s and a barrier E_n contribution from each nearest-neighbor bond formed parallel to the substrate. The homonuclear bond energy of Ga is 1.71 eV [78] and the Ga-N bond energy is determined to be 3.1 eV using Pauling's approximation [79]. The larger activation energy of Ga migration on GaN compared with Ga on GaAs is understandable since GaN has a larger E_s (ionic bonding) than the E_s (covalent bonding) of GaAs.

A model has been developed to explain the RHEED specular reflection beam intensity behavior observed during Ga exposure and subsequent Ga-delay time phases of growth. The discussion of the model will be presented in terms of three stages, namely, the Ga exposure stage, the first stage of recovery and the second stage of recovery. These three stages are illustrated in Fig. 5.2 with regard to a typical RHEED intensity trace recorded in this work during a cycle of AEEE growth.

Ga Exposure Stage:

As can be seen from Fig. 5.2, the specular reflection beam intensity initially decreases, goes through a minimum and then increases again during the Ga exposure. What is not illustrated in this figure is the fact that for Ga exposures longer than 5 seconds, the specular reflection beam intensity saturates at the intensity level corresponding to a 5 second Ga exposure.

An attempt is made to explain the "Ga exposure stage" behavior with reference to the illustrations presented in Fig. 5.3. As mentioned in the previously section, dislocation densities in the range, 10^8 - 10^{10} cm^{-2}, have been reported for typical GaN films grown on c-plane sapphire [25,26,54,61] and most of these dislocations are pure edge type, existing on $\{1\ \bar{1}\ 0\ 0\}$ planes. However, screw, or mixed type, dislocations are also present and account for ~30% of the total dislocation density [79]. The magnitude of the Burger's vector is equal to the lattice parameter, c, for screw dislocations (5.18 Å in GaN) and a/3 $[1\ 1\ \bar{2}\ 0]$ for edge dislocations (a is equal to 3.19 Å in GaN). Therefore, because the dislocation nucleation energy increases linearly with k. b^2, where b is the magnitude of the Burger's vector and k is a constant, edge dislocations account for a large fraction of the total dislocation density because of their lower formation energy. The edge dislocations which formed on $\{1\ \bar{1}\ 0\ 0\}$ during the coalescence of 3D-islands in the early stage of GaN / sapphire growth will terminate on (0001) surfaces. These points of termination disrupt the orderly array of surface atoms as seen from Fig. 5.3 (a).

Consideration of mechanical equilibrium among the interfacial tensions in the case of heterogeneous nucleation yields Young's Equation $\gamma_f \cos\theta = \gamma_{sv} - \gamma_{fs}$ as shown in Fig.5.4 (b), where f, s, v and θ represent film, N-covered GaN surfaces, vapor and contact angle, respectively. ΔG* (energy barrier to the nucleation) will depend on the surface energy of the cluster (γ_f) and contact angle between the cluster and the surface (θ) for the heterogeneous nucleation case and can be represented as:

$$\Delta G^* = 16\pi(\gamma_f)^3 f(\theta) / 3(\Delta G_V)^2 \quad \text{----------(5.2)}$$

where $f(\theta) = (2 + \cos\theta)(1-\cos\theta)^2 / 4$, and ΔG_V is the free energy change per unit volume accompanying of the of formation of small clusters. Lattice mismatch between film and substrate will increase the overall energy barrier (ΔG*) because the strain energy is involved in ΔG_V. However, ΔG* will decrease when the surface defects are presented.

When a surface having a large dislocation density [as shown in Fig. 5.3 (a)] is exposed to the Ga flux, Ga adatoms will nucleate on the termination sites of dislocations

as seen in Fig. 5.3 (b). Ga aggregates having radii smaller than r* will shrink and disappear, lowering the free energy. At the same time, because of their lower energy barrier (ΔG^*) to the nucleation process, nuclei having radii larger than r* will grow to supercritical dimensions by the further addition of atoms as shown in Figs. 5.3 (c)-(d) and Fig. 5.4 (a). After 2-2.5 sec. Ga exposure (circle c and d on the RHEED intensity variation curve in Fig 5.3), islands several atomic-layers high are formed and the RHEED specular reflection beam intensity drops rapidly to the lowest level, indicating a rough surface. The RHEED specular reflection beam intensity recovers after a 2.5 sec. Ga exposure and it is proposed that the small Ga islands merge to form larger Ga clusters, flattening the cluster surfaces which in turn decreases the surface roughness.

For 5 sec. Ga exposures and longer (circle e on the RHEED intensity variation curve in Fig. 5.3), the RHEED intensity starts to saturate. For this condition, it is proposed that Young's equation for partial wetting conditions, $\gamma_f > (\gamma_{sv} - \gamma_{fs}) > -\gamma_f$, is balanced at a critical contact angle. Further Ga deposition will be limited by increasing $f(\theta)$ [Fig. 5.4 (c)] which increases the energy barrier for the nucleation process (ΔG^*).

First Stage of Recovery:

As can be seen from Fig. 5.2, following closure of the Ga shutter, which prevents further Ga exposure, there is a fast recovery phase which lasts for about 15 seconds (for a substrate of 600° C). During this first stage of recovery, it is expected that Ga adatoms migrate fairly rapidly (in the absence of N atoms) on the terraces to the steps which results in a smoothing of the growth front as illustrated in Figs. 5.5 and 5.6. Large Ga clusters are unlikely to move freely on the terraces, however, the Ga adatoms can detach themselves from the edges of the clusters and migrate quickly to the step (kink or ledge) sites. Also at this stage, the probability of Ga finding incorporation sites is high and the

mean free path for Ga adatom migration is large. It must be pointed out that the Ga adatoms have equal chance to either migrate to the upper or the lower terraces.

Second Stage of Recovery:

As can be seen from Fig. 5.2, for Ga-delay times in excess of 15 seconds (at 600°C), a second recovery stage begins in which recovery (surface smoothing) is not as rapid as in the previous stage. During this stage, it is expected that a rearrangement of the terraces takes place which impacts longer range order as shown in Fig. 5.5 [67,69,70]. For Ga delays longer than 30 sec. the RHEED intensity drops slightly. It is speculated that step bunching occurs in these cases in which the terrace width locally decreases [80].

As can be seen from Figs. 4.11-14 (low-temperature PL spectra recorded from AEEE-grown samples with different Ga-delay times, namely, 0 sec, 15 sec, 30 sec and 50 sec.), the near-band-edge emission intensity is about an order of magnitude higher from the 30 sec. delay sample compared to the 0 sec. or 15 sec. delay samples. Also, weak deep level emission centered around 450 nm is present at room temperature from the 0 sec. and 15 sec. delay samples but not from the 30 sec. delay sample as shown in Figs. 4.15 and 4.16. These results considered together with the model suggest that the achievement of long-range order (as indicated by the observation of the second stage recovery of the RHEED intensity) produces the highest quality epilayers. However, as shown in Figs. 4.14 and 4.18, the near-band-edge emission intensity is again lower from the 50 sec. delay sample (compared with the 30 sec. delay sample) and so it appears that epilayer quality is degraded when step bunching is involved.

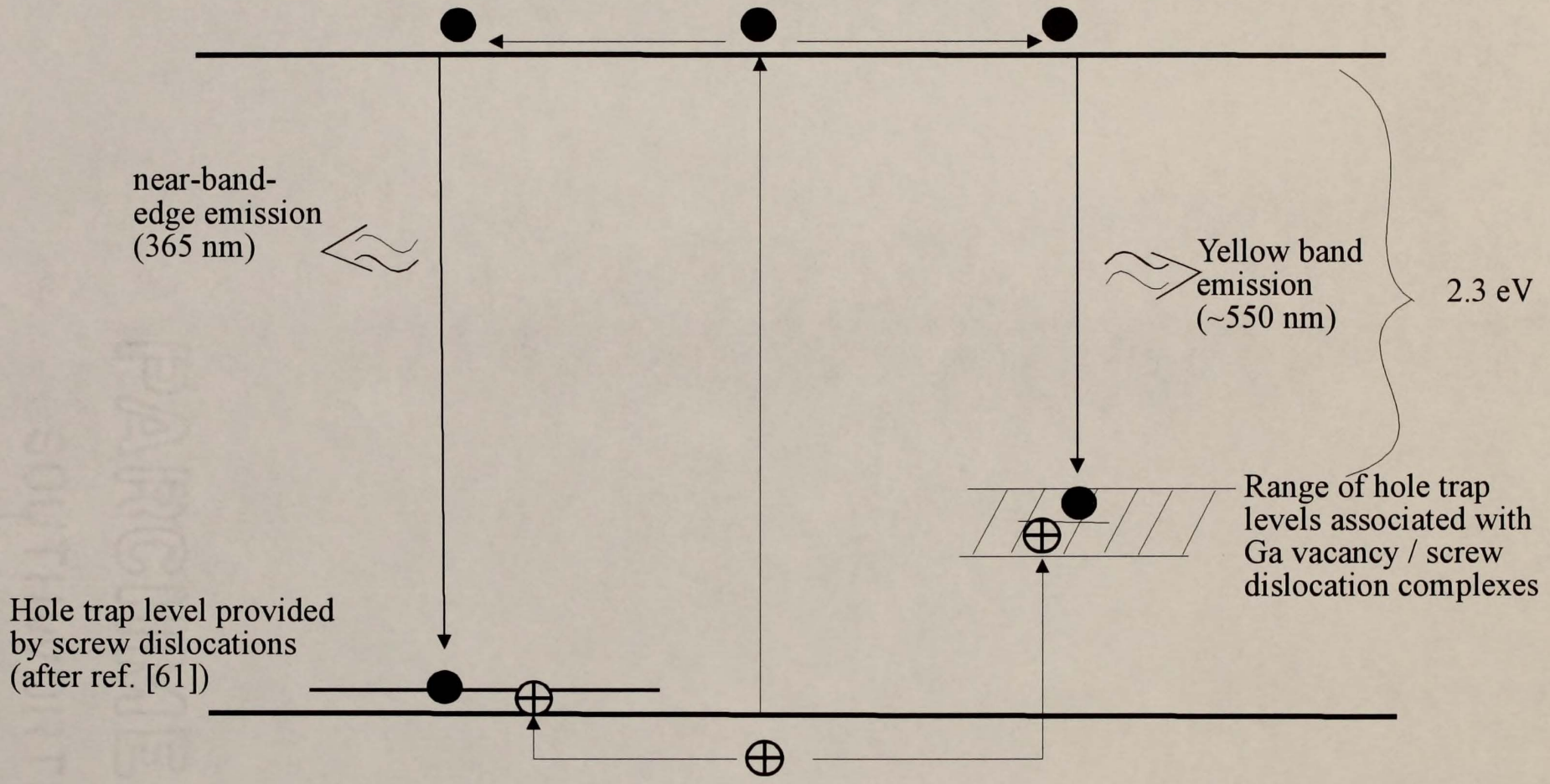

Fig. 5.1 In defective GaN epilayers, efficient radiative transitions are associated which screw dislocations that are either isolated or are in association with native point defects.

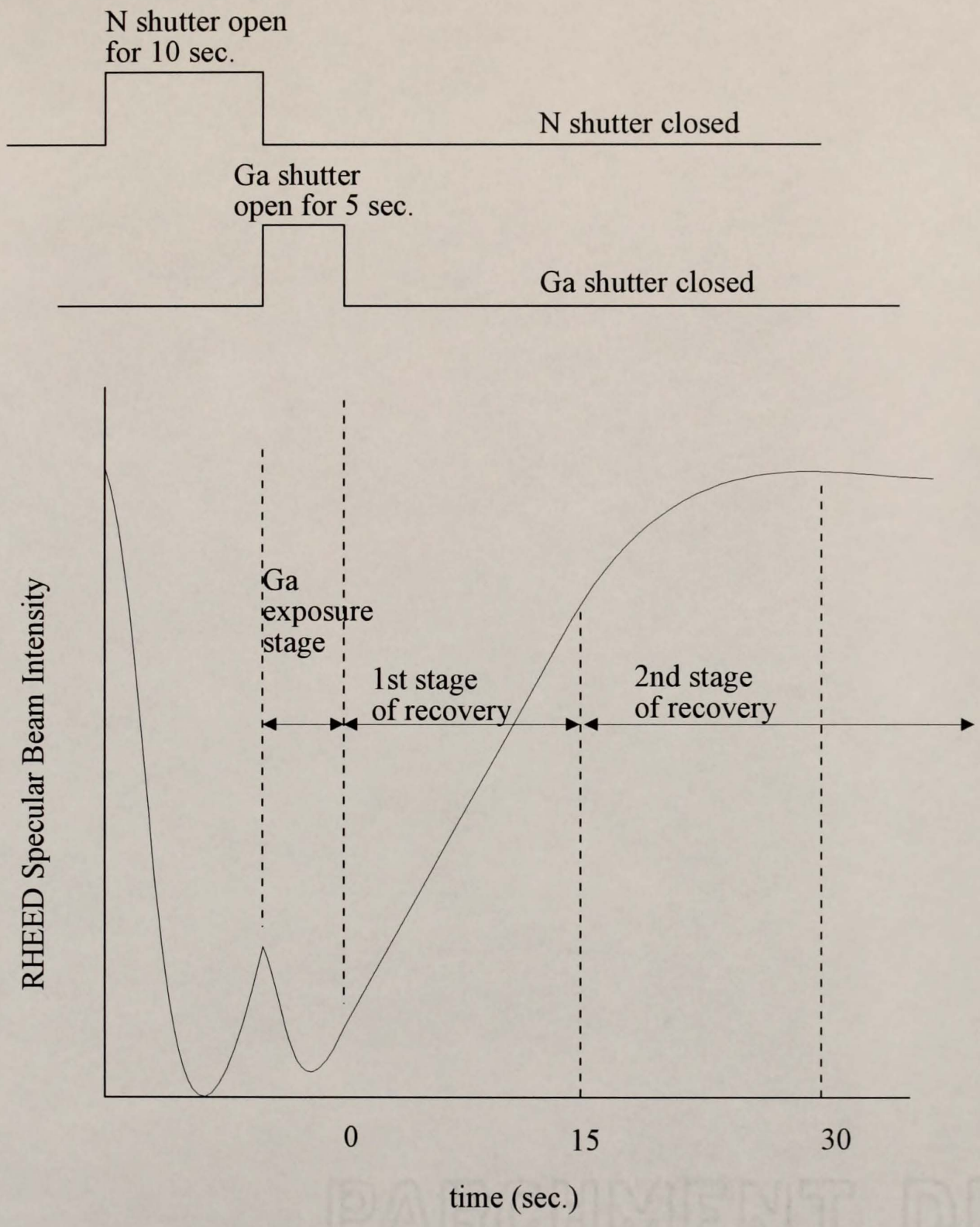

Figure 5.2 A typical trace of the RHEED specular reflection beam intensity recorded during one cycle of AEEE illustrating the three stages of the process discussed in the model presentation.

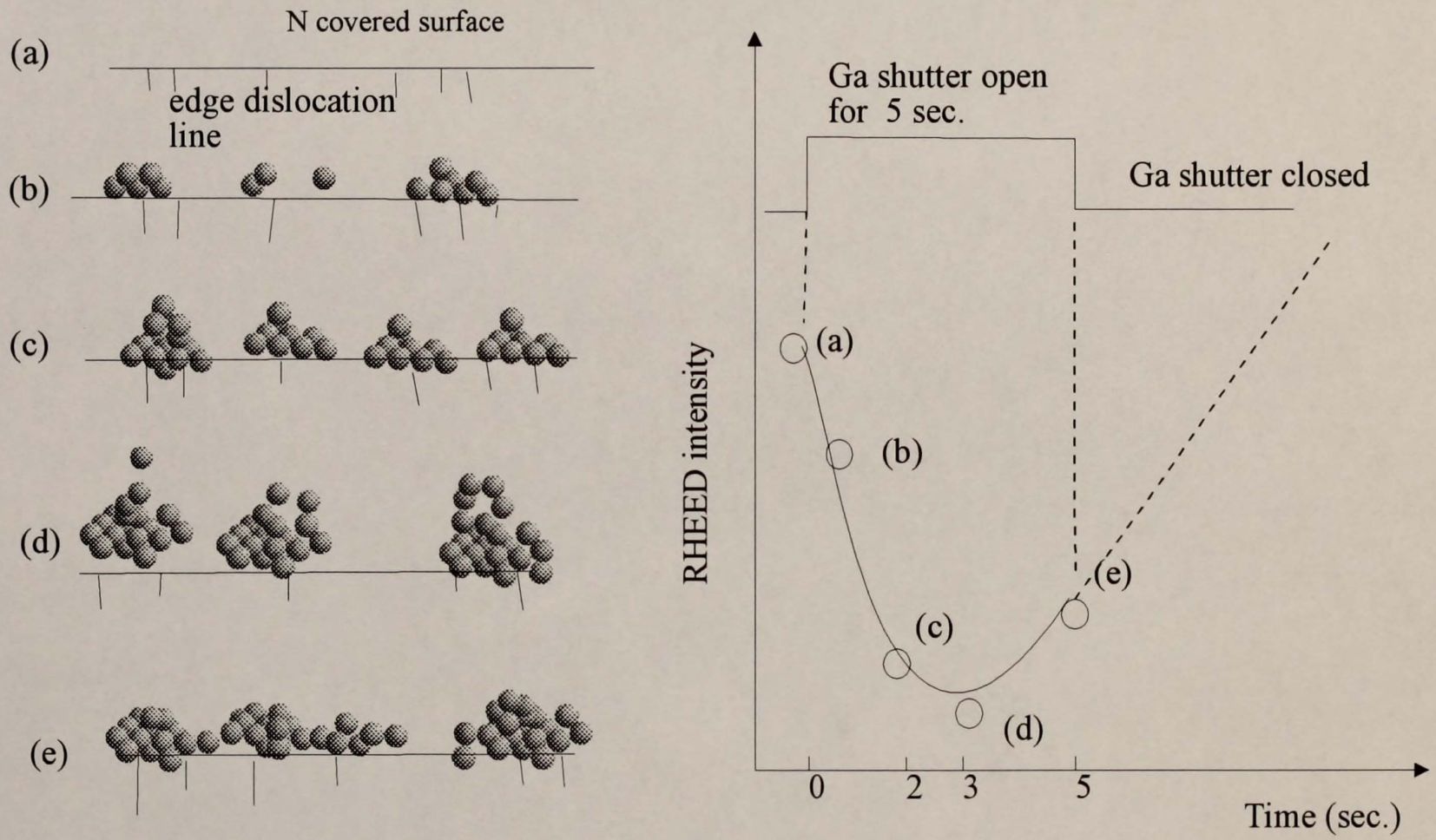

Figure 5.3 Ga cluster nucleation and evolution during the Ga exposure phase (in the absence of nitrogen) as suggested from the RHEED intensity observations.

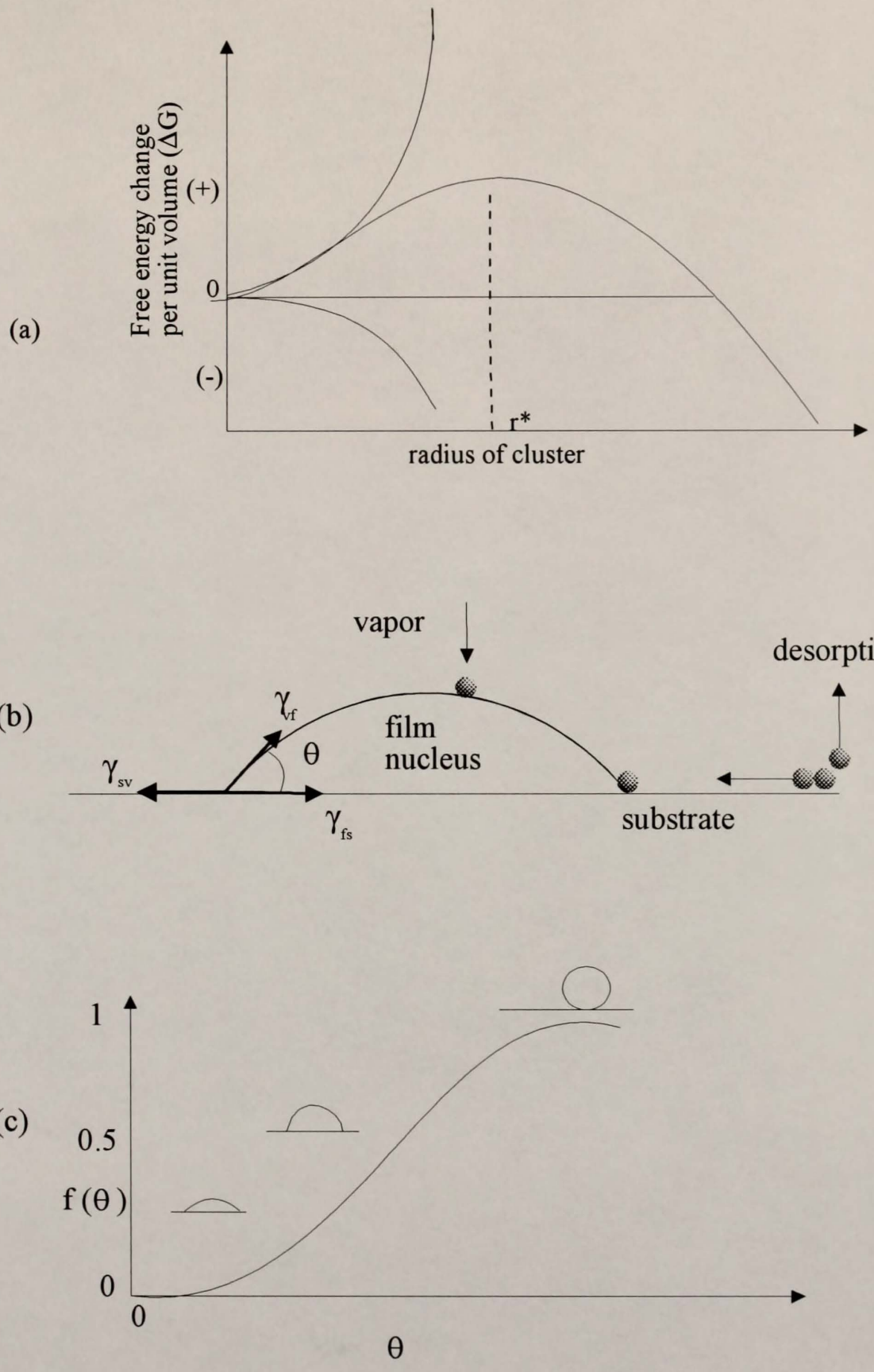

Figure 5.4 (a) Free energy change per unit volume as a function of cluster size. (b) Young's equation, film-vapor interface coming to some equilibrium contact angle, with the substrate surface. (c) Variation of the efficiency factor for nucleation by solid surface, f(θ), with the contact angle θ .

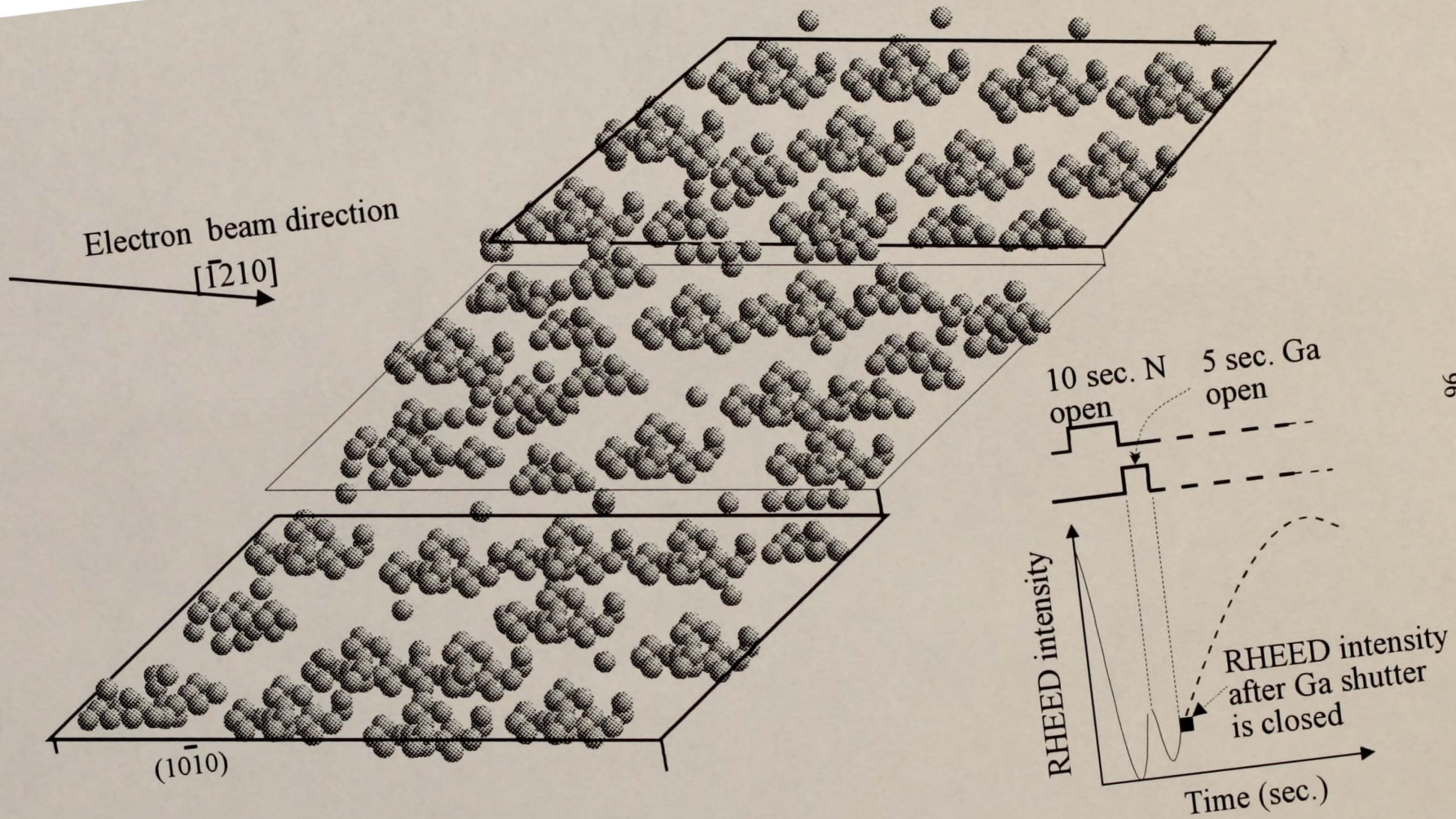

Figure 5.5 Ga cluster distribution on the N-covered terraces following a 5 sec. Ga exposure. (at T_{sub} = 600° C).

Figure 5.6 Ga adatom distribution after about 16 sec. (at T_{sub} = 600° C) during Ga delay stage (both Ga and N shutters closed).

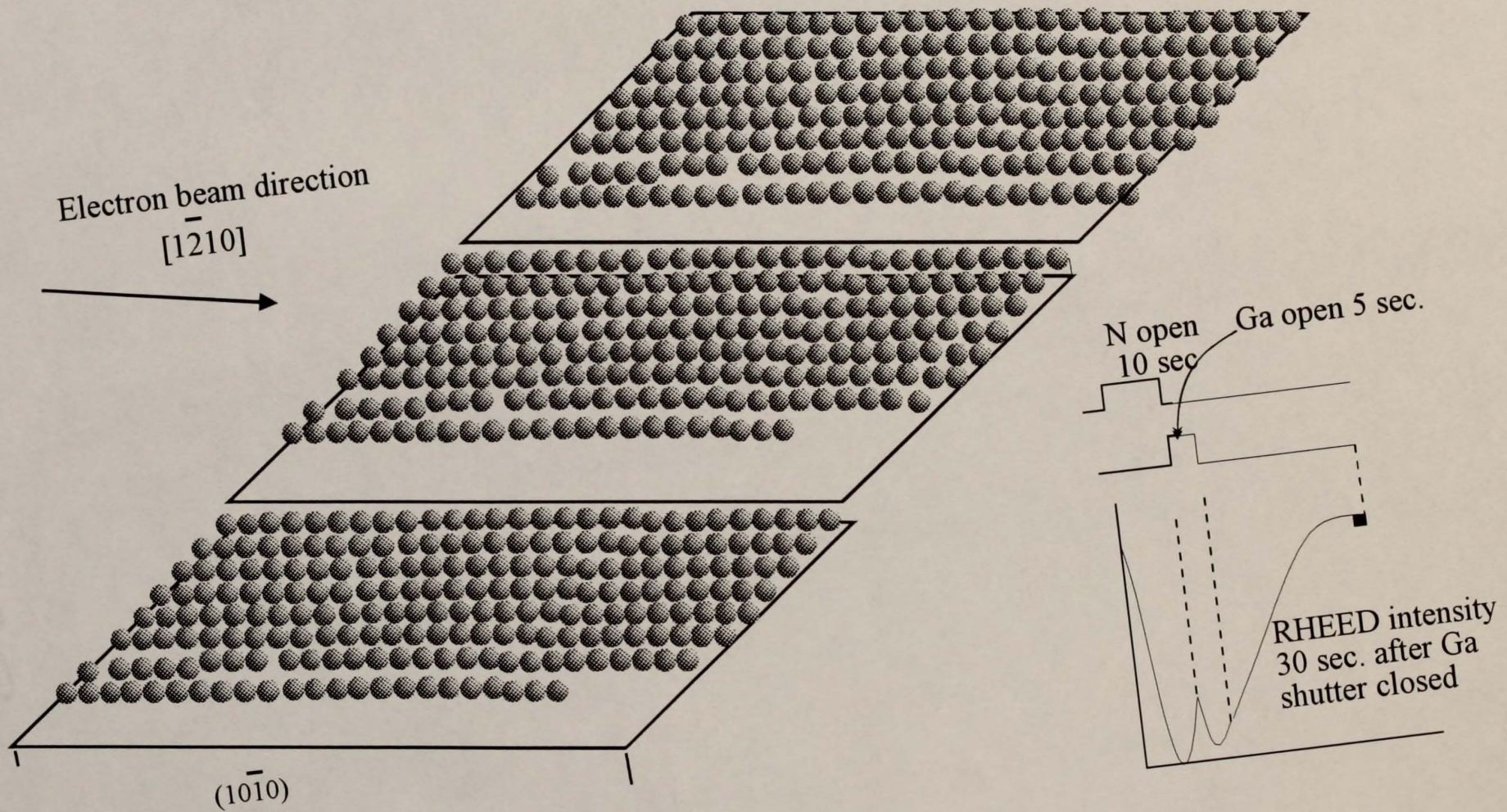

Figure 5.7 Ga adatom distribution after about 30 sec. (at T_{sub} = 600° C) during Ga delay stage (both Ga and N shutters closed).

CHAPTER 6
CONCLUSIONS AND RECOMMENDATIONS

Yellow band luminescence is commonly observed in the PL spectra recorded from GaN films regardless of the crystal growth technique and the substrate employed. This yellow band emission is associated with radiative transitions involving deep-level defects in GaN. In this research, the impact of the growth kinetics on the production of these deep centers has been systematically studied.

Several GaN films were grown by conventional MBE using a variety of growth parameters as reference samples. Ga droplets were observed on the surfaces of conventionally-grown samples, particularly those grown at low temperatures. The yellow band emission appeared in the PL spectra recorded from all of the conventionally-grown samples. In contrast, Ga droplets were not observed on the surfaces of samples grown by the alternate element exposure method, even in the case of samples grown at 600°C. In addition, the yellow band emission was suppressed in the PL spectra recorded from the AEEE-grown samples.

It is concluded that the role of Ga adatom migration on growing GaN surfaces is critical with regard to the production of deep level defects. It is essential, in fact, to promote Ga adatom migration with a view to minimizing the concentration of the deep centers responsible for the yellow band luminescence.

It is also imperative, as shown in this work, to minimize the probability of N desorption occurring from growing GaN surfaces, as this process generates other levels in the GaN energy-gap (due to N vacancies) which themselves provide for radiative transitions.

An additional conclusion from this work is that further optical finality improvement can be realized by the provision of an optimum delay time following a Ga exposure (prior to a subsequent N exposure) which promotes further Ga adatom migration (in the absence of N atoms and N_2 molecules) and also allows time for terrace re-arrangement (growth front smoothing) to occur. Figure 6.1 summarizes the impact that enhanced Ga migration has on the quality of GaN epilayers.

It is recommend that the novel AEEE-growth mode be applied to the growth of InGaN and AlGaN, which are difficult to grow using conventional MBE because of large growth temperature differences for InN, GaN and AlN. It is also recommend that the AEEE-growth mode be applied to doping of III-V nitride materials.

GaN epilayer grown by conventional MBE at 600° C

GaN epilayer grown by migration enhanced epitaxy (MEE) at 600° C

GaN epilayer grown by migration enhanced epitaxy at 600° C with inclusion of optimum Ga-delay times

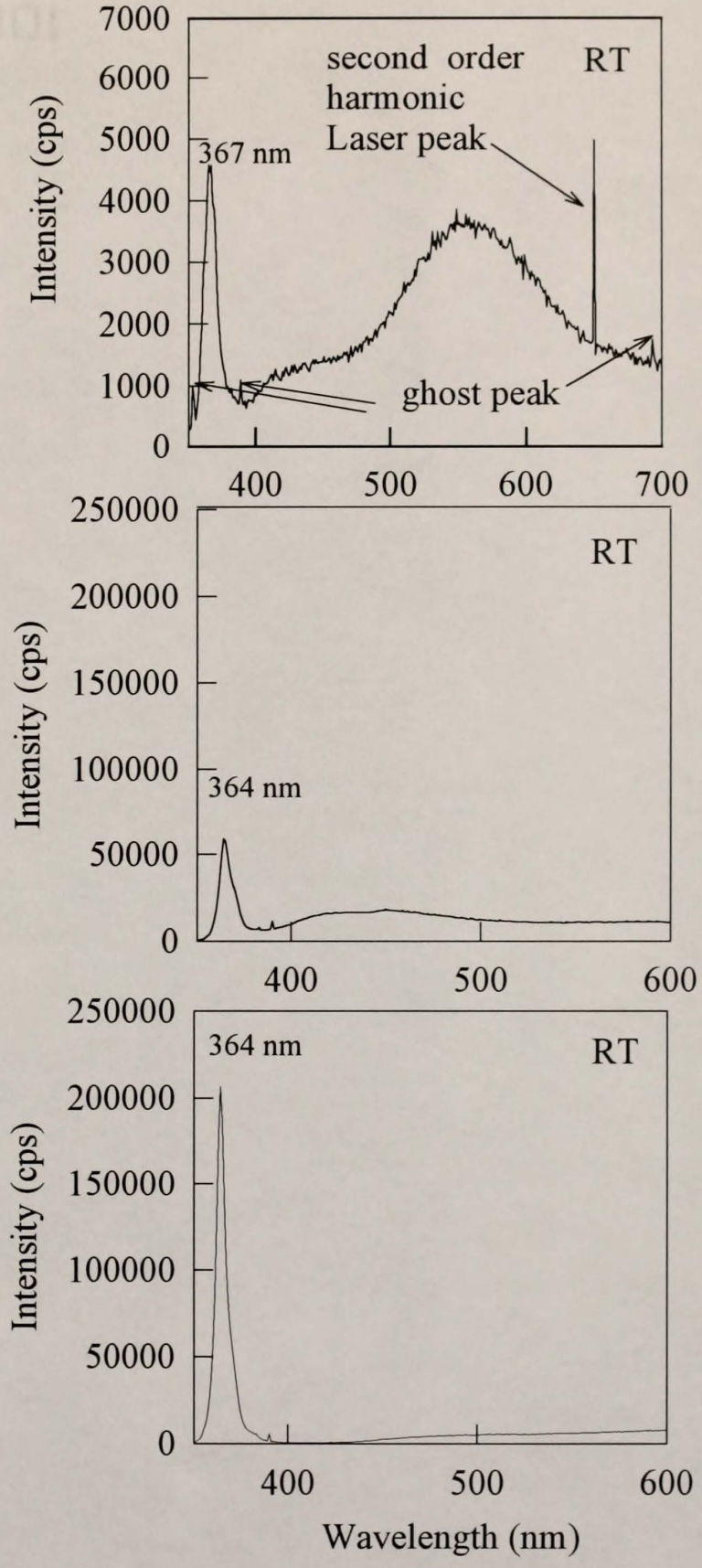

Figure 6.1 Room temperature PL spectra recorded from variously-grown GaN epilayers

LIST OF REFERENCES

1. S. Nakamura, M. Senoh, S. Nagahama, N. Iwasa, T. Yamada, T. Matsushita, H. Kiyoku, and Y. Sugimoto, Jpn. J. Appl.Phys., 35 (1B), L74 [1996].

2. K. Doverspike, L.B. Rowland, D.K. Gaskill, S.C. Binari, J.A. Freitas, W.Qian, and M. Skowronski, Inst. Phys. Conf. Ser. No 141, 101 [1995].

3. P. Kung, X. Zhang, D. Walker, A. Sazier, J. Piotrowski, and A. Rogaiski, Appl. Phys.Lett. 67 (25), 3792 [1995].

4. W. Rieger, T. Metzger, H. Angerer, R. Dimitrov, O. Ambacher, and M. Stuzmann, Appl. Phys. Lett. 68 (7), 970 [1996].

5. T. Saaki and T. Matsuoka, J. Appl. Phys. 77 (1), 192 [1994].

6. N. Grandjean, J. Massies, and M. Leroux, Appl. Phys. Lett. 69 (14), 2071 [1996].

7. T.W. Weeks, M.D. Bremser, K.S. Ailey, E.Carison, W.G. Perry, and R.F. Davis, Appl. Phys. Lett. 67 (3), 401 [1995].

8. I.P. Nikitina and V.A. Dmitriev, Proceeding of the 21st International Symposum of Compound Semiconductors, 431 [1994], edited by H. Goronkin and V. Mishra.

9. A. Ohtani, K.S. Stevens, and R. Beresford, Appl. Phys. Lett. 65 (1), 61 [1994].

10. A. Gassmann, T. Suski, N. Newman, C. Kisielowski, E. Jones, E.R. Wwber, Z.L. Weber, D.M. Rubin, H.I. Helava, I. Grzegory, M. Bockowski, J. Jun, and S. Porowski, J. Appl. Phys. 80 (4), 2195 [1996].

11 F.A. Ponce, D.P. Bour, W. Gotz, and N.M. Johnson, Appl. Phys. Lett. 68 (7), 917 [1995].

12. S. Nakamura, T. Mukai, M. Senoh, and S. Nagahama, J. Appl. Phys. 74 (6), 3911 [1993].

13. C. Wetzel, S. Fischer, J. Kruger, and E.E. Haller, Appl.Phys. Lett. 68 (18), 2556 [1996].

14. C. T. Cowan, K.P. O'Donnell, S.E. Hooper, and C.T. Foxon, Appl. Phys. Lett. 68 (3), 355 [1995].

15. M. Ramsteiner, J. Menniger, O. Brandt, H. Yang, and K.H. Ploog, Appl.Phys. Lett. 69 (9), 1276 [1996].

16. C.G. Van de Walle and J. Neugebauer, Mat. Res. Soc. Symp. Proc. 378, 467 [1995], edited by S. Ashok, J. Chevallier, I. Akasaki, N.M. Johnson and B.L. Sopori.

17. J. Neugebauer and C.G. Van de Walle, Proceedings of the 22nd International Conference on the Physics of Semiconductors, 3, 2327, [1995], edited by D.J. Lockwood.

18. J. Neugebauer and C.G. Van de Walle, Phys. Rev. B, 50, 8067 [1994].

19. J. Neugebauer and C.G. Van de Walle, Mat. Res. Soc. Symp. Proc. 339, 687 [1994], edited by C.H. Carter, Jr., G. Gildenblat, S. Nakamura, R.J. Nemananich.

20. T.L. Tansley and R.J. Egan, Phys. Rev. B, 45, 10942 [1991].

21. D.W. Jenkins and J.D. Dow, Phys. Rev. B, 39, 3317 [1987].

22. P. Perlin, T. Suski, H. Teisseyre, M. Leszczynski, I. Grzegory, J. Jun, S. Porowski, P. Boguslawski, J. Bernholc, J.C. Chervin, A. Polian, and T.D. Moustakas, Phys. Rev. Lett., 75, 296 [1995].

23. P. Boguslawski, E. Briggs, T.A. White, M.G. Wensell, and J. Bernholc, Mat. Res. Soc. Proc. Vol. 339, 693 [1994], edited by C.H. Carter, Jr., G. Gildenblat, S. Nakamura, R.J. Nemanich.

24. P.Boguslawski, E.L. Briggs, and J. Bernholc, Phys. Rev. B, 51, 17255 [1995].

25. F.A. Ponce, D.P. Bour, W. Gotz, and P.J. Wright, Appl. Phys. Lett. 68 (1), 57 [1996].

26. Z. L. Weber, H. Sohn, N. Newman, and J. Washbum, J. Vac. Sci. Technol. B 13 (4), 1578 [1995].

27. C.R. Eddy Jr. and T.D. Moustakas, J. Appl. Phys. 73 (1), 448 [1993].

28. D. Crawford, R. Held, A.M. Johnston, A.M. Dabiran, and P. I. Cohn, http://nsr.mij.mrs.org, MRS Internet J. Nitride Semicond. Res. 1, 12 [1996].

29. Y. Horikoshi, M. Kawashima, and H. Yamaguchi, Jpn. J. Appl.Phys. 27, 169 [1987].

30. R.E. Ewing and P.E. Greene, J. Electrochem. Soc. 11, 1266 [1964].

31. T. Ogino and M. Aoki, Jpn. J. Appl. Phys. 19, 2395 [1980].

32. X. Zhang, P. Kung, A. Saxier, D. Walker, T.C. Wang, and M. Razeghi, Appl. Phys. Lett. 67 (12), 1745 [1995].

33. E.R. Glaser, T.A. Kennedy, K. Doverspike, L.B. Rowland, D.K. Gaskill, M. Asif Khan, D.T. Olson, and J.N. Kuznia, Phys, Rev. B 51, 13326 [1995].

34 W. Shan, T.J. Schmidt, R.J. Hauenstien, and J.J. Song, Appl. Phys. Lett. 66 (25), 3492 [1995].

35. M. Asif Khan, D.T. Olson, J.N. Kuznia, W.E. Carlos, and J.A. Freitas, Jr., J. Appl. Phys. 74 (9), 5901 [1993].

36. W. Shan, X.C. Xie, J.J. Song, and B. Goldenberg, Appl. Phys. Lett. 67 (17), 2512 [1995].

37. W. Gotz, N.M. Johnson, R.A. Street, H. Amano, and I. Akasaki, Mat. Res. Soc. Symp. Proc. 378, 491 [1995], edited by S. Ashok, J. Chevallier, I. Akasaki, N.M. Johnson, B.L. Aopori.

38. P. Hacke, T. Detchprohm, K. Hiramatsu, N. Sawaki, K. Tadatomo, and K. Miyake, J. Appl. Phys. 76 (1), 304 [1994].

39. F.J. Sanchez, D. Basak, M.A. Sanchez-Garcia, E. Calleja, E. Munoz, I. Izpura, F. Calle, J.M.J. Tijero, B. Beaumont, P. Lorenzini, P. Gibart, T.S. Cheng, C.T. Foxon and J.W. Orton, http://nsr.mij.mrs.org, MRS Internet J. Nitride Semicond, Res. 1, 7 [1996].

40. M.E. Lin, B.N. Sverdlov ,and H. Morkoc, Appl. Phys, Lett. 63 (26), 3625 [1993].

41. S.D. Kim, H. Lee, and J.S. Harris, Jr., J. Electrochem. Soc.142 (5), 1667 [1995].

42. Y. Horikoshi and M. Kawaahima, J. Cryst. Growth 95, 17 [1989].

43. Y. Horikoshi, M.. Kawashima, and H. Yamaguchi, Jpn. J. Appl. Phys. 25, L868-870 [1986].

44. J.H. Neave, P.J. Dobson, B.A. Joyce, and J. Zhang, Appl. Phys. Lett. 47 (2), 100 [1985].

45. B.A. Joyce, P.J. Dobson, J.H. Neave,and J. Zhang, Proc. 2nd Conf. on Modulated Semiconductor Structures, Kyoto, Surface Science 174. 1 [1986].

46. S. Nagata and T. Tanaka, J. Appl. Phys. 48 (3), 940 [1977].

47. R.J. Field and S.K. Ghandhi, J. Cryst. Growth 74, 551 [1986].

48. C.T. Foxon and B.A. Joyce, Surface Science 50, 434 [1975].

49. S. Kurtin, T. C. McGill, and C.A. Mead, Phys. Rev. Lett. 22 (26), 1433 [1969].

50. J.S. Foresi and T.D. Moustakas, Appl. Phys. Lett. 62 (22), 2859 [1993].

51. S.D. Lester, F.A. Ponce, M.Craford, and D.A. Steigerwald, Appl.Phys. Lett. 66 (10),1249 [1994].

52. S. Strite and H. Morkoc, J. Vac. Sci. Technol. B 10 (4), 1237 [1992].

53. R.C. Powell, N.E. Lee, Y.W. Kim, and J.E. Greene, J. Appl. Phys. 73 (1), 189 [1993].

54. C.Y. Hwang, P. Lu, W.E. Mayo, Y. Lu, and H. Liu, Mat. Res. Soc. Symp. Proc. 326, 347 [1994], edited by G. Gumbs, S. Luryi, B. Weiss, G.W. Wicks.

55. J. Sumakeris, Z. Sitar, K.S. Ailey-Trent, K.L. More, and R.F. Davis, Thin Solid Films 225, 244 [1993].

56. M. Asif Khan, R. A. Skogman, J. M. Van Hove, D.T. Olson, and J.N. Kuznia, Appl. Phys. Lett. 60 (11), 1366 [1992].

57. R.M. Park, M.B. Troffer, C.M. Rouleau, J.M. DePuydt, and M.A. Haase, Appl. Phys. Lett. 57 (20), 2127 [1990].

58. M.A. Haase, J. Qiu, J.M. DePuydt, and H. Cheng, Appl. Phys. Lett. 59 (11), 1272 [1992].

59. J.G. Kim, A.C. Frenckel, H. Liu, and R.M. Park, Appl. Phys. Lett. 65 (1), 91 [1994].

60. H. Liu, A.C. Frenkel, J.G. Kim, and R.M. Park, J. Appl. Phys. 74 (10), 6124 [1993].

61. Y.G. Shreter and Y.T. Rebane, International Conference "Extended Defects in Semiconductors-96", Gien, France, Sept. [1996].

62. Y. Tokura, H. Saito, and T. Fukui, J. Cryst. Growth, 94, 46 [1989].

63. K. Pond, A.C. Gossard, A. Lorke, and P.M. Petroff, Materials Science and Engineering B 30, 121 [1995].

64. A. Madhukar, J. Cryst. Growth, 163, 149 [1996].

65. S.A. Chalmers, J.Y. Tsao, and A.C. Gossard, Appl. Phys. Lett. 61 (6), 645 [1992].

66. J.P.A. van der Wagt and J.S. Harris, Jr., J. Cryst. Growth, 127, 1025 [1993].

67. J.H. Neave, B.A. Joyce, P.J. Dobson, and N. Norton, Appl. Phys. A. 31, 1 [1983].

68. T. Isu, Y. Morishita, S. Goto, Y. Normura, and Y. Katayama, J. Vac. Sci. Tecnol. A, 12 (4), 1176 [1994].

69. P.B. Dobson, B.A. Joyce, J.H. Neave, and J. Zhang, J. Cryst. Growth, 81, 1 [1987].

70. X.M. Zhang, D.W.Pashley, I. Kamiya, J.H. Neave, and B.A. Joyce, J. Cryst. Growth, 147, 234 [1995].

71. B.F. Lewis, F.J. Grunthaner, A. Madhukar, T.C. Lee, and R. Fernandez, J. Vac. Sci. Technol. B 3, 1317 [1985], reprinted in Molecular Beam Epitaxy AIP Press, Woodbury, NY. 295 [1994], edited by A. Cho.

72. S. Strite, J. Ruan, Z. Li, A. Salvador, H, Chen, D. J. Smith, W.J. Choyke, and H. Morkoc, J. Vac. Sci. Technol. B 9 (4), 1924 [1991].

73. M.A Khan, J.N. Kuznia, D.T. Olson, and R. Kaplan, J. Appl. Phys., 73, 3108 [1993].

74. R.C. Schoonmaker, A. Buhl, and J. Lemley, J. Phys. Chem. 69, 3455 [1965].

75. J.R. Arthur, Jr. J. Appl. Phys. 39, 4032 [1968], reprinted in Molecular Beam Epitaxy AIP Press, Woodbury, NY. 51 [1994], edited by A. Cho.

76 F.Brones and A. Ruiz, J. Cryst. Growth, 111, 194 [1991].

77. R. T. Sanderson, J. Am. Chem. Soc. 105, 2259 [1983].

78. L. Pauling, The Chemical Bond, Cornell University Press, Ithaca, NY [1967].

79 D. Kapolnek, X. H. Wu, B. Heying, S. Keller, B.P. Keller, U. K. Mishra, S. P Denbaars and J. S. Speck Appl. Phys. Lett. 67 (11), 1541 [1995].

80. T. Ide, A. Yamashita, and T. Mizutani, Surface Science, 287/288, 1013 [1993].

BIOGRAPHICAL SKETCH

Hsing-Long Liu, received his Bachelor of Industrial Education from National Taiwan Normal University, Taipei, Taiwan, in June 1981. After graduating, he taught at San Chung Technology School. He then continued his education at Auburn University, Alabama, where he earned a Master of Science degree in materials science, in August 1990. His M.S. thesis topic was, "Synthesis of SiC / SiC Ceramic Composites by CVD". He then proceeded to the Department of Materials Science and Engineering at the University of Florida where he has been investigating the growth of GaN by molecular beam epitaxy, working toward his Ph.D.

I certify that I have read this study and that in my opinion it conforms to acceptable standards of scholarly presentation and is fully adequate, in scope and quality, as a dissertation for the degree of Doctor of Philosophy.

Robert M. Park

Robert M. Park, Chairman
Professor of Materials
Science and Engineering

I certify that I have read this study and that in my opinion it conforms to acceptable standards of scholarly presentation and is fully adequate, in scope and quality, as a dissertation for the degree of Doctor of Philosophy.

Paul H. Holloway

Paul H. Holloway
Professor of Materials
Science and engineering

I certify that I have read this study and that in my opinion it conforms to acceptable standards of scholarly presentation and is fully adequate, in scope and quality, as a dissertation for the degree of Doctor of Philosophy.

Joseph H. Simmons

Joseph H. Simmons
Professor of Materials
Science and Engineering

I certify that I have read this study and that in my opinion it conforms to acceptable standards of scholarly presentation and is fully adequate, in scope and quality, as a dissertation for the degree of Doctor of Philosophy.

Kevin S. Jones

Kevin S. Jones
Associate Professor of Materials
Science and Engineering

I certify that I have read this study and that in my opinion it conforms to acceptable standards of scholarly presentation and is fully adequate, in scope and quality, as a dissertation for the degree of Doctor of Philosophy.

Sheng S. Li
Professor of Electrical
and Computer Engineering

This dissertation was submitted to the Graduate Faculty of the College of Engineering and to the Graduate School and was accepted as partial fulfillment of the requirements for the degree of Doctor of Philosophy.

December, 1996

Winfred M. Phillips
Dean, College of Engineering

Karen A. Holbrook
Dean, Graduate School